University of Ottawa

A PHENOMENOLOGICAL EXPERIMENTAL METHOD FOR THE INVESTIGATION OF FUEL SPRAY EVAPORATION

BY

JOHN KUO SUN WONG

Submitted in Partial Fulfillment of the
Requirements for the Degree
of Doctor of Philosophy in Mechanical Engineering
in the Graduate School of
The University of Ottawa

Approved_____
Adviser

Ottawa, Ontario, Canada
June, 1972

To my father, the Late
Mr. Bing Fung Wong

ACKNOWLEDGEMENTS

The author wishes to express his sincere appreciation to his advisors, Dr. J. A. Newman, acting chairman of the Mechanical Engineering Department, University of Ottawa, and Dr. R. Sandri, senior research officer of the Mechanical Engineering Division, National Research Council of Canada for their continued assistance and guidance in the work reported.

Thanks are especially due to Dr. R. B. Whyte, Head, Fuels and Lubricants Section, Mechanical Engineering Division, National Research Council, for reviewing the manuscript and making valuable suggestions.

The author also wishes to thank Messrs. F. R. Billingham; F. Chellingworth, and N. N. Kallio, for helping in assembling the apparatus.

This work was carried out in the Fuels and Lubricants Laboratory of the Mechanical Engineering Division, National Research Council of Canada.

CONTENTS

	ACKNOWLEDGEMENTS		iii
	ABSTRACT		vii
	NOMENCLATURE		ix
I	INTRODUCTION		1
II	LITERATURE SURVEY - THEORETICAL STUDIES		9
	2.1	Single droplet evaporation - At low and moderate pressures.	10
	2.1.1	Evaporation rate from the rate of mass transfer approach.	11
	2.1.2	Evaporation rate from the rate of heat transfer approach.	14
	2.2	Single droplet evaporation - At pressures near to or above the critical pressure of the liquid fuel.	15
	2.3	Physical properties of sprays.	17
	2.4	Spray evaporation.	20
III	LITERATURE SURVEY - EXPERIMENTAL STUDIES		26
	3.1	Single droplet evaporation studies.	27
	3.2	Spray evaporation studies.	30
IV	SPRAY EVAPORATION - ANALYTICAL STUDY		37
	4.1	Description of phenomenon and outline of analytical treatment.	37
	4.2	Theoretical model spray.	41
	4.3	Basic equations.	45
	4.4	Development of hypothetical instantaneous temperature and pressure drop formulae.	47
	4.4.1	Case I. Fuel vapour is considered an ideal gas.	51
	4.4.2	Case II. Fuel vapour considered as a non-ideal gas.	57

4.4.3 Sample calculation of the difference between ideal and non-ideal instantaneous pressure decrease for ethyl alcohol. 63
4.5 Determination of the liquid fuel mass existing in the evaporation chamber during injection. 65
4.6 Conditions during injection and lifetime of spray. 71
4.6.1 Case I. Fuel vapour is considered an ideal gas. 73
4.6.2 Case II. Fuel vapour is considered a non-ideal gas. 83
4.7 Conditions during the transient period. 90
4.7.1 Case I. Fuel vapour is considered an ideal gas. 92
4.7.2 Case II. Fuel vapour is considered a non-ideal gas. 101
4.8 Warm-up period.
4.8.1 Case I. Fuel vapour is considered an ideal gas. 106
4.8.2 Case II. Fuel vapour is considered an non-ideal gas. 107

V SPRAY EVAPORATION - EXPERIMENTAL STUDY, METHODS AND APPARATUS 110

5.1 Description of phenomenon and outline of study. 110
5.2 Experimental details. 113
5.3 Description of apparatus. 116
5.4 Instrumentation and calibration of instruments. 121
5.5 Experimental procedure. 125

VI EXPERIMENTAL RESULTS - EVALUATION AND DISCUSSIONS 130

6.1 Experimental parameters. 130

6.2 Experimental data. 131

6.3 Evaluation of data and analysis of results. 134

6.4 Discussions. 142

6.5 Conclusions. 148

REFERENCES

APPENDICES

A. ETHYL ALCOHOL PRESSURE vs. ENTHALPY GRAPH.

B. FIGURES AND GRAPHS OF EXPERIMENTAL APPARATUS AND INSTRUMENT CALIBRATIONS.

C. PHOTOGRAPHIC RECORDINGS.

D. SAMPLE EVALUATION OF EXPERIMENTAL DATA IDEAL GAS EXPRESSIONS.

E. SAMPLE EVALUATION OF EXPERIMENTAL DATA NON-IDEAL GAS EXPRESSIONS.

F. LIFETIME OF ETHYL ALCOHOL SPRAYS AT VARIOUS INITIAL EVAPORATION CHAMBER TEMPERATURES AND PRESSURES.

G. SELECTED PHYSICAL PROPERTIES OF ETHYL ALCOHOL.

H. EXPERIMENTAL PARAMETER COMBINATIONS AND LIFETIME OF SPRAYS.

ABSTRACT

A PHENOMENOLOGICAL EXPERIMENTAL METHOD FOR THE INVESTIGATION OF FUEL SPRAY EVAPORATION

In this study, a new concept for the investigation of fuel spray evaporation from a phenomenological approach is introduced. This concept is based upon the physically observed fact that when a liquid spray evaporates in a closed high temperature environment, the heat for evaporation is taken solely from the environment. The total amount of heat transferred to the fuel at any time is governed by the characteristics of the spray, and the heat and mass transfer processes of the system. This heat also controls the amount of fuel evaporated, and the states of the fuel and its vapour at that time. These in turn are functions of certain physical and thermodynamic properties of the fuel. Therefore, if the total heat loss of the environment can be measured, the amount of fuel evaporated can be estimated. From this, some spray evaporation characteristics may be predicted. Based on this concept, an experimental method is devised. This approach then offers an alternative to the existing mechanistic approach.

The technique involves injecting a predetermined mass of liquid fuel into an evaporation chamber at constant rate and measuring the pressure decrease and the amount of injected fuel as functions of time. From these data, and provided that certain thermodynamic and physical properties of the fuel are known, two important characteristics of the spray

can then be calculated. These are:

a). The lifetime of the spray, which is an average lifetime of all droplets in the spray, and

b). The fraction of environmental gas cooled by the mixing of the fuel vapour and the surrounding gas.

The present technique has many advantages. Most significant of all is that it can be applied over any pressure range as long as a quadratic law of droplet evaporation holds true. Data on latent heat of evaporation near the thermodynamic critical point of the fuel, on diffusion coefficient, and on vapour pressure of the fuel at pressures equal to or above the critical pressure which were necessary in all previous theoretical studies, are no longer required. The present technique also serves to integrate automatically all the governing parameters of spray evaporation.

Even when there are no available physical and thermodynamic properties of the fuel, this technique can still be used to compare different injector nozzle designs for identical operating conditions.

To verify this concept and the experimental method, a total of five series of spray evaporation experiments were carried out with three different injector-plates.

Nomenclature

$$a = \left[\left(\frac{\partial e_2(T,P)}{\partial T}\right)_P - \left(\frac{\partial e_2(T,1)}{\partial T}\right)_P\right]$$

$a_{10} = -\kappa$
$a_{11} = \beta_n + \zeta - \kappa\zeta$ } equation (4-78)

a_c a constant

$$b = \left(\frac{\partial e_2(T,P)}{\partial P}\right)_T$$

$b_{10} = \kappa$
$b_{11} = \gamma_n + \kappa\zeta$
$b_{12} = \zeta\mu$ } equation (4-78)

b_c a constant

$$B_i = [m_1 c_{v_1} + m_{2f} (\bar{c}_{P_2} - \frac{R}{M_2})]/HS$$

$$B_n = \frac{m_1 c_{v_1} + m_{2f} (\gamma_n + \zeta + \zeta\chi_f\mu)}{HS}$$

c Specific heat

C Integration constant

D Diffusion coefficient

e Specific internal energy

f Wind factor

$$f_{11}(u) = \varepsilon_i \frac{u + 5\sigma_i u^4}{1-\varepsilon_i\sigma_i u^5} \approx \varepsilon_i(u + 5\sigma_i u^4) + \varepsilon_i^2(\sigma_i u^6 + 5\sigma_i^2 u^9)$$

$$f_{12}(u) = \varepsilon_i \frac{u - 5\tau_i u^4}{1 - \varepsilon_i \sigma_i u^5} \approx \varepsilon_i(u-5\tau_i u^4) + \varepsilon_i^2(\sigma_i u^6 - 5\sigma_i \tau_i u^9)$$

G	Vapour concentration
h	Specific enthalpy
H	Overall heat transfer coefficient

$$K = \frac{m_1 HS}{\dot{m}_2^2 c_{v_1}} \frac{(\beta_i+\gamma_i)}{\kappa(\beta_i+\gamma_i-\mu)}$$

$$K_c = 2\Pi DMP_{r_d}/RT$$

L	Latent heat of evaporation
m	Mass
$\dot{m}$	Mass injection rate
M	Molecular weight
n_c	Distribution constant in Rosin - Rammler law.
P	Pressure
P_c	Constant
q	Heat supplied
q_c	Constant
r	Liquid droplet radius
r_{si}	Radius of the sphere of influence
R	Universal gas constant
S	Evaporation chamber inside surface area
t	Time
t'	Age of liquid droplet
T	Temperature

$u = \sqrt{1-t'/t_L}$, Equation (4-90)

v Specific volume

V Volume of evaporation chamber

$\vec{V}$ Velocity vector

$\underline{x} = \chi-\lambda$ Integration variable

r, θ, ϕ Spherical polar co-ordinate

GREEK LETTERS

$\alpha = HS/2\dot{m}_2 C_{v_1}$

$\alpha'' = \frac{\lambda\zeta\mu}{20\alpha}$

$\beta_i = \frac{1}{C_{v_1} T_o} [L_2 + \int_{T_{2,0}}^{T_S} C_2 dT + \int_{T_S}^{T_o} C_{p_2} dT - \overline{C}_{p_2} T_o]$, Dimensionless constant.

$\beta_n = \beta_i + \frac{[e_2(T_o,P_o) - e_2(T_o,1)]}{C_{v_1} T_o} - \frac{[aT_o + bP_o]}{C_{v_1} T_o}$ Dimensionless Constant.

$\beta_n'' = \beta_n + \zeta(1-\kappa)$

$\gamma_i = \frac{\overline{C}_{p_2} - R/M_2}{C_{v_1}}$

$\gamma_n = \gamma_i + \frac{a}{C_{v_1}}$

$\gamma_n'' = \gamma_n + \zeta(\kappa+\chi_f\mu)$

δ Coefficient of volume expansion

δ_c Size constant in Rosin-Rammler law

δ_d Liquid droplet diameter

$$\varepsilon_i = \frac{10\lambda\alpha}{\kappa+\chi_f\gamma_i}$$

$$\varepsilon_n = \frac{10\lambda^*\alpha}{1+\chi_f\gamma_n''}$$

$$\zeta = \frac{bP_o}{C_{v_1}T_o}$$

$$\zeta'' = \zeta\lambda\mu$$

η Dimensionless constant

$\kappa = \chi/\chi' = m_1'/m_1$, vapour spread coefficient

$\lambda = 0.4\ \dot{m}_2 t_L/m_1$

$$\lambda'' = -(P-P_i)/\frac{dP}{d\chi}$$

$\lambda^* = \lambda/\kappa$

$\mu = M_1/M_2$

$$\sigma_i = 0.1\ \frac{\gamma_i}{\alpha}$$

$$\sigma_n = 0.1\ \frac{\gamma_n''}{\alpha}$$

$$\tau_i = 0.1\ \frac{\beta_i}{\alpha}$$

$$\tau_n = 0.1\ \frac{\beta_n''}{\alpha}$$

$\phi'' = \gamma_n + \beta_n + \zeta - \mu$

$$\chi = \frac{m_2}{m_1}$$

ρ	Density

$$\chi' = \frac{m_2'}{m_1}$$

$$\chi_f = \frac{m_{2f}}{m_1}$$

$$\omega_i = 0.1\ (\gamma_i - \mu)\kappa/\alpha(\kappa+\mu\chi_f)$$

Superscripts

$'$	Conditions when only a fraction of the inert gas inside the evaporation chamber is cooled.
$-$	Average
(ℓ)	Liquid state

Subscripts

0	Initial condition
1	Inert gas
2	Fuel
at	Atmospheric condition
c	Constant
d	Liquid droplet
e	End of evaporation of drops
f	Total amount of fuel
i	Ideal gas
L	Life of droplet
m	Value corresponding to minimum pressure
n	Non-ideal gas
p	Constant pressure

r	Reference point
r_d	Droplet surface
s	Normal boiling point of fuel
sp	Spray
v	Constant volume

Symbols

Δ	Finite change
∞	At infinite distance
$\rightarrow$	Approaches

Chapter 1

Introduction

In modern liquid fuel internal combustion engines, one of the components which requires considerable attention is the combustion chamber. Normally, a combustion chamber is designed to give high combustion efficiency and intensity, long service life and freedom from deposits and pollutant emissions. An essential prerequisite to achieve these ends is good fuel injection, atomization and mixing, since it is well known that these physical processes are the limiting factors. Also, it is often necessary to operate these engines at pressures well in excess of the critical pressure of the fuel. In recognition of these facts, many investigators have devoted much effort to the study of fundamental liquid fuel combustion mechanisms at low and high pressures. However the application of the results obtained for single droplets to obtain the characteristics of the combustion of sprays is not an easy matter and remains an outstanding problem fundamental to spray combustion research.

The function of an injector is to introduce and to meter the flow of fuel or fuels to the combustion chamber. It also serves to atomize and to mix the fuel and oxidizer in such a manner that a correctly proportioned mixture will result. A standard procedure employed in the evaluation of injector performance is full scale

testing, an expensive yet necessary proposition at the present.

Usually, the fuel is introduced into the combustion chamber in the form of a spray. The physical processes which take place when a spray is formed are evaporation of fuel and mixing of fuel vapour with the surrounding gaseous mixture. Both of these are highly dependent on injector performance.

Spray evaporation is an extremely complicated process. It involves such phenomena as fuel atomization, droplet motion, evaporation of moving droplets, droplet size and spatial distribution, and interference between droplets. Each of these phenomena in turn is dependent on one or more of three groups of controlling factors. These are:

a). Mechanical - the type and physical dimensions of the atomizer.

b). Operational - the conditions of operation such as injection pressure differential, temperature and pressure.

c). Fuel - the physical properties such as heat of vaporization, specific heat, viscosity, surface tension and density of the fuel.

Many investigators have treated spray evaporation theoretically and experimentally. In general, their

analytical methods consist of applying the single droplet evaporation empirical relation and integrating with an assumed drop size distribution function. In so doing, it is assumed that the semi-empirical relations obtained from single droplet studies are valid for the evaporation of individual droplets of varying size which constitute the ensemble of the spray. These analytical methods do not take into consideration influencing factors such as:

a). Single droplet evaporation experiments normally employ a much larger droplet than those normally encountered in a spray and results obtained from these studies may be of questionable applicability to the analysis of the spray.

b). The size distribution and droplet spatial distribution change with time, and are not accounted for in any existing theory.

c). The role of boundary layer transport under conditions of motion whereby forced convection effects become predominant.

d). The influence of surface deformation on the rate of evaporation.

e). Interference between neighboring drops during evaporation.

In addition, many of the assumptions in the single droplet evaporation analysis, even though valid at low and moderate pressure ranges, fail to remain valid at pressures equal to and above the critical pressure of the fuel. At this high pressure level, coupled with high surrounding temperature, the surface tension of the liquid can become very low. This can lead to substantial departures from the assumed spherical shape and furthermore can lead to droplet shattering. It is also difficult to determine the latent heat of vaporization, the diffusion coefficient, and the vapour pressure of the fuel under these conditions.

In view of these many uncertainties, and the unmanageable task of setting up the differential equations to take into account all the governing parameters of spray evaporation, the best approach seems to be experimental.

The present study introduces a new concept for the investigation of spray evaporation from a phenomenological approach. This concept is based on observed physical phenomena of spray evaopration in a high temperature environment and the relationship between the evaporated fuel mass and the heat transfer within a closed system. To verify the validity of this concept, an experiment method is devised for spray evaporation studies. The results so obtained would be significant advantage in injector design considerations. The present method has many advantages. Most significant of all is that it can be applied over any pressure range as long as a quadratic

law* of droplet evaporation holds true. It has been found that the quadratic law holds true except in extremely high pressures, i.e. at pressures several times that of the critical pressure of the fuel. Also, by making use of the fact that the thermodynamic properties are point functions and by conveniently choosing the various processes between the initial and final states of the fuel under investigation, it is possible to eliminate the use of the latent heat of evaporation near to the critical point of the fuel. Data on diffusion coefficient and vapour pressure of the fuel at pressures equal to or above the critical pressures are also no longer required.

The major feature of the present technique is that it serves as an automatic integrator of all the governing parameters of spray evaporation. The input to this integrator is a known mass of liquid fuel injected in the form of a conical spray. This input is then combined automatically with all the influencing factors to give certain data which can simply be transformed into two important characteristics of the spray. These are:

a). The lifetime of the spray, which is an average lifetime of all droplets in the spray, and

---

*d^2-law of droplet evaporation states that the drop surface area changes linearly with time during evaporation.

b). The fraction of environmental gas cooled by the mixing of the fuel vapour and the surrounding gas. This provides information on both the spread of the spray and the mixing of the gases.

Since these are important characteristics in spray combustion, application of this technique should furnish valuable information on combustion chamber and fuel injector designs.

The technique involves injecting at constant rate a predetermined mass of liquid fuel into an evaporation chamber and monitoring the pressure decrease and the amount of injected fuel as functions of time. Both of these are dependent on the physical properties of the fuel, of the inert gas and the operating conditions. Corresponding to any injected mass of fuel, there is a maximum pressure decrease which would occur if the gas and fuel vapour mixture is perfectly insulated from the evaporation chamber. This is true regardless of the time period which would be required for complete evaporation. However, in order to provide a standard reference time and pressure, the fuel is assumed to evaporate instantaneously and to produce a maximum pressure decrease in the evaporation chamber. This pressure decrease, resulting from an idealized process, will be referred to as a hypothetical instantaneous pressure decrease so as to eliminate the probable confusion with the ideal gas treatments in the present study. It is

obvious that this hypothetical pressure decrease can only be achieved experimentally at some later time, since fuel evaporation cannot occur instantaneously. The difference between this time and the time at which the same pressure would be obtained if evaporation were instantaneous is termed the Evaporation Lag. In other words, the actual spray evaporation process is lagging behind the idealized process by an amount which is called the Evaporation Lag.

From the Evaporation Lag, the lifetime of a spray and the spread coefficient can be calculated if certain physical and thermodynamic properties of the fuel are known. The spread coefficient is defined here as the fraction of environmental gas which is cooled by spray evaporation.

Even when physical and thermodynamic properties of the fuel are not available, this technique can still be used to compare different nozzle designs. In this case, a more efficient nozzle will give a faster rate of pressure drop under identical operating conditions.

In Chapter II, a review of theoretical studies on spray evaporation and related phenomena is given. Chapter III contains the review of experimental studies on the same phenomena. Theoretical analysis of the present study is given in Chapter IV. The corresponding experimental technique and apparatus are reported in Chapter V. Chapter VI is devoted entirely to the evaluation and discussion of the present experimental technique and results

of the ethyl alcohol and water spray evaporation experiments.

The present investigation is one of several projects on liquid-fuel rocket-engine research at the National Research Council of Canada.

Chapter II

Literature Survey - Theoretical Studies

Since all available studies on spray evaporation are based upon the single droplet evaporation treatment, it is necessary to review certain analytical solutions for the single droplet evaporation problem. The main requirements of any theoretical treatment of droplet evaporation is that it gives an insight into the dependence of evaporation on the physical processes that occur. It must also be in agreement with the experimental results. These criteria have been met by a number of theoretical analyses.

The procedure of discussion in this chapter will be as follows. First, single droplet evaporation treatments will be reviewed. This is followed by a brief discussion of the physical properties of sprays. Finally, a literature survey on spray evaporation is given.

2.1 Single droplet evaporation - At low and moderate pressures

The most fundamental process in spray evaporation is the evaporation of the individual drops comprising the spray. Because the general phenomenon is one of heat and mass transfer, the rate of evaporation can be calculated from either the rate of mass transfer or the rate of heat transfer approach.

The usual simplifying assumptions in the derivation of the fundamental equation for the evaporation rate are:

1). The drop is spherical.

2). The droplet is considered to be a single, pure component.

3). The surrounding atmosphere extends unbounded in all directions.

4). The atmosphere is at uniform temperature and pressure. The change of droplet temperature is neglected.

5). The evaporation process is quasi-steady.

6). The vapour is saturated on the surface of the drop.

7). The vapour pressure of the drop is small in comparison with the total pressure.

8). There are no convection effects.

2.1.1 Evaporation rate from the rate of mass transfer approach.

The theory of the evaporation process in a gas environment owes its origins to Maxwell (ref. 2-1) and Stefan (ref. 2-2). Their theory is based on the assumption that the vapour in the immediate surrounding of the liquid droplet surface is completely saturated, and that consequently the evaporation rate depends only on the velocity of diffusion of the vapour into the surrounding space. In its most general form, the diffusion equation may be written:

$$\text{div}(D \text{ grad } G) = \frac{\partial G}{\partial t} + \vec{v} \cdot \text{grad } G \qquad (2\text{-}1)$$

where D is the diffusion coefficient, G the concentration of vapour in gas phase, and $\vec{v}$ is the velocity vector. Equation (2-1) when applied to a droplet can be expressed in spherical polar co-ordinates as:

$$D\left[\frac{\partial^2 G}{\partial r^2} + \frac{2}{r}\frac{\partial G}{\partial r} + \frac{1}{r^2 \sin\theta}\frac{\partial}{\partial \theta}\left(\sin\theta \frac{\partial G}{\partial \theta}\right) + \frac{1}{r^2 \sin^2\theta}\frac{\partial^2 G}{\partial \theta^2}\right] \qquad (2\text{-}2)$$

$$= \frac{\partial G}{\partial t} + V_r \frac{\partial G}{\partial r} + \frac{V_\theta}{r}\frac{\partial G}{\partial \theta} + \frac{V_\theta}{r \sin\theta}\frac{\partial G}{\partial \phi}$$

The vapour concentration distribution is obtained by solving equation (2-2). Because the size of the droplet changes continuously, equation (2-2) is subjected to the existence of a free boundary. This introduces a non-linearity into the equation and consequently, only a few

exact solutions are known.

The case of a single, stationary, isolated drop was solved by Fuchs (ref. 2-3). He discarded the time dependence of the vapour distribution by introducing the concept of a stagnant boundary layer surrounding the drop. The convective terms in the diffusion equation, equation (2-2), were also neglected in evaluating the diffusive flux. This gives the quasi-steady theory of droplet evaporation.

The droplet evaporation rate obtained by Fuchs is

$$-\frac{dm}{dt} = 4\pi D r_d M(G_{r_d} - G_\infty) \qquad (2-3)$$

where dm/dt is the evaporation rate in mass per unit time, "r_d" the drop radius, M the molecular weight, G_∞ the vapour concentration in moles per unit volume at $r \to \infty$, and G_{r_d} the vapour concentration at the drop surface. Fuchs also examined the simplifying assumptions one by one and corresponding corrections were introduced into equation (2-3).

The case of a moving drop was investigated by Frössling (ref. 2-4). The evaporation rate of a droplet in an air stream obtained by Frössling is given by the semi-empirical formula:

$$-\frac{dm}{dt} = 4\pi D r_d M(G_{r_d} - G_\infty) f \qquad (2-4)$$

where all the terms are the same as in equation (2-3). The factor "f" is the wind-factor which was determined

experimentally. Nearly all of the subsequent works in spray evaporations are, in part, based upon Frössling's original analysis.

2.1.2 Evaporation rate from the rate of heat transfer approach

Ranz (ref. 2-5) analyzed the evaporation of a drop of volatile liquid in high-temperature surroundings in terms of the rate of heat transfer. This approach was followed because the rate of heat transfer is better understood and values of thermal conductivity are more readily available than values of diffusivity. The only drawback of this method is that the droplet surface temperature must be known. Usually, for surroundings with temperatures several hundred degrees above the boiling point, the surface temperature is taken as very nearly the boiling point. Also, since a dynamic balance exists between the rate of heat transfer and the rate of mass transfer, the calculation of evaporation rate from this approach requires some knowledge of the rate of mass transfer.

Both analytical approaches gave an evaporation rate proportional to the diameter of the evaporating drop and hence the drop surface area changes linearly with time. The latter is generally known as the quadratic or "d^2" law of single droplet evaporation. These analyses have been found to be satisfactory at low and moderate pressures. However, it was pointed out by Kirkaldy (ref. 2-6) that the operation of neglecting the time dependence in the derivation of the evaporation rate from the quasi-steady theory is mathematically untenable.

2.2 Single droplet evaporation - At pressures near to or above the critical pressure of the liquid fuel

Weiber (ref. 2-7) applied the heat transfer rate approach of the low pressure quasi-steady evaporation model in his study. He calculated the steady-state temperatures and temperature, mass, and trajectory histories of heptane and oxygen droplets in high-pressure and high-temperature environments. In this case, steady state implies that all the energy arriving at the droplet is carried away entirely by the mass transfer. Weiber found that at sufficiently high pressure, both heptane and oxygen droplets would be heated up to their respective critical temperatures. He stated that above critical conditions, mass transfer from these droplets cannot be calculated because of the lack of theory for this region. He suggested that his finding sets an upper limit to the applicable regime of the present low-pressure vaporization theory. However, no consideration was given to the non-ideal effects which are encountered at high pressures in this study. Weiber also neglected the effects of pressure on the physical properties of the substances.

Manrique and Borman (ref. 2-8) calculated the steady state droplet evaporation in the region of its thermodynamic critical point. They took into consideration the effects of non-ideal mixtures, solubility of the ambient gas in the liquid drop, variation of the physical properties due to difference in vapour concentration, the effect of total pressure on vapour pressure, and the non-ideality of

the latent heat of vaporization. They found that there is a linear relationship between the steady-state vaporization time and the square of the droplet radius.

Brzustowski (ref. 2-9) discussed the applicability of the quasi-steady droplet theory. He stated that the evaporation kinetics would become the limiting factor in droplet combustion whenever the maximum diffusion rate exceeds the maximum evaporation rate. In such a case, the quasi-steady droplet theory becomes invalid. Brzustowski also pointed out that when the difference in density between vapour and liquid phases of a fuel is no longer large, the liquid surface regression velocity and the storage of mass in the vapour phase can not be neglected. This, therefore, rendered invalid the quasi-steady droplet theory at high pressures. A pressure of 1/10 of the critical pressure of the fuel was suggested to be the upper limit for the quasi-steady droplet theory in describing droplet combustion.

Kotake and Okazaki (ref. 2-10) treated the droplet evaporation process as an unsteady diffusion-controlled phenomenon. Their results indicated that during the process, both mass and heat transfer at the droplet surface can not reach a quasi-steady state. However, they did not take into consideration the variable physical properties of the fuel in their calculation and their findings have yet to be verified experimentally.

2.3 Physical properties of sprays

These properties will be briefly reviewed.

a). Atomization (ref. 2-11) - Very briefly, atomization generally takes place in three steps; (i) the initial disturbance of the surface of the jet of liquid, (ii), the formation of ligaments which then break up into fragments, and (iii) the further breakup of the fragments into smaller droplets. The problem of determining theoretically the form of disturbance that most rapidly leads to jet instability has been solved for several typical cases. For the impinging nozzles, a mathematical treatment would be very difficult due to the complexity of the spray. The nozzle used in the present study is of this type.

b). Droplet size distribution (ref. 2-11) - The most important factors that influence drop size are (i) nozzle design, (ii), operating conditions, especially pressure, (iii) the properties of the liquid and of the gas into which the fuel is injected, and (iv), the relative velocity between the liquid and the gas. In general, sprays consist of dispersed drops of a range of sizes. The relative abundances of the various sizes of drops varies over the range. A number of useful mathematical expressions describing the size distribution of a spray have the same general form:

$$\frac{dN}{d\delta_d} = a_c \delta_d^{p_c} \exp(-b_c \delta_d^{q_c}) \qquad (2\text{-}5)$$

where N is the cumulative number of droplets having diameters less than a given size δ_d, and a_c, b_c, p_c, q_c are independent constants. Among these mathematical expressions, the more important are:

(i). the Rosin-Rammler equation which is useful for sprays produced by vortex-type atomizing nozzles,

(ii). the Nukiyama - Tanasawa expression which is most useful for air atomization, and

(iii). the logarithmico - normal equation which is useful for impinging jet types of atomizers.

It has been found that the above three equations can correlate the results for a large number of different types of atomizers. However, because they are not based on any fundamental theoretical analysis, their usefulness depends largely on the excellence of fitting the experimental results.

c). Spray mass distribution (ref. 2-11) - Most nozzles develop a spray which is closely conical in shape. However, depending upon the nozzle design, the concentration of drops in the radial direction can be changed. The concentration of drops may be a maximum along the axis of the nozzle and gradually decrease to zero at the edge of the conical surface. Another distribution is that the concentration along the nozzle axis is at a value lower than the maximum and rises to a maximum at some distance from the

nozzle axis, and then falls to zero at the conical surface.

d). Spray angle - In the case of conical sprays, the spray angle is defined as that total included angle which takes in some specific fraction of the total mass in the spray. The specific fraction is chosen arbitrarily.

e). Drop velocity - The velocity of the drops in the entire spray has not been measured. However, based on some short time droplet velocity measurements in certain parts of the spray, it is correct to assume that there is a distribution of velocities among the drops. It is also safe to assume that the velocity of any single drop changes with time as the drop evaporates.

2.4 Spray evaporation

Available spray evaporation literature can be divided into four main groups according to practical applications. Only those studies which are related to internal combustion engines will be considered here. It is found that the general theoretical approach in treating spray evaporation problems is to integrate the available single droplet evaporation rate equation over an assumed drop-size distribution relation for a spray to obtain the total evaporation rate. Therefore, in the light of the existing evaporation theory for individual drops in motion, it is not surprising that any analytical solution on spray evaporation rate would be, at best, an approximation. It is also unfortunate that, in order to utilize the semi-empirical relations for the evaporation of the individual drops, numerous doubtful assumptions were made in order to circumvent certain mathematical difficulties which were encountered in analyzing the spray.

The earliest theoretical study on spray evaporation was done by Probert (ref. 2-12). The problem was examined using the Rosin-Rammler relation for size distribution in a spray and an experimental law concerning the effect of size on the evaporation of single droplets. He studied the effects of size and distribution on the evaporation rate of a spray. One of his assumptions was that the single drop evaporates at a rate proportional to its diameter.

Sacks (ref. 2-13) calculated theoretically the rate of spray evaporation. By assuming that the spray obeys the Rosin-Rammler distribution law, he integrated the evaporation rate for individual drops over this distribution to obtain the evaporation rate for the spray.

For a single droplet in still air, assuming that $G_\infty = 0$ and $G_{r_d} = P_{r_d}/RT$, the evaporation rate of a droplet in still air at atmospheric pressure is given by the Langmuir expression

$$-\frac{dm}{dt} = 2\pi D\delta_d M \frac{P_{r_d}}{RT} \tag{2-6}$$

At constant pressure and temperature, equation (2-6) becomes

$$-\frac{dm}{dt} = K_c\delta_d \tag{2-7}$$

where $K_c = 2\pi DMP_{r_d}/RT$ is a constant of evaporation. If δ_d is in microns, the number of droplets having diameters between δ_d and $\delta_d + d\delta_d$ per cubic centimeter is, according to the Rosin-Rammler distribution

$$Nd\delta_d = \frac{dV}{\frac{\pi\delta_d^3}{6}} = \frac{6\times10^{12}}{\pi} n_c \frac{\delta_d^{n_c-4}}{\delta_c^{n_c}} e^{-\left(\frac{\delta_d}{\delta_c}\right)^{n_c}} d\delta_d \tag{2-8}$$

where n_c is the distribution constant in Rosin-Rammler law. Therefore, for a spray, the evaporation rate is given by:

$$-\left.\frac{dm}{dt}\right)_{sp.} = \int_o^\infty K_c N \delta_d d\delta_d \qquad (2\text{-}9)$$

$$= \frac{6\times10^{12}}{\pi\delta_c^{\,n_c}} K_c \int_o^\infty n_c \delta_d^{\,n_c-3} e^{-\left(\frac{\delta_d}{\delta_c}\right)^{n_c}} d\delta_d$$

Transforming to the gamma function, equation (2-9) becomes

$$-\frac{dm}{dt} = \frac{12\times10^{12}}{\delta_c^{\,2}} \frac{DMP}{RT} r_d \Gamma\left(1 - \frac{2}{n_c}\right) \qquad (2\text{-}10)$$

The calculated result was found to be 100 times greater than the experimentally determined evaporation rate. This difference is introduced mainly through the usage of inaccurate values of the diffusion coefficient and vapour pressure in equation (2-10).

By applying the Frössling single droplet evaporation rate equation to the unidirectional spray, Fledderman and Hanson (ref. 2-14) attempted to develop an equation for predicting the total evaporation rate of a spray. The Nukiyama-Tanasawa relation was used to describe the drop size distribution of the spray.

Benson (ref. 2-15) proposed a method for predicting the rate of evaporation of a spray in which the mutual effects of adjacent drops are important. This theoretical study appeared to be the first to take into consideration the effects of adjacent drops. However, the assumption that the drop size variation during evaporation is small, makes

the analysis applicable only to low volatility fuels. His method is to define a sphere of influence associated with each drop. This surface is defined by the condition that the net flux of vapour is zero. The problem then reduces to the solution of

$$\frac{\partial G}{\partial t} = \frac{D}{r^2} \frac{\partial}{\partial r} \left(r^2 \frac{\partial G}{\partial r}\right) \qquad (2\text{-}11)$$

for a single droplet and subject to the boundary conditions

$$G = G_{r_d} \quad \text{at} \quad r = r_d \quad \text{when} \quad t \geq 0 \qquad (2\text{-}12a)$$

$$G = 0 \quad \text{at} \quad r > r_d \quad \text{when} \quad t = 0 \qquad (2\text{-}12b)$$

$$\frac{\partial G}{\partial r} = 0 \quad \text{at} \quad r = r_{si} \quad \text{when} \quad t \geq 0 \qquad (2\text{-}12c)$$

where r_{si} is the radius of the sphere of influence. From the single droplet evaporation rate, a semi-empirical expression was derived to describe the evaporation rate of the spray.

Hoffman and Gauvin (refs. 2-16, 2-17, 2-18) studied spray evaporation in a high temperature environment. Their investigation is in three parts. The first part deals with radiant heat transfer to clouds of droplets and particles. The difficulties inherent in the calculation of the absorption of thermal radiation by clouds of particles suspended in an absorbing gas medium was discussed. The method of formulating radiation configuration factors for a cylindrical column containing an absorbing medium was

presented and some of these configuration factors have been calculated for their particular experimental equipment. Part two deals with the calculation of the evaporative load distribution in a spray of droplets suspended in an absorbing gas medium contained in a cylindrical column after a temperature profile for the gas has been assumed. Their calculated results emphasize the importance of the physical characteristics of the spray, such as initial drop size and distribution, drop velocities and spray angle. Part three deals with the method of calculating the heat flux distribution along the hot walls of a vertical cylindrical column containing a suspension of evaporating droplets in an absorbing atmosphere flowing downward.

Dickinson and Marshall Jr. (ref. 2-19) developed the mathematical equations for the evaporation of sprays with non-uniform drop size distribution. The problem was divided into two cases. Case I dealt with sprays which have sufficiently low relative velocities, so that the rate of evaporation corresponded to zero velocity conditions. Case II dealt with sprays which have appreciable relative velocity. The heat transfer rate approach was used to calculate the rate of evaporation of a single drop. To obtain the evaporation rate of sprays, four types of drop size distribution were considered. These are: (i) Log-normal, (ii) Square-root normal, (iii) Rosin-Rammler, and (iv) Nukiyama-Tanasawa relations for drop size distributions.

In summary, all theoretical developments of the spray evaporation problem can be criticized on a multiplicity of points. The principal objection is that dynamic spray evaporation is either treated from (i) the standpoint of the behavior of some average droplet in the ensemble, following an empirical evaporation law for a moving droplet, or (ii) from a consideration of the entire drop ensemble following the Maxwellian evaporation law for a static drop. Except in Benson's work, the evaporation of individual drops has been considered as taking place in an infinite medium, thus neglecting the mutual influence of neighboring drops. Another objection is the use of the various drop-size distribution relations which are assumed to be valid throughout the life-time of the spray. This is certainly not the case since the evaporation rates of the drops change with time and the drop-size distribution in the spray also changes.

It would appear that much experimental work on spray evaporations is needed, before any radical development can be made in the theory of spray evaporation in combustion chambers.

Chapter III

Literature Survey - Experimental Studies

To obtain a full understanding of the spray evaporation process, it is necessary to have complete knowledge of the mechanism of evaporation of the individual droplets that make up the spray. It is therefore appropriate to briefly survey experimental studies on single droplet evaporation before reviewing spray evaporation studies.

3.1 Single droplet evaporation studies

Nearly all measurements of droplet evaporation in a moving gas stream were carried out on droplets which were suspended from filaments. This technique appears to be due to Frössling (ref. 2-4) and has been adopted by most other workers. The method involves picking up a liquid drop and suspending it on the end of the filament. This is then placed in the air stream which is maintained at a fixed temperature and linear velocity. The change of the drop diameter as function of time is obtained from successive photographs of the drop. The droplet evaporation rate is calculated from these data.

Frössling pointed out the principal sources of error which arise in connection with his method. Since these errors apply generally to all such single droplet evaporation studies, they will be listed below:

a). Deviation from spherical shape - Appreciable distortion occurs only to comparatively large drops.

b). Compressibility of the surrounding gas. - For flows over a sphere, the radially dependent pressure variations are of the order of magnitude of the dynamic pressure. Only in the range of low velocities may the compressibility of the gas stream be neglected at the leading point of a small

evaporating droplet.

c). Effect of Turbulence - At low intensities of stream turbulence, the effect of turbulence on droplet evaporation of small drops is negligible.

Other sources of error include transient condition of evaporation, assumption of saturated vapour pressure at the drop surface, and the deviation of the vapour from the Ideal-Gas Law.

Frössling's measurements were obtained from evaporating drops of nitrobenzene, aniline, water and naphthalene in an air stream maintained at an ambient temperature of 20°C. The time rate of change of d^2 was shown to be directly proportional to the square root of the stream Reynold's number.

Bradley et al. (ref. 3-1) studied the droplet evaporation rate at low pressures by means of a microbalance. Their experimental data verified Fuch's theory on droplet evaporation at atmospheric pressure.

Ranz and Marshall Jr. (ref. 3-2) investigated the factors which influence the rate of evaporation of pure liquid drops. Their results confirmed the analogy between heat and mass transfer of droplet evaporation at low Reynold's numbers.

Hoffman and Gauvin (ref. 3-3) measured the evaporation rate of stationary droplets of water, methanol,

cumene, pentane and benzene in high temperature surroundings. Their results satisfied the d^2-law of droplet evaporation.

Priem et al. (ref. 3-4) measured temperature, mass and radius histories of small drops of different hydrocarbon fuels. They found that an appreciable portion of the drop may be vaporized during the "heating-up" period of droplet evaporation. They also showed that a quasi-steady film theory could accurately predict droplet histories at atmospheric pressure and a wide range of ambient temperature, air velocity, and droplet size.

Savery and Borman (ref. 3-5) measured the size and temperature histories of vaporizing n-heptane and Freon-13 droplets suspended in a hot air stream of pressures up to 100 atmospheres. The quasi-steady film theory, which was reported by Priem and co-workers, was modified and applied to high pressure evaporation studies. All their calculated size and temperature histories of droplet evaporation were found to agree with their experimental data within the estimated uncertainties.

3.2 Spray evaporation studies

Measurement of spray evaporation in a moving gas stream is difficult because it requires a rather complete knowledge of the drop-size distribution at several points along the air stream. An experimental technique is satisfactory only if it can measure the drop-size distribution without disturbing the flow. The earliest significant experimental work on spray evaporation is largely concerned with the ignition and combustion of liquid fuels in compression-ignition engines.

Wollers and Ehmcke (ref. 3-6), in connection with their work on diesel engines, studied spray evaporation on a variety of fuel oils. Their technique was to inject a fuel spray into a preheated bomb at relatively high pressures. The pressure-time and temperature data were then used to determine the spray evaporation rate. They concluded that ignition in the diesel engine does not require fuel vaporization. Unfortunately, this conclusion was misinterpreted by a number of other investigators, who concluded that not only did vaporization have no effect on the combustion process, but that ignition started in the liquid phase.

Rothrock and Waldron (ref. 3-7) used high-speed cinematography as a means of measuring the variation of fuel-spray vaporization with engine speed. They found that considerable vaporization of the injected spray

occurred between injection and combustion and that spray evaporation markedly influenced the rate of combustion in a high-speed compression-ignition engine.

Selden and Spencer (ref. 3-8) investigated the evaporation of fuel-oil sprays by injecting the fuel into a heated and pressurized bomb. Pressure change in the bomb was monitored. This study furnished considerable data concerning the initial heat exchange between the inert gas in the bomb and the fuel spray. However, the rate of evaporation can not be determined from this experimental data.

Godsave (ref. 3-9) in his study of fuel spray combustion concluded that spray evaporation was controlled by two distinct rate-determining mechanisms. At relatively low temperature, the evaporation is governed by diffusion. In this case, vapour pressure of the fuel is the predominant parameter. At elevated temperatures, heat transfer rate to the spray is the most important quantity.

Sacks (ref. 2-13) studied the evaporation rate of a kerosine spray which was produced by a pressure-jet atomizer operating at 50 and 80 psi fuel injection pressure. The ambient air had a temperature of 22°C and the pressure was approximately equal to the standard atmosphere. His experimental method consisted of passing a slow stream of air at a constant rate through a spray. The rate of evaporation was estimated by determining the concentration of fuel vapour in the air leaving the chamber.

Bahr (ref. 3-10) investigated experimentally the evaporation and spreading of isooctane sprays over a range of inlet-air conditions common in ram-jet engines. The distribution profiles were measured over the following ranges of variables: inlet-air temperature, 540°R to 850°R; inlet-air velocities, 100 to 350 feet per second; inlet-air static pressure, 18 to 35 inches of mercury absolute; fuel-injection pressure drop, 25 to 85 psi; diameter of fuel injector orifice, 0.024 to 0.041 inch; and axial distance from fuel injector, 5 to 18 inches. Empirical expressions were obtained which related the evaporation rate and the degree of spreading of the sprays to the experimental variables.

It was found that:

a). Evaporation rate increased with increasing air temperature. This was attributed to the greater heat transfer to the evaporating liquid drops.

b). Higher temperature decreased air density, thus allowed greater upstream penetration of the spray and longer residence time.

c). The degree of spray evaporation was found to increase with air velocity. This influence was probably the result of a combination of factors. Finer atomization of the injected fuel and higher heat

transfer coefficients between the air and droplets would be expected at the higher air velocities. These factors served to increase spray evaporation. However, greater air velocities would also be expected to decrease the residence time of the spray. Shedding of the vapour boundary layer of the drop is also a factor.

d). An increase in air pressure decreased the degree of spray evaporation. An increase in air density caused a shorter upstream penetration, thus shorter spray residence time.

e). Higher injection pressure produced finer spray and as a result, a higher evaporation rate.

f). The degree of spray evaporation was unaffected by changes in the diameter of the injection nozzle.

Ingebo (ref. 3-11) used a droplet camera to obtain drop-size distribution and drop-velocity data for isooctane sprays injected into a turbulent air stream. Evaporation rates and drag coefficients were calculated for isooctane drops accelerating and evaporating in air stream having velocities of 140 and 180 feet per second. The

evaporation rate of a drop was determined from the heat-transfer equation, and a semi-empirical expression for spray evaporation was obtained from this single droplet analysis.

Fledderman and Hanson (ref. 2-14) investigated the effect of turbulence and relative velocity upon the evaporation of a liquid fuel spray. A hollow-cone-spray, with the maximum mass distribution located away from the nozzle axis, was used. It was found that an increase in turbulence intensity increases the evaporation rate of the spray. They also concluded that the effect of turbulence did not appear to work through the Reynolds number but seemed to be due rather to an increase in the coefficient of diffusion.

Benson (ref. 3-12) measured the rate of evaporation of a spray in an air stream. His method is based on the cooling produced when a spray evaporates adiabatically. By measuring the air stream temperature at various downstream locations, the rate of evaporation was determined. The equipment works well when the air stream is at room temperature. However, when high temperatures and pressures are involved, this experimental technique would require very complicated equipment.

Sjenitzer (ref. 3-13) studied the evaporation of a liquid spray injected into a gas stream. In order to make the problem manageable mathematically, he assumed a uniform spray droplet size. The analysis is based on

Frössling's empirical formula for the evaporation of a spherical liquid droplet in a moving gas stream and Ingebo's expression for the instantaneous, unsteady-state drag coefficient of evaporating droplets.

Sandri and Wong (ref. 3-14) determined experimentally the average life time of sprays at high temperatures, and pressures. The method involves injecting liquid fuel, such as ethyl alcohol or n-pentane, into a closed chamber filled with nitrogen gas at high temperature and pressure. The evaporation of the liquid droplets in the chamber decreases the gas temperature and consequently causes a pressure decrease. Since the duration of the experiments is of the order of 100 milliseconds, the amount of heat transferred from the chamber wall to the gas is not appreciable. Thus, by measuring the pressure drop corresponding to the known amount of liquid fuel injected, the evaporation lag can be determined. The limitations of the apparatus were pointed out to be:

(1) The evaporation chamber was not large enough, and

(2) only liquid fuels that wet glass and metal surfaces well could be examined, because of the particular fuel injection quantity measuring method used.

Newman and Brzustowski (ref. 3-15) investigated the behaviour of liquid sprays at pressure and temperature

close to the critical properties of the injected liquid. The geometry of the spray was studied by photographic means. Data on the dynamic and thermal characteristics of the spray were also collected. Six different regimes of jet behaviour have been identified. The two-phase spray was treated analytically as a turbulent submerged jet. Conservation equations of mass, momentum, energy, and a modified jet propagation equation were solved to give the axial velocity, concentration and temperature difference decay rates.

The problem of spray evaporation under high temperature and low pressure conditions appears to have received considerably more attention from both theoretical and experimental standpoints. The reason for the lack of experimental data on spray evaporation under high temperature and high pressure conditions can be traced to the inherent difficulties associated with measuring spray evaporation under such conditions. It would appear that experimental techniques for studying spray evaporation at high pressure and high temperature are needed.

An extensive literature survey on sprays can be found in "Spray Literature Abstracts" by De Juhasz (ref. 3-16).

Chapter IV

Spray Evaporation - Analytical Study

4.1 Description of phenomenon and Outline of Analytical Treatment

When liquid fuel is sprayed through an injector into an enclosure filled with an inert gas at high temperature and pressure, heat transfer takes place between the droplets of the liquid spray and the surrounding gas. The ensuing evaporation of the droplets decreases the gas temperature and consequently causes a pressure drop within the enclosure. The pressure drop at any time after the beginning of injection will always be smaller than that which would occur if all the injected fuel were immediately vaporized. The condition that would be required for such instantaneous evaporation is that the heat transfer rate between the hot gas and the droplets in the spray be infinite. This of course cannot be achieved in practice. However, the theoretical pressure drop for this hypothetical case can be calculated and thence the Evaporation Lag, previously defined, can be determined. From the Evaporation Lag, the lifetime of the spray can then be calculated.

The object of this chapter is the derivation of an expression of the lifetime of a spray. In this analytical development, the following sequence of steps take place.

Section 4.2 contains the theoretical description of the spray, the formulation of the problem and the

justification of assumptions. Section 4.3 gives the basic equations. The ideal gas P-V-T relationship is used. In section 4.4.1, the basic equations are solved to give a total of four sets of expressions for the hypothetical instantaneous temperature and pressure decreases as functions of injected fuel mass to inert gas mass ratio, χ, or the mass ratio of the injected fuel to the cooled portion of the inert gas, χ'. Normally, the last set of expression will be used as the reference standard because it is the most general solution. The other three sets are special cases of the general solution. Therefore, a certain amount of repetition in the analytical treatment will be evident in this section. However, it was decided to present the analysis in this manner to show the theoretical development sequence of the present study. Consequently, in section 4.4.1, the most simplified special case, i.e. by treating the fuel vapour as an ideal gas during isothermal compression, is considered first. The specific internal energy of the fuel vapour remains constant during this process. Also, the entire inert gas mass is assumed to be cooled uniformly. When solutions of the basic equations were obtained, the next logical step for improving the solutions was taken. This is accomplished by assuming that only a portion of the inert gas in the evaporation chamber, i.e. the portion occupying the same volume as the spray and the fuel vapour, is cooled to a uniform temperature while the remaining

portion maintains its original temperature. This means that the continuous mixture temperature profile at any cross section is replaced by a rectangular curve. This curve has a discontinuity at the boundaries of the spray cone and a magnitude equivalent to the average temperature decrease within the spray cone. The governing equations again can be solved. In section 4.4.2, real vapour properties are considered in solving the basic equations to further improve the analysis. Changes in specific internal energy of the fuel vapour during isothermal compression is accounted for. Again, the entire inert gas mass was considered, in the first case, to have been cooled to a uniform temperature. In the second and most general case, only a portion of the inert gas mass is assumed to be cooled uniformly. A comparison of the hypothetical pressure decrease for ethyl alcohol between the ideal gas and non-ideal gas solutions is presented in section 4.4.3. In section 4.5, a formula which describes the liquid fuel mass existing in the evaporation chamber at any time during the fuel injection period is derived. This formula is used in the development of equations in the following sections and is valid for both ideal and non-ideal cases. In section 4.6, the conditions in the evaporation chamber during fuel injection are considered. The energy balance equation and the basic equations of section 4.3 are solved to give expressions for the actual temperature and pressure drop as functions of injected fuel mass and the

mixing characteristic, κ. From these expressions and those in section 4.4, the lifetime of a spray is derived (equation 4-69d for an ideal gas; equation 4-85 for a non-ideal gas). However, certain experimental information is required before this expression can be used. In the derivation, one has to introduce into the energy balance equation a certain heat transfer characteristic of the equipment. This heat transfer characteristic is unique for any given set of operating conditions and can not be determined theoretically. Therefore, experimental data must be used for an estimation of this characteristic. Section 4.7 results in relationships describing the end of liquid fuel evaporation. These are necessary in order to fix a reference time on the experimental data. The heat transfer characteristic of the equipment is then estimated from the experimental data beyond the reference time. Section 4.8 then contains equations for estimating the heat transfer characteristic of the equipment for the ideal gas and non-ideal gas cases.

With this additional information, the lifetime of the spray can be calculated.

4.2 Theoretical Model Spray

A theoretical analysis will be performed modelling the continuous liquid fuel injection and the subsequent breaking up and evaporation processes in a closed chamber at high temperature and pressure. The theoretical model spray is assumed to possess the following characteristics.

a). The liquid fuel mass injection rate is constant. In any real situation, the fuel injection rate varies from zero at time zero and increases to a constant value in a very short time. By keeping the initial transient period to less than 1% of the total fuel injection period, the constant mass injection rate assumption gives a good description of the actual phenomenon.

b). The initial droplet size is uniform and constant at formation. It has been pointed out by Giffin and Lamb (ref. 4-1) that both the fineness and uniformity of a liquid spray improve with increase in surrounding gas pressure. At 400 and 600 psi, the droplet diameter varies within a narrow range only. Therefore, the above assumption is a good approximation for this study. It also simplifies the mathematical treatment and description of the spray.

c). The mass evaporation rate of all droplets having the same size is the same. However, local conditions such as vapour concentration, droplet spatial distribution, will create some deviations. Nevertheless, the mathematical simplicity introduced by this assumption justifies its adoption in the present analysis.

d). The mass evaporation rate of the spray is constant over the entire fuel injection period and is the same as the mass injection rate. This assumption is valid except for a short initial transient period.

e). There is no wall effect. The surrounding is considered infinite.

f). The evaporation process of the spray is assumed to be quasi-steady. Since the temperature drop and consequently the pressure drop is kept small, this assumption should not introduce any significant error in the analysis. The initial transient behavior of the spray is not considered because it covers only a relatively short period.

For the analysis, the whole physical evaporation process is divided into five distinct periods. These are:

1). Before injection - A period up to the moment

of liquid fuel injection into the evaporation chamber, for which the state of both the liquid fuel and the inert gas are well defined.

2). Transient period of liquid fuel injection or liquid fuel build-up period - A relatively short period beginning at the instant of fuel injection and ending at the instant when the evaporation rate equals the injection rate. Droplet build-up terminates at this point.

3). Quasi-steady state fuel injection - A period during which the temperature and pressure of the mixture of fuel vapour and inert gas in the evaporation chamber change only very little. The liquid fuel injection rate remains constant and is identical to the evaporation rate. Approximate mathematical expressions for both temperature and pressure of the mixture can be developed as a function of the injected fuel mass.

4). After fuel injection; evaporation of remaining droplets resulting in further temperature drop - During this period, the remaining liquid fuel mass decreases with time and tends to decrease the temperature of the fuel vapour and gas mixture. On the

other hand, heat transfer takes place from the chamber wall to the mixture and tends to increase the mixture temperature. As long as the effect of the first phenomenon is predominant, the mixture temperature and consequently the pressure will continue to drop until both phenomena have equal effects, and the mixture temperature and pressure attain minimum values. For this period, a mathematical formula can be derived to describe the remaining liquid fuel mass at any specific time within the period.

5). After fuel injection; warm-up period - At the beginning of this period, some liquid fuel still remains. However, droplet evaporation has less influence on the mixture temperature than that of heat transfer. The net result is a slow rise in mixture temperature. When all liquid has evaporated, the mixture temperature continues to rise because of heat transfer. The final mixture temperature is identical to the initial temperature of the inert gas. The final pressure, on the other hand, will be above the original value due to an increase of mass within the evaporation chamber. Approximate mathematical expressions for this period can be developed.

4.3 Basic Equations

Theoretical calculations of temperature and pressure drops are based on the Ideal Gas Law, the internal energy equation and the conservation of mass for the inert gas and fuel system. Let V be the volume of the evaporation chamber, m_1 the mass of inert gas in the chamber, M_1 its molecular weight, m_2 the mass of injected fuel and M_2 its molecular weight. Then, assuming that the gas is cooled uniformly by the spray, we have before injection

$$P_o V = \frac{m_1}{M_1} R\, T_o \qquad (4\text{-}1)$$

where the subscript "o" refers to initial conditions, subscript "1" refers to the inert gas.

After evaporation of the fuel, one has

$$P\, V = \left(\frac{m_1}{M_1} + \frac{m_2}{M_2}\right) R\, T \qquad (4\text{-}2)$$

where subscript "2" refers to the fuel.

Neglecting the kinetic energy of the liquid fuel, the internal energy of the gas and fuel system must be constant and is given by the internal energy balance

$$m_1 e_1 + m_2 e_2 = m_1 e_{1,0} + m_2 e_{2,0} \qquad (4\text{-}3)$$

where e_1 and e_2 are the specific internal energies of the inert gas and fuel respectively.

If only part of the gas is cooled by the spray, equation (4-1) still holds. However equations (4-2) and (4-3) must be modified. Assume that m_1' is the mass of gas which is cooled, then after fuel injection, one has

$$P\ V = \frac{m_1 - m_1'}{M_1} R\ T_o + \left(\frac{m_1'}{M_1} + \frac{m_2}{M_2}\right) R\ T \qquad (4-4)$$

The internal energy equation for the system is now given by

$$(m_1 - m_1')\ e_{1,0} + m_1'\ e_1 + m_2 e_2 = m_1 e_{1,0} + m_2 e_{2,0} \qquad (4-5)$$

4.4 Development of Hypothetical Instantaneous Temperature and Pressure Drop Formulae

Solution of the basic equations gives the "Hypothetical Instantaneous Temperature and Pressure Drop Formulae", when heat transfer from the chamber wall and evaporation lag are neglected. Four sets of solutions will be given. Case I, the fuel vapour is considered an ideal gas. Case II, the fuel vapour is considered a non-ideal gas. For each case, the gas in the chamber is cooled either uniformly or partially.

Consider the case when the gas is uniformly cooled. The specific internal energy of the gas at the end of fuel evaporation is:

$$e_1 = e_{1,0} + c_{v_1} (T - T_o) \qquad (4\text{-}6)$$

where c_{v_1} is the specific heat of the gas at constant volume.

For the fuel, an arbitrary path is chosen such that the physical properties of the liquid fuel being investigated are available for all processes between the end states. Since the specific internal energy is a property, i.e. a point function, its change between any two states is independent of the processes which brought about the change. The arbitrarily chosen path is:

a). Decrease of initial pressure to 1 atmosphere at constant temperature. The specific internal energy of the liquid fuel remains the same when it is assumed to be independent

of pressure.

b). Heating-up of the liquid fuel to its boiling temperature at constant atmospheric pressure. Increase of the specific internal energy of the fuel is accounted for by the term

$$\int_{T_{2,0}}^{T_s} c_2 \, dT$$

where c_2 is the specific heat of the liquid fuel, T_s its normal boiling point, $T_{2,0}$ the initial temperature of the liquid fuel.

c). Isobaric evaporation of the liquid fuel at atmospheric pressure. To derive an expression which describes the specific internal energy increase during this process, the definition of enthalpy and the first law of thermodynamics are used. The specific enthalpy is given as

$$h = e + P\,v \; *$$

where P is the pressure, v the specific volume. In differential form, it becomes

$$dh = de + P\,dv + v\,dP \qquad (4\text{-}7)$$

*Units must be consistent

From the first law of thermodynamics, one has

$$de = dq - P\,dv \qquad (4\text{-}8)$$

where dq is the heat transferred to the fuel. Elimination of "de" from these two equations gives

$$dh = dq + v\,dP \qquad (4\text{-}9)$$

The heat supplied Δq to the fuel increases the enthalpy by an amount Δh. In this case, the change in enthalpy is termed the latent heat of evaporation and is denoted by L_2. Referring back to the definition of the specific enthalpy, the change in specific internal energy due to a phase change is given by

$$\Delta e = \Delta h - P_{at}\Delta v = L_2 - P_{at}\Delta v$$

where P_{at} is atmospheric pressure and $\Delta v \approx v_{at,s}$ where $v_{at,s}$ is the specific volume of the vapour at atmospheric pressure and temperature T_s.

d). Heating-up of the fuel vapour to its final temperature by a constant pressure process. The specific internal energy increase is given by

$$\int_{T_s}^{T} c_{p_2}\, dT - P_{at}(v_{at} - v_{as}) = \int_{T_s}^{T} c_{p_2}\, dT - \frac{R\,T}{M_2} + P_{at} v^{*}_{at,s}$$

where v_{at} is the specific volume at atmospheric pressure and the final temperature T.

e). Increase of vapour pressure to its final value by a constant temperature process. This has two possibilities depending on whether the vapour is considered an ideal gas or a non-ideal gas.

---

*The ideal gas approximation is used, since at low pressure and high temperature this assumption is valid.

4.4.1 Case I. Fuel Vapour is considered an ideal gas

In process (e), compression of the vapour at constant temperature does not change its specific internal energy. The work done on the fuel vapour is extracted from it in the form of heat loss. In equation form, the specific internal energy of the fuel is therefore

$$e_2 = e_{2,0} + \int_{T_{2,0}}^{T_s} c_2 \, dT + L_2 - \frac{R\,T}{M_2} + \int_{T_s}^{T} c_{p_2} \, dT$$

The specific heat at constant pressure c_{p_2} which appears in the last integral is variable with temperature. However, the final temperature T of the gas decreases from its original value T_o only by a comparatively small amount during fuel injection. It is therefore possible to simplify the above equation by letting

$$\int_{T_s}^{T} c_{p_2} \, dT = \int_{T_s}^{T_o} c_{p_2} \, dT + \bar{c}_{p_2} \, (T - T_o)$$

where $\bar{c}_{p_2}$ is an average value of c_{p_2} for the comparatively small interval $T_o - T$ and the first integral on the right-hand side has a constant value. So one has

$$e_2 = e_{2,0} + \int_{T_{2,0}}^{T_s} c_2 \, dT + L_2 - \frac{R\,T}{M_2} + \int_{T_s}^{T_o} c_{p_2} \, dT + \bar{c}_{p_2} \, (T - T_o) \qquad (4\text{-}10)$$

If c_2 is not constant, the integral

$$\int_{T_{2,0}}^{T_s} c_2 \, dT$$

is integrated either analytically or numerically.

With the assumption that all the heat for evaporation comes from the hot gas, the resulting formulae for the hypothetical instantaneous pressure and temperature decreases of the system must then be functions of the fuel to gas mass ratio

$$\chi = \frac{m_2}{m_1} \tag{4-11}$$

Next, by introducing three dimensionless constant

$$\beta_i = \frac{1}{c_{v_1} T_o} \left[L_2 + \int_{T_{2,0}}^{T_s} c_2 \, dT + \int_{T_s}^{T_o} c_{p_2} \, dT - \bar{c}_{p_2} T_o \right] \tag{4-12a}$$

$$\mu = \frac{M_1}{M_2} \tag{4-12b}$$

$$\gamma_i = \frac{\bar{c}_{p_2} - (R/M_2)}{c_{v_1}} \tag{4-12c}$$

equation (4-10) becomes

$$e_2 = e_{2,0} + \gamma_i c_{v_l} T_i + \beta_i c_{v_l} T_o \qquad (4\text{-}10a)$$

where T_i is the hypothetical temperature when the vapour is considered an ideal gas. Substitution of equations (4-6) (4-10a) into equation (4-3) gives

$$m_1(T_i - T_o) + m_2 (\beta_i T_o + \gamma_i T_i) = 0 \qquad (4\text{-}3a)$$

Making use of equation (4-11), equation (4-3a) can be re-arranged to give the instantaneous temperature decrease

$$\Delta T_i = T_o - T_i = T_o \chi \frac{(\beta_i+\gamma_i)}{(1+\gamma_i\chi)} \qquad (4\text{-}13)$$

The corresponding pressure decrease expression is obtained from equations (4-1) and (4-2). Dividing equation (4-2) by equation (4-1) gives

$$\frac{P_i}{P_o} = \frac{T_i}{T_o} \left(1 + \frac{m_2 M_1}{m_1 M_2}\right) = \frac{T_i}{T_o} (1 + \chi\mu) \qquad (4\text{-}14)$$

Making use of equation (4-13) and eliminating T_i/T_o from equation (4-14) gives

$$\Delta P_i = P_o - P_i = P_o \chi \frac{(\beta_i+\gamma_i-\mu) + \beta_i\mu\chi}{1 + \gamma_i\chi} \qquad (4\text{-}15)$$

Equation (4-15) gives the instantaneous pressure decrease in the evaporation chamber due to liquid fuel spray evaporation.

If only part of the gas is cooled, equations (4-4) and (4-5) must be used in the derivation of the hypothetical instantaneous temperature and pressure decrease expressions. Now define

$$\chi' = \frac{m_2}{m_1'} \tag{4-16}$$

Substitution of equations (4-6) and (4-10a) into equation (4-5) gives

$$m_1'T_i' + m_2\gamma_i T_i' = m_1'T_o - m_2\beta_i T_o \tag{4-17}$$

where T_i' is the hypothetical temperature when part of the gas is cooled and the vapour is considered an ideal gas. Dividing equation (4-17) by m_1' and making use of equation (4-16) gives

$$\frac{T_i'}{T_o} = \frac{(1 - \chi'\beta_i)}{(1 + \chi'\gamma_i)} \tag{4-18}$$

or

$$\Delta T_i' = T_o - T_i' = T_o\chi' \frac{\beta_i + \gamma_i}{1 + \gamma_i\chi'} \tag{4-19}$$

Equation (4-19) expresses the hypothetical instantaneous temperature decrease when the cooled portion of the hot gas is m_1'.

The corresponding pressure decrease expression is obtained by dividing equation (4-4) by equation (4-1) and making use of equations (4-12b), (4-16) and (4-18). The

resulting expression is

$$\Delta P_i = P_o - P_i' = P_o \chi \left[\frac{(\beta_i + \gamma_i - \mu) + \beta_i \mu \chi'}{1 + \gamma_i \chi'} \right] \qquad (4\text{-}20)$$

Equation (4-20) can be simplified further if $\gamma_i \chi' << 1$ because

$$\frac{1}{1 + \gamma_i \chi'} \approx 1 - \gamma_i \chi'$$

Making this substitution, equation (4-20) becomes

$$\Delta P_i' \approx P_o \chi \left[(\beta_i + \gamma_i - \mu) - (\beta_i + \gamma_i)(\gamma_i - \mu) \chi' \right] \qquad (4\text{-}21)$$

The validity of the approximation can be investigated with the following typical example.

Consider the initial conditions of the evaporation chamber as follows:

a). Inert gas - Nitrogen

b). Temperature - 800°F (689.8°K)

c). Pressure - 400 psig.

d). Volume - 82.36 liters (constant)

The mass of nitrogen gas in the evaporation chamber is 1132.6 grams. Assume that 20 c.c. of ethyl alcohol is injected. At 0°C, ethyl alcohol has a density of 0.80 gm/c.c. The mass of ethyl alcohol injected is 16 grams.

Assume that only one third of the nitrogen gas is cooled, then

$$\chi' = 0.042,38$$

For this combination and initial conditions, Cp_2 is given by (Ref. 4-2)

$$Cp_2 = 4.946 + 0.049,08T - 0.000,023,855T^2 + .000,000,004,5T^3$$

and $\overline{Cp}_2 \approx 0.628$ cal/g.°C. $R = 83.15 \times .0244$. $M_2 = 46.07$g. and $Cv_1 = 0.197,32$ (Ref. 4-3).

From equation (4-12c)

$$\gamma_i = \frac{0.628 - .0244 \times 83.15/46.07}{0.197} = 2.964$$

and $\gamma_i\chi' = 0.126$. The error introduced through the approximation is

$$\frac{\frac{1}{(1+\gamma_i\chi')} - (1-\gamma_i\chi')}{\frac{1}{(1+\gamma_i\chi')}} \approx 1.6\%$$

and is within the limit of experimental accuracy.

4.4.2 Case II. Fuel vapour considered as a non-ideal gas

The first four processes listed in section 4.4 still apply. Process (e), the increase of vapour pressure to its final value by a constant temperature process will however in the non-ideal case cause a change in the specific internal energy. This change is calculated in two parts. The first part consists of a change from the initial state of the process, $T = T_o$ and $P = 1$ atm. to the initial conditions existing in the chamber, $T = T_o$ and $P = P_o$. This is given by

$$e_2(T_o, P_o) - e_2(T_o, P = 1 \text{ atm.})$$

The second part consists of changes due to deviation of temperature from T_o and pressure from P_o and is given by

$$d[e_2(T,P) - e_2(T,P = 1 \text{ atm})]$$

$$= \left[\left(\frac{\partial e_2(T,P)}{\partial T}\right)_P - \left(\frac{\partial e_2(T,1)}{\partial T}\right)_P\right] dT + \left(\frac{\partial e_2(T,P)}{\partial P}\right)_T dP$$

For small changes in temperature and pressure, the partial derivatives can be determined by assuming the changes follow a linear relationship.

Let $$\left[\left(\frac{\partial e_2(T,P)}{\partial T}\right)_P - \left(\frac{\partial e_2(T,1)}{\partial T}\right)_P\right] = a$$

and $$\left(\frac{\partial e_2(T,P)}{\partial P}\right)_T = b$$

Then, the total change in specific internal energy for the process is

$$e_2(T_o,P_o) - e_2(T_o,1) + a(T-T_o) + b(P-P_o)$$

where a and b are to be determined from available data for the fuel vapour. For ethyl alcohol, a and b are calculated from figure (5-1).

The specific internal energy of the fuel is therefore,

$$e_2 = e_{2,0} + \int_{T_{2,0}}^{T_s} C_2 dT + L_2 - \frac{RT}{M_2} + \int_{T_s}^{T} C_{p_2} dT + e_2(T_o,P_o) \qquad (4\text{-}22)$$

$$- e_2(T_o,1) + a(T-T_o) + b(P-P_o)$$

Equation (4-22) is simplified as in section 4.4.1 to give

$$e_2 = e_{2,0} + \int_{T_{2,0}}^{T_s} C_2 dT + L_2 - \frac{RT}{M_2} + \int_{T_s}^{T_o} C_{p_2} dT + \overline{C}_{p_2}(T-T_o) \qquad (4\text{-}22a)$$

$$+ e_2(T_o,P_o) - e_2(T_o,1) + aT - aT_o + bP - bP_o$$

Values for $e_2(T,P)$ are obtained from figure (5-1) by letting

$$e_2(T,P) = h_2(T,P) - Pv_2 \ .$$

Again, assuming that all the heat for evaporation comes from the hot gas and that the heat transfer rate is infinite between the two substances, the temperature and pressure decreases caused by immediate complete evaporation of injected liquid fuel may again be expressed in terms of dimensionless constants and the fuel-to-gas mass ratio, χ.

To derive the formula for the hypothetical instantaneous temperature decrease we introduce two new dimensionless constants

$$\beta_n = \frac{1}{C_{v_1} T_o} \left[L_2 + \int_{T_{2,0}}^{T_s} C_2 dT + \int_{T_s}^{T_o} C_{p_2} dT + e_2(T_o,P_o) - e_2(T_o,1) \right. \tag{4-23a}$$

$$\left. - \overline{C}_{p_2} T_o - aT_o - bP_o \right]$$

$$\gamma_n = \frac{\overline{C}_{p_2} + a - \frac{R}{M_2}}{C_{v_1}} \tag{4-23b}$$

Substitution of equations (4-12b), (4-23a), and (4-23b) into equation (4-22a) gives

$$e_2 = e_{2,0} + \gamma_n C_{v_1} T_n + \beta_n C_{v_1} T_o + bP_n \tag{4-22b}$$

where T_n and P_n are the hypothetical temperature and pressure respectively for the non-ideal gas case.

Next, equations (4-6), (4-22b) are substituted into equation (4-3) to give

$$m_1(T_n-T_o) + m_2(\beta_n T_o + \gamma_n T_n + \frac{bP_n}{C_{v_1}}) = 0 \qquad (4\text{-}24)$$

Making use of equation (4-11), equation (4-24) after re-arranging gives the instantaneous temperature decrease for the non-ideal gas case

$$\Delta T_n = T_o - T_n = T_o\chi \left[\frac{\gamma_n + \beta_n + \frac{b}{C_{v_1}}\frac{P_n}{T_o}}{1 + \gamma_n\chi}\right] \qquad (4\text{-}25)$$

Eliminating T_n/T_o from equations (4-14) and (4-25) gives the corresponding pressure formula

$$\frac{P_n}{P_o} = \frac{(1 + \chi\mu)}{(1 + \chi\gamma_n)}\left(1 - \chi\beta_n - \chi\frac{b}{C_{v_1}} \cdot \frac{P_n}{T_o}\right) \qquad (4\text{-}26)$$

Rearranging of equation (4-26) gives the instantaneous pressure decrease as

$$\Delta P_n = P_o - P_n = P_o\chi \frac{(\beta_n + \gamma_n + \zeta - \mu) + (\zeta + \beta_n)\mu\chi}{1 + (\gamma_n + \zeta)\chi + \mu\zeta\chi^2} \qquad (4\text{-}26a)$$

where $$\zeta = \frac{b}{C_{v_1}} \cdot \frac{P_o}{T_o} \qquad (4\text{-}26b)$$

Equation (4-26a) gives the pressure drop caused by instantaneous spray evaporation when the fuel vapour is considered a non-ideal gas. It has the same form as equation (4-15) which is an expression for the pressure drop when the vapour is considered an ideal gas. If non-ideal effects are neglected, equation (4-26a) becomes identical to equation (4-15).

When only part of the gas in the chamber is cooled, we have from equations (4-5), (4-6), and (4-22b)

$$m_1' T_n' + m_2 \gamma_n T_n' = m_1' T_o - m_2 \beta_n T_o - m_2 \frac{b}{C_{v_1}} P_n' \qquad (4\text{-}27)$$

Dividing equation (4-27) by m_1' and making use of equation (4-16) gives

$$\frac{T_n'}{T_o} = \frac{(1 - \chi' \beta_n - \chi' \frac{b}{C_{v_1}} \cdot \frac{P_n'}{T_o})}{1 + \chi' \gamma_n} \qquad (4\text{-}27a)$$

or

$$\Delta T_n' = T_o - T_n' = T_o \chi' \frac{(\gamma_n + \beta_n + \frac{b}{C_{v_1}} \frac{P_n'}{T_o})}{1 + \chi' \gamma_n} \qquad (4\text{-}27b)$$

The corresponding pressure decrease formula is obtained by combining equations (4-1), (4-4), (4-12b), (4-16)

and (4-27a) to give

$$\Delta P_n' = P_o - P_n' = P_o \chi \left[\frac{(\beta_n + \gamma_n + \zeta - \mu) + (\zeta + \beta_n)\mu\chi'}{1 + \chi' \gamma_n + \chi\zeta + \chi\chi'\mu\zeta} \right] \tag{4-28}$$

It can be readily observed that this equation is the same as equation (4-20) when non-ideal gas properties are neglected.

4.4.3 Sample calculation of the difference between ideal and non-ideal instantaneous pressure decrease for ethyl alcohol

It can be readily observed from equations (4-15), (4-20), (4-26a) and (4-28) that the instantaneous pressure decrease is proportional to $P_o \dot{\chi}$. The influences of non-ideal gas effects and partial cooling of the inert gas are accounted for in the fraction which follows this product. This fraction varies with both fuel and operating conditions.

Consider a typical example using nitrogen as the inert gas and ethyl alcohol as fuel. The initial chamber conditions are:

$$T_o = 900°F \ (755.\dot{3}) \ °K$$

and

$$P_o = 414.7 \text{ psia.} \quad \text{For}$$

$$\chi = 0.01 \quad \text{and} \quad \chi' = .01/.3 = .0\dot{3}.$$

$\beta_i = -.144{,}735$ (section 4.4.1 , equation (4-12a))

$\gamma_i = 3.142{,}1$ (section 4.4.1 , equation (4-12c))

From figure (4-1), appendix A

$$e_2(T_o,P_o) = h(T_o,P_o) - Pv = \frac{20{,}400-28.21\times24.205\times1.9}{46.07} =$$

$$= 414.644 \text{ cal/g.}$$

and

$$e_2(T_o,1) = h(T_o,1) - v = 444.3 \text{ cal/g.}$$

$$e_2(480°C, \text{ 1 atm.}) = 443 \text{ cal/g.}$$

$$e_2(420°C, \text{ 1 atm.}) = 406.276 \text{ cal/g.}$$

$$e_2(480°C,\ 30\ atm.) = 411.67\ cal/g.$$

$$e_2(420°C,\ 30\ atm.) = 375.098\ cal/g.$$

$$e_2(480°C,\ 20\ atm.) = 426.27\ cal/g.$$

$$\left[\frac{\partial e_2(T,1)}{\partial T}\right]_P = \frac{e_2(480°C,\ 1\ atm) - e_2(420°C,\ 1\ atm)}{480°C - 420°C} = .612,06\dot{}$$

$$\left[\frac{\partial e_2(T,30)}{\partial T}\right]_P = \frac{e_2(480°C,\ 30) - e_2(420°C,\ 30)}{480°C - 420°C} = .597,633$$

$$a = \left[\frac{\partial e_2(T,30)}{\partial T}\right]_P - \left[\frac{\partial e_2(T,1)}{\partial T}\right]_P = -0.015,433$$

$$b = \left[\frac{\partial e_2(480,\ P)}{\partial P}\right]_T = \frac{e_2(480,30) - e_2(480,20)}{30-20} = -1.460$$

$$\zeta = \frac{bP_o}{C_{v_1} T_o} = -.281,333,5$$

$\beta_n = 0.020,04$ (section 4.4.2 , equation (4-23a))

$\gamma_n = 3.062,431$ (section 4.4.2 , equation (4-23b))

The two instantaneous pressure decreases are:

$\Delta P_i' = P_o\chi(2.160)$ (Ideal gas formula, section 4.4.1, equation (4-20))

$\Delta P_n' = P_o\chi(1.990)$ (Non-ideal gas formula, section 4.4.2 , equation (4-28))

It can be seen that the two differ by approximately 10%.

4.5 Determination of the Liquid Fuel Mass existing in the Evaporation Chamber during Injection

If we now consider the fact that evaporation of the droplets require a finite time period, then the mass of fuel existing in the liquid phase during injection is determined in the following manner. The initial radius of all droplets is assumed to be r_o. Theory (Refs. 4-4, 2-3) and experiments (Refs. 4-5, 4-6) have shown that the evaporation of droplets follows a quadratic law so that

$$r^2 = r_o^2 \, (1 - t'/t_L) \tag{4-29}$$

where t' is the age of the droplet, i.e. the time elapsed after injection of the droplet, t_L is the lifetime of the droplet, and r is the droplet radius at age t'. For each droplet having an age t', its radius compared to its initial radius is

$$\frac{r}{r_o} = (1 - \frac{t'}{t_L})^{\frac{1}{2}} \tag{4-30}$$

The corresponding volume of the droplet compared to its initial volume is proportional to

$$(1 - \frac{t'}{t_L})^{\frac{3}{2}} \tag{4-31}$$

Consider an infinitely small period of time, dt', the liquid fuel mass injected during this time is

$$\dot{m}_2 dt' \tag{4-32}$$

If the density of the liquid fuel is assumed constant, the droplet mass at any time t' when expressed as a ratio of the initial injected mass is proportional to its volume ratio. The mass of all droplets of an age between t' and t' + dt' will therefore be the product of the mass injected during dt', given by equation (4-32), and the ratio given by equation (4-31). In equation form, this is

$$dm^{(\ell)} = \dot{m}_2 dt' \, (1-t'/t_L)^{3/2} \qquad (4-33)$$

where $\dot{m}_2$ is the rate of fuel injection.

During the initial transient period, if the quadratic law is assumed, the liquid mass build-up is given by integrating equation (4-33) from t'=o to t'=t. This gives

$$\int_o^t dm^{(\ell)} = \dot{m}_2 \int_o^t (1-\frac{t'}{t_L})^{3/2} \, dt' = \frac{2}{5} \dot{m}_2 t_L \left[1-(1-\frac{t}{t_L})^{5/2}\right] \qquad (4-34)$$

for $t < t_L$.

The validity of equation (4-34) hinges on the assumption that droplet evaporation follows the quadratic law. As long as the quadratic law remains valid, equation (4-34) will give the order of magnitude of the transient period. This is of the order of t_L.

The total mass of liquid fuel at any time during fuel injection other than the initial transient period is obtained by integrating equation (4-33) between t'=o and

$t'=t_L$. This gives

$$m^{(\ell)} = \int_0^{t_L} dm^{(\ell)} = \frac{2}{5}\dot{m}_2 t_L \qquad (4\text{-}35)$$

This amount is constant during the injection period except for the initial transient period.

So far in the analysis all liquid drops were assumed to have constant density regardless of their temperature changes. However, when the decrease in density of the droplets is considered, equation (4-33) requires modification. For a fixed mass, the change in volume, as a result of temperature increase, is inversely proportional to the change in density. Therefore, the equation which describes the liquid fuel mass existing during injection is

$$dm^{(\ell)} = \frac{\dot{m}_2(1 - \frac{t'}{t_L})^{3/2}}{(1 + \delta\Delta T)}\, dt' \qquad (4\text{-}36)$$

where δ is the volume expansion coefficient of the liquid fuel, ΔT is the temperature change of the droplets. For ethyl alcohol, $\delta = 0.745 \times 10^{-3}/°C$ and the critical temperature of ethyl alcohol is $T_c = 243.1°C$. If the injection temperature of ethyl alcohol is set at 0°C and the final temperature reached by the fuel droplets is the critical temperature, then

$$\Delta T = 243.1°C$$

However, a majority of the liquid fuel droplets is at a temperature closer to the initial injection temperature. Taking the average change in droplet temperature equal to one-third of the maximum temperature change and that the temperature change is a linear function of the droplet lifetime, then for ethyl alcohol, equation (4-36) becomes

$$dm^{(\ell)} = \frac{\dot{m}_2\left(1 - \frac{t'}{t_L}\right)^{3/2}}{\left(1 + .745 \times 10^{-3} \times 243\, \frac{t'}{3t_L}\right)} dt' = \dot{m}_2 \frac{\left(1 - \frac{t'}{t_L}\right)^{3/2}}{\left(1 + .060{,}345\, \frac{t'}{t_L}\right)} dt \qquad (4\text{-}37)$$

Since $0.060345\, \frac{t'}{t_L} \leq .060{,}345 << 1$ for $0 \leq t' \leq t_L$,

$$\frac{1}{1 + .060{,}345\, \frac{t'}{t_L}} \approx 1 - .060{,}345\, \frac{t'}{t_L}$$

Using the above approximation, equation (4-37) can be written as

$$dm^{(\ell)} \approx \dot{m}_2\left(1 - \eta \frac{t'}{t_L}\right)\left(1 - \frac{t'}{t_L}\right)^{3/2} dt' \qquad (4\text{-}38)$$

where $\eta = .060{,}345$.

Integration of equation (4-38) gives

$$m^{(\ell)} = \frac{2}{5}\dot{m}_2 t_L - \eta \frac{\dot{m}_2}{t_L}\int_o^{t_L} t'(1 - \frac{t'}{t_L})^{3/2}\, dt' \qquad (4\text{-}39)$$

$$= \frac{2}{5}\dot{m}_2 t_L\,(1 - \frac{2}{7}\eta)$$

Comparison of equations (4-35) and (4-39) shows that the two calculated liquid masses during injection differ by the factor $(1-2\eta/7)$. This factor can be considered as a correction factor to the idealized condition. For the case of ethyl alcohol, this factor has a value of 0.98276. The error introduced in the liquid mass calculation is less than 2% if the thermal expansion of the liquid fuel is neglected.

For liquid fuel with high $\delta\Delta T$ value, the term $1/(1 + \delta\Delta T)$ would be expressed in power series of the form

$$\frac{1}{(1 + \delta\Delta T)} = 1 - \delta\Delta T + (\delta\Delta T)^2 - (\delta\Delta T)^3 + \text{---} \qquad (4\text{-}40)$$

Taking only the first four terms, equation (4-37) becomes

$$dm^{(\ell)} \approx \left[1 - \eta\frac{t'}{t_L} + \left(\eta\frac{t'}{t_L}\right)^2 - \left(\eta\frac{t'}{t_L}\right)^3\right]\dot{m}_2\left(1 - \frac{t'}{t_L}\right)^{3/2} dt' \qquad (4\text{-}41)$$

Integration of equation (4-41) gives

$$m^{(\ell)} \approx \frac{2}{5} \dot{m}_2 t_L (1 - \frac{2}{7} \eta + \frac{4}{63} \eta^2 - \frac{48}{693} \eta^3) \qquad (4\text{-}42)$$

where the correction factor is now $(1 - \frac{2}{7} \eta + \frac{4}{63} \eta^2 - \frac{48}{693} \eta^3)$.

4.6 Conditions during Injection and Lifetime of Spray

We shall now consider the real conditions in the evaporation chamber during fuel injection, taking into account the finite lifetime of the droplets, heat transfer from the wall and the fact that the entire mass of gas in the evaporation chamber is not at a uniform temperature. We shall, however, still make some simplifying assumptions in addition to the ones outlined in section 4.2. These are:

a). The liquid droplets are considered to remain at their initial temperature throughout their lifetime. Many theoretical calculations have been performed to determine the droplet temperature and arrived at conflicting results. For small droplets, verification of these theoretical studies by direct measurement is difficult.

b). The fuel vapour, on the other hand, is considered to be at the temperature T of the gas, neglecting the fact that part of the vapour will still be at lower temperature between T_s and T.

c). For the inert gas it is assumed that part of it remains at the original temperature T_o while another portion (of mass m_1') is at temperature T.

d). The chamber wall, during the whole process, is considered to remain at constant initial temperature, T_o. This is very close to the actual case because of the large mass and heat capacity of the evaporation chamber used.

e). The volume of the liquid spray droplets is neglected. The volume of the evaporation chamber is 82.36 liters and the volume of the liquid spray droplets is approximately 0.025 liters.

With these assumptions, we can now write the energy balance equation for the different cases.

4.6.1 Case I. Fuel vapour is considered an ideal gas

The energy balance equation is

$$m_1'(e_1-e_{1,0}) + [m_2(t) - \int_o^t dm^{(\ell)}](e_2-e_{2,0}) = HS\int_o^t (T_o-T)dt \qquad (4-43)$$

Here, H is the overall heat transfer coefficient and S is the evaporation chamber inside surface area, and

$$m_2(t) = \dot{m}_2\int_o^t dt \ . \qquad (4-44)$$

The term $\int_o^t dm^{(\ell)}$ has two forms depending on the time t. These are given by equations (4-34) and (4-35). Therefore equation (4-43) also has two forms. For $t < t_L$, equation (4-43) can be written as

$$m_1'(e_1-e_{1,0}) + \{m_2(t) - \frac{2}{5}\dot{m}_2 t_L[1-(1-\frac{t}{t_L})^{5/2}]\}(e_2-e_{2,0}) = \qquad (4-45)$$
$$= HS\int_o^t (T_o-T)dt$$

During this initial transient fuel injection period, the right-hand side term of equation (4-45) is negligible because of the small temperature gradient existing between the evaporation chamber wall and the inert gas.

For $t_L \leqslant t$, equation (4-43) becomes

$$m_1'(e_1-e_{1,0}) + [m_2(t) - 0.4\dot{m}_2 t_L](e_2-e_{2,0}) = \\ = HS\int_{t_L}^{t}(T_o-T)dt \approx HS\int_{o}^{t}(T_o-T)dt \qquad (4\text{-}46)$$

Making use of equations (4-6), (4-10), (4-11), (4-12's) and (4-16), equation (4-46) can be written as

$$\kappa(T-T_o) + (\chi-\lambda)(\beta_i T_o + \gamma_i T) = \frac{HS}{m_1 C_{v_1}}\int_{o}^{t}(T_o-T)dt \qquad (4\text{-}47)$$

where $$\lambda = 0.4\ \dot{m}_2 t_L/m_1 \qquad (4\text{-}48)$$

$\kappa = \chi/\chi' = m_1'/m_1 \approx$ constant (within the time interval of interest) (4-49)

κ is a mixing or jet spread coefficient. Equation (4-47) can best be solved by approximation. The term on the right-hand side of equation (4-47) while not negligible, is still small compared to the other terms. Hence one finds a first approximation for T by letting the right-hand side equal to zero. This gives, after rearranging the term on the left-hand side of equation (4-47).

$$T_o - T \approx T_o\,\frac{(\beta_i + \gamma_i)(\chi-\lambda)}{\kappa + \gamma_i(\chi-\lambda)} \qquad (4\text{-}50)$$

Substitution of equation (4-50) into the integral in equation (4-47) gives

$$\int_o^t (T_o - T)dt = T_o(\beta_i + \gamma_i) \frac{m_1}{\dot{m}_2 \gamma_i^2} \left[\gamma_i \chi - \kappa \ell n\left[1 + \frac{\gamma_i \chi}{\kappa - \gamma_i \lambda}\right]\right] \quad (4\text{-}51)$$

In view of the fact that $\chi << 1$ and $\lambda << \chi$, the logarithm can be expanded into a series. Taking only the first two terms in the series expansion, one has

$$\gamma_i \chi - \kappa \ell n\left[1 + \frac{\gamma_i \chi}{\kappa - \gamma_i \lambda}\right]$$

$$= \gamma_i \chi - \kappa\left[\frac{\gamma_i \chi}{\kappa - \gamma_i \lambda} - \frac{\gamma_i^2 \chi^2}{2(\kappa - \gamma_i \lambda)^2}\right]$$

$$= \frac{[2(\kappa - \gamma_i \lambda)^2 \gamma_i \chi - 2\gamma_i \chi\ \kappa(\kappa - \gamma_i \lambda) + \kappa \gamma_i^2 \chi^2]}{2(\kappa - \gamma_i \lambda)^2}$$

$$= \frac{[-2\kappa\gamma_i \lambda + 2\gamma_i^2 \lambda^2 + \kappa \gamma_i \chi]\gamma_i \chi}{2(\kappa - \gamma_i \lambda)^2}$$

$$\approx \frac{\kappa \gamma_i^2 (\chi^2 - 2\chi\lambda)}{2(\kappa - \gamma_i \lambda)^2}$$

$$\approx \gamma_i^2 \frac{(\chi - \lambda)^2}{2\kappa} \quad (4\text{-}52)$$

In the derivation of equation (4-52), terms of lower order of magnitude were dropped.

Now, from equations (4-47), (4-51) and (4-52)

$$\kappa(T-T_o) + (\chi-\lambda)(\beta_i T_o+\gamma_i T) = \frac{HS}{\dot{m}_2 C_{v_1}} T_o(\beta_i+\gamma_i)\frac{(\chi-\lambda)^2}{2\kappa} = \alpha\, T_o(\beta_i+\gamma_i)\frac{(\chi-\lambda)^2}{\kappa} \tag{4-53}$$

where $$\alpha = HS/2\dot{m}_2 C_{v_1} \tag{4-53a}$$

Rearranging (4-53) gives

$$T\left[1 + \frac{\gamma_i}{\kappa}(\chi-\lambda)\right] = T_o\left\{1 - \beta_i\frac{\chi-\lambda}{\kappa} + \alpha(\beta_i+\gamma_i)\frac{(\chi-\lambda)^2}{\kappa^2}\right\}$$

or $$T = T_o\left\{1 - \beta_i\frac{(\chi-\lambda)}{\kappa} + \alpha(\beta_i+\gamma_i)\frac{(\chi-\lambda)^2}{\kappa^2}\right\}\left[1 + \frac{\gamma_i}{\kappa}(\chi-\lambda)\right]^{-1} \tag{4-54}$$

The term $\left[1 + \frac{\gamma_i}{\kappa}(\chi-\lambda)\right]^{-1}$ can be expressed in series as

$$\left[1 + \frac{\gamma_i}{\kappa}(\chi-\lambda)\right]^{-1} = 1 - \frac{\gamma_i}{\kappa}(\chi-\lambda) + \frac{\gamma_i^2(\chi-\lambda)^2}{\kappa^2} - \cdots \tag{4-55}$$

Substituting equation (4-55) into (4-54) and dropping terms containing $(\chi-\lambda)^3$ and higher order terms, equation (4-54)

becomes

$$T \approx T_o \left\{ 1 - (\beta_i+\gamma_i) \left[\frac{(\chi-\lambda)}{\kappa} - (\alpha+\gamma_i)\frac{(\chi-\lambda)^2}{\kappa^2} \right] \right\} \quad (4\text{-}56)$$

Equation (4-56) gives an approximation to the evaporation chamber temperature as a function of the injected fuel quantity. The accuracy of this approximation may be tested as follows:

First, differentiate equation (4-47) with respect to t to obtain

$$[\kappa + (\chi-\lambda)\gamma_i]\frac{dT}{dt} + (\beta_i T_o + \gamma_i T)\frac{d\chi}{dt} = \frac{HS}{m_1 C_{v_1}} (T_o-T) \quad (4\text{-}57)$$

where

$$\frac{d\chi}{dt} = \frac{\dot{m}_2}{m_1} . \quad (4\text{-}58)$$

Making use of the expression for α, equation (4-57) may be written as

$$[\kappa + (\chi-\lambda)\gamma_i]\frac{dT}{dt} + [(\beta_i-2\alpha)T_o + (\gamma_i+2\alpha)T]\frac{d\chi}{dt} = 0 \quad (4\text{-}59)$$

If the expression for T as given by equation (4-56) is exact, the left-hand side of equation (4-59) shall be identical to zero. When T is not exact, substitution of T, and dT/dt into equation (4-59) would not satisfy the equality. The resulting value, which differs from zero, is the deviation due to approximation. This temperature approximation will now be

checked in the following manner.

Differentiation of equation (4-56) gives

$$\frac{dT}{dt} = - T_o(\beta_i+\gamma_i)[1 - (\alpha+\gamma_i)(\chi-\lambda)\frac{2}{\kappa}]\frac{1}{\kappa}\frac{d\chi}{dt} \qquad (4\text{-}60)$$

Substitution of equations (4-56), and (4-60) into the left-hand side of equation (4-52) gives, after simplifying,

$$\frac{2T_o}{\kappa^2}(\beta_i+\gamma_i)(\alpha+\gamma_i)(\alpha + \frac{3\gamma_i}{2})(\chi-\lambda)^2 \qquad (4\text{-}61)$$

which is of second order in $(\chi-\lambda)$, and is small compared to the other terms.

The corresponding approximate expression for the evaporation chamber pressure is derived from

$$PV = \frac{m_1-m_1'}{M_1} RT_o + \left[\frac{m_1'}{M_1} + \frac{m_2 - 0.4\dot{m}_2 t_L}{M_2}\right] RT \qquad (4\text{-}62)$$

and equations (4-1), (4-48) and (4-49) to give

$$P = P_o\{(1-\kappa) + [\kappa+\mu(\chi-\lambda)]\frac{T}{T_o}\} \qquad (4\text{-}63)$$

Substituting equation (4-56) for T/T_o into equation (4-63) gives

$$P \approx P_o\{1 - (\beta_i+\gamma_i-\mu)(\chi-\lambda) + (\beta_i+\gamma_i)(\alpha+\gamma_i-\mu)\frac{(\chi-\lambda)^2}{\kappa}\} \qquad (4\text{-}64)$$

Equation (4-64) is the approximation of the real evaporation chamber pressure during fuel injection, developed from the assumptions outlined at the beginning of this section. It is noted that the ratio κ appears only in a term of small order of magnitude, i.e. the term containing $(\chi-\lambda)^2$. Therefore, the spatial distribution of the spray droplets has no more influence on the actual pressure than it has on the ideal pressure, (see section 4.4.1, equation 4-21). One interesting observation regarding equation (4-64) is that when $m_1' \to 0$, i.e. $\chi' \to \infty$ and $\kappa \to 0$, P becomes infinite. Therefore, equations (4-56) and (4-64) are valid only when $\kappa \neq 0$. For the present study, χ' has the same order of magnitude as χ, the value of κ lies between 1/5 and 1. During the fuel injection period, κ is much closer to the lower range.

The accuracy of equation (4-64) can be estimated by comparing it to the ideal pressure decrease of equation (4-21). If $\lambda = 0$, i.e. no liquid droplets in the evaporation chamber during injection; and $\alpha = 0$, i.e. no heat transfer, equation (4-64) becomes after rearranging

$$P_o - P_i = P_o \chi[(\beta_i+\gamma_i-\mu) - (\beta_i+\gamma_i)(\gamma_i-\mu)\frac{\chi}{\kappa}] \qquad (4-65)$$

which is identical to equation (4-21) since $\chi/\kappa = \chi'$.
To derive the expression for the lifetime of the spray, one requires the quantity

$$-(P-P_i)/\frac{dp}{d\chi}$$

where both P and $dp/d\chi$ are to be determined experimentally. We will define this quantity as λ''.

$$\lambda'' = -(P-P_i)/\frac{dp}{d\chi} \tag{4-66}$$

Calculating λ'' from equations (4-64) and (4-65a), one finds

$$\lambda'' = \frac{\lambda + \frac{(\beta_i+\gamma_i)}{\kappa(\beta_i+\gamma_i-\mu)}[(\alpha+\gamma_i-\mu)(\chi-\lambda)^2 - (\gamma_i-\mu)\chi^2]}{1 - \frac{2(\beta_i+\gamma_i)}{\kappa(\beta_i+\gamma_i-\mu)}(\alpha+\gamma_i-\mu)(\chi-\lambda)} \tag{4-66a}$$

Expanding the denominator of equation (4-66a) in series gives

$$\left[1 - \frac{2(\beta_i+\gamma_i)(\chi-\lambda)}{\kappa(\beta_i+\gamma_i-\mu)}(\alpha+\gamma_i-\mu)\right]^{-1} = 1 + \frac{2(\beta_i+\gamma_i)(\chi-\lambda)}{\kappa(\beta_i+\gamma_i-\mu)}(\alpha+\gamma_i-\mu)$$

$$+ \frac{4(\beta_i+\gamma_i)^2(\chi-\lambda)^2(\alpha+\gamma_i-\mu)^2}{\kappa^2(\beta_i+\gamma_i-\mu)^2} + \frac{8(\beta_i+\gamma_i)^3(\chi-\lambda)^3(\alpha+\gamma_i-\mu)^3}{\kappa^3(\beta_i+\gamma_i-\mu)^3} + \cdots \tag{4-67}$$

Making use of equation (4-67), one obtains

$$\lambda'' = \left\{\lambda + \frac{(\beta_i+\gamma_i)}{\kappa(\beta_i+\gamma_i-\mu)}\left[(\alpha+\gamma_i-\mu)(\chi-\lambda)^2 - (\gamma_i-\mu)\chi^2\right]\right\}$$

$$\left[1 + \frac{2(\beta_i+\gamma_i)(\chi-\lambda)(\alpha+\gamma_i-\mu)}{\kappa(\beta_i+\gamma_i-\mu)} + \frac{4(\beta_i+\gamma_i)^2(\chi-\lambda)^2(\alpha+\gamma_i-\mu)^2}{\kappa^2(\beta_i+\gamma_i-\mu)^2} + \cdots\right] \tag{4-68}$$

Dropping terms containing λ^2, $\chi\lambda$, and χ^3, equation (4-68) can be simplified to give

$$\lambda'' \approx \lambda + \frac{\alpha(\beta_i+\gamma_i)}{\kappa(\beta_i+\gamma_i-\mu)}\chi^2 \tag{4-69}$$

Solving equation (4-69) for λ gives

$$\lambda \approx \lambda'' - \frac{\alpha(\beta_i+\gamma_i)}{\kappa(\beta_i+\gamma_i-\mu)}\chi^2 \tag{4-69a}$$

Using the definitions of λ and λ'', equations (4-48) and (4-66), one obtains

$$0.4t_L\frac{\dot{m}_2}{m_1} \approx \frac{-(P-P_i)}{dP/d\chi} - \frac{\alpha(\beta_i+\gamma_i)}{\kappa(\beta_i+\gamma_i-\mu)}\chi^2 \tag{4-69b}$$

or
$$0.4t_L \approx -(P-P_i)/\left(\frac{dP}{d\chi}\cdot\frac{\dot{m}_2}{m_1}\right) - \frac{\alpha(\beta_i+\gamma_i)m_1}{\kappa(\beta_i+\gamma_i-\mu)\dot{m}_2}\chi^2 \tag{4-69c}$$

However, $\frac{\dot{m}_2}{m_1} = \frac{d\chi}{dt}$, therefore

$$0.4t_L \approx -(P-P_i)/\frac{dP}{dt} - K\chi^2 \tag{4-69d}$$

where $$K = \frac{m_1 HS}{\dot{m}_2^2 c_{v_1}} \cdot \frac{(\beta_i+\gamma_i)}{\kappa(\beta_i+\gamma_i-\mu)} \qquad (4\text{-}70)$$

For the evaluation of formula (4-69d), P and dP/dt are taken from the actual pressure-time curve while P_i is calculated from equation (4-20). The constant K, which has the dimension of time, can be determined from a slow warm-up curve as will be described in section (4.8). The first term on the right-hand side of equation (4-69d) (which is positive) is the evaporation lag as defined in the introduction. Apart from the term $-K\chi^2$ which allows for the influence of heat transfer, the evaporation lag is therefore proportional to the lifetime t_L of the droplets by the factor 0.4.

It will be noted that the correction term in formula (4-69d) is negative and proportional to χ^2, hence to the square of time. The formula is, of course, only an approximation because the heat transfer coefficient H is not necessarily the same during the slow warm-up as during injection. Neither will the ratio κ be quite constant. However, H and κ appear only in small correction terms.

4.6.2 Case II. Fuel vapour is considered a non-ideal gas

The energy balance equation is obtained by combining equations (4-6), (4-22b), and (4-46) to give, for $t_L \leq t$

$$m_1' C_{v_1}(T-T_o)+(m_2-.4\dot{m}_2 t_L)(\gamma_n C_{v_1} T+\beta_n C_{v_1} T_o+bP) = HS\int_{t_L}^{t}(T_o-T)dt \qquad (4\text{-}71)$$

From the modified equation (4-4), one obtains a relationship between T and P as

$$P = \left(1 - \frac{m_1'}{m_1}\right)P_o + \left[\frac{m_1'}{m_1} + \frac{m_2}{m_1}\mu - \frac{.4\dot{m}_2 t_L}{m_1}\mu\right]\frac{P_o}{T_o}T \qquad (4\text{-}72)$$

or
$$bP = (1-\kappa)\, bP_o + (\kappa+\chi\mu-\lambda\mu)\, b\,\frac{P_o}{T_o}T \qquad (4\text{-}73)$$

Substituting equation (4-73) into equation (4-71) and dividing by $m_1 C_{v_1}$ gives

$$\kappa(T-T_o)+(\chi-\lambda)[\gamma_n T+\beta_n T_o+(1-\kappa)\zeta T_o+(\kappa+\chi\mu-\lambda\mu)\zeta T]=\frac{HS}{m_1 C_{v_1}}\int_o^t (T_o-T)dt \qquad (4\text{-}71a)$$

Equation (4-71a) is solved by means of the approximation technique of section (4.6.1).

Let
$$\int_o^t (T_o-T)dt = 0$$

Then, equation (4-71a) gives

$$\frac{T}{T_o} = \frac{\kappa-(\chi-\lambda)\beta_n-(\chi-\lambda)(1-\kappa)\zeta}{\kappa+(\chi-\lambda)\gamma_n+(\chi-\lambda)(\kappa+\chi\mu-\lambda\mu)\zeta} \qquad (4-74)$$

and $$1 - \frac{T}{T_o} = \frac{T_o-T}{T_o} = (\chi-\lambda)\ \frac{(\gamma_n+\beta_n)+(1+\chi\mu-\lambda\mu)\zeta}{\kappa+(\chi-\lambda)\gamma_n+(\chi-\lambda)(\kappa+\chi\mu-\lambda\mu)\zeta}$$

Therefore,

$$T_o-T \approx T_o(\chi-\lambda)\ \frac{(\gamma_n+\beta_n)\ +\ (1+\chi\mu-\lambda\mu)\zeta}{\kappa+(\chi-\lambda)\gamma_n+(\chi-\lambda)(\kappa+\chi\mu-\lambda\mu)\zeta} \qquad (4-75)$$

$$= T_o\left[1\ +\ \frac{(\beta_n+\zeta-\kappa\zeta)(\chi-\lambda)-\kappa}{\mu\zeta\chi^2+(\gamma_n+\kappa\zeta-2\lambda\mu\zeta)(\chi-\lambda)-\lambda^2\mu\zeta+\kappa}\right]$$

But

$$\zeta\mu\chi^2 = \zeta\mu(\chi-\lambda)^2 + 2\chi\lambda\zeta\mu - \lambda^2\zeta\mu \qquad (4-76)$$

Elimination of the term $\zeta\mu\chi^2$ from equations (4-75) and (4-76) gives

$$T_o-T \approx T_o\left[1\ +\ \frac{(\beta_n+\zeta-\kappa\zeta)(\chi-\lambda)-\kappa}{\zeta\mu(\chi-\lambda)^2+(\gamma_n+\kappa\zeta)(\chi-\lambda)+\kappa}\right] \qquad (4-75a)$$

and

$$\int_o^t (T_o - T)dt \approx T_o t + T_o \int_o^t \frac{(\beta_n+\zeta-\kappa\zeta)(\chi-\lambda)-\kappa}{\zeta\mu(\chi-\lambda)^2+(\gamma_n+\kappa\zeta)(\chi-\lambda)+\kappa}\, dt$$

$$= T_o t + \frac{m_1}{\dot{m}_2} T_o \int_o^{\chi} \frac{(\beta_n+\zeta-\kappa\zeta)(\chi-\lambda)-\kappa}{\zeta\mu(\chi-\lambda)^2+(\gamma_n+\kappa\zeta)(\chi-\lambda)+\kappa}\, d\chi \qquad (4\text{-}77)$$

Let $\bar{X} = \chi-\lambda$, equation (4-77) can be written as

$$\int_o^t (T_o - T)dt \approx T_o t + \frac{m_1}{\dot{m}_2} T_o \int_{-\lambda}^{\chi-\lambda} \frac{(\beta_n+\zeta-\kappa\zeta)\bar{X}-\kappa}{\zeta\mu\bar{X}^2+(\gamma_n+\kappa\zeta)\bar{X}+\kappa}\, d\bar{X} \qquad (4\text{-}77a)$$

The integrand of equation (4-77a) can be expressed in power series

$$\frac{a_{10}+a_{11}\bar{X}}{b_{10}+b_{11}\bar{X}+b_{12}\bar{X}^2} = \frac{a_{10}}{b_{10}} + \left[\frac{a_{11}}{b_{10}} - \frac{a_{10}b_{11}}{b_{10}^2}\right]\bar{X} + \left[\frac{a_{10}b_{11}^2}{b_{10}^3} - \frac{a_{10}b_{12}}{b_{10}^2} - \frac{a_{11}b_{11}}{b_{10}^2}\right]\bar{X}^2 + \cdots \qquad (4\text{-}78)$$

where $a_{10} = -\kappa$, $a_{11} = (\beta_n+\zeta-\kappa\zeta)$, $b_{10} = \kappa$, $b_{11} = \gamma_n+\kappa\zeta$,

$b_{12} = \zeta\mu$.

Taking only the first two terms in the power series and substituting into equation (4-77a) gives

$$\int_o^t (T_o - T)dt \approx T_o t + \frac{m_1}{\dot{m}_2} T_o \left\{ -\int_{-\lambda}^{\chi-\lambda} d\bar{X} + \int_{-\lambda}^{\chi-\lambda} \frac{(\beta_n+\gamma_n+\zeta)}{\kappa} \bar{X}\, d\bar{X} \right\}$$

$$= \frac{1}{2} \frac{m_1}{\dot{m}_2} T_o \frac{(\beta_n+\gamma_n+\zeta)}{\kappa} (\chi^2 - 2\chi\lambda) \tag{4-79}$$

Substitution of equation (4-79) into equation (4-71a) gives

$$\kappa(T-T_o) + (\chi-\lambda)[\gamma_n T + \beta_n T_o + (1-\kappa)\zeta T_o + (\kappa+\chi\mu-\lambda\mu)\zeta T$$

$$= \frac{HST_o}{2\dot{m}_2 C_{v_1}} \frac{(\beta_n+\gamma_n+\zeta)}{\kappa} (\chi^2 - 2\lambda\chi) \tag{4-80}$$

or after rearrange

$$T \approx T_o \frac{[\frac{\alpha}{\kappa}(\beta_n+\gamma_n+\zeta)(\chi^2-2\lambda\chi)+\kappa-(\chi-\lambda)\beta_n-(\chi-\lambda)(1-\kappa)\zeta]}{\kappa+(\chi-\lambda)\gamma_n+(\chi-\lambda)(\kappa+\chi\mu-\lambda\mu)\zeta} \tag{4-80a}$$

The accuracy of this approximate solution may be investigated by comparing equation (4-74) with equation (4-80a). These two equations differ by the amount

$$\frac{\frac{\alpha}{\kappa}(\beta_n+\gamma_n+\zeta)(\chi^2-2\lambda\chi)}{\kappa+(\chi-\lambda)\gamma_n+(\chi-\lambda)(\kappa+\chi\mu-\lambda\mu)\zeta} \tag{4-81}$$

Using the numerical values of section 4.4.3 and $\alpha \approx 1$, the numerator of equation (4-81) equals approximately to 0.001. The relative magnitude of this fraction compared to the numerator of equation (4-74) is

$$\frac{\frac{\alpha}{\kappa}(\beta_n+\gamma_n+\zeta)(\chi^2-2\lambda\chi)}{\kappa-(\chi-\lambda)\beta_n-(\chi-\lambda)(1-\kappa)\zeta} < 1\%$$

Since the denominator of both equations are the same, one can conclude that the approximation is satisfactory.

The corresponding formula for the pressure is obtained by eliminating T from equations (4-73) and (4-80a). This gives

$$P \sim P_o \left\{ 1-\kappa+ \frac{[\kappa+\mu(\chi-\lambda)][1-\beta_n\frac{(\chi-\lambda)}{\kappa} - \zeta\frac{(\chi-\lambda)}{\kappa} + \zeta(\chi-\lambda)+\alpha(\beta_n+\gamma_n+\zeta)\frac{(\chi-\lambda)^2}{\kappa^2}]}{[1 + \frac{\gamma_n}{\kappa}(\chi-\lambda) + (\chi-\lambda)\zeta + \mu\zeta\frac{(\chi-\lambda)^2}{\kappa}]} \right\}^*$$

$$\approx P_o\{1-(\chi-\lambda)(\gamma_n+\beta_n+\zeta-\mu) + (\chi-\lambda)^2\zeta(\beta_n+\zeta-\gamma_n-\mu)$$

$$+ \frac{(\chi-\lambda)^2}{\kappa}(\beta_n+\gamma_n+\zeta)(\alpha+\gamma_n-\mu)\} \qquad (4\text{-}82)$$

Equation (4-82) is the approximation of the actual evaporation chamber pressure during fuel injection, developed for a non-ideal gas.

---

*When λ and $\alpha = 0$, this equation simply gives the hypothetical pressure as specified by equation (4-28).

To obtain a formula for the lifetime of the spray, we equate the theoretical and experimental quantities in the following form:

$$-(P-P_n')/\frac{dp}{d\chi}$$

the theoretical part is derived by making use of equations (4-28) and (4-82) and then solve the resulting equation for λ.

Let $$\phi'' = \gamma_n + \beta_n + \zeta - \mu$$

Equation (4-82) becomes

$$P \approx P_o\{1-\phi''\chi+\phi''\lambda + (\chi-\lambda)^2\zeta(\phi''-2\gamma_n) + \frac{(\chi-\lambda)^2}{\kappa}(\phi''+\mu)(\alpha+\gamma_n-\mu)\} \tag{4-82a}$$

$$\frac{dp}{d\chi} \approx P_o\{-\phi''+2(\chi-\lambda)\zeta(\phi''-2\gamma_n) + 2(\chi-\lambda)\frac{(\phi''+\mu)}{\kappa}(\alpha+\gamma_n-\mu)\} \tag{4-83}$$

Making the similar substitutions and rearranging, equation (4-28) becomes

$$P_n' \approx P_o\{1 - \phi''\chi-(\zeta+\beta_n)\mu\frac{\chi^2}{\kappa} + (\gamma_n+\zeta)\phi''\frac{\chi^2}{\kappa}\} \tag{4-28a}$$

From equations (4-28a), (4-82a) and (4-83), one has

$$-\frac{P-P_n'}{\frac{dp}{d\chi}} = \frac{\{\lambda\phi''+(\chi-\lambda)^2\zeta(\phi''-2\gamma_n)+[(\zeta+\beta_n)\mu-(\gamma_n+\zeta)\phi'']\frac{\chi^2}{\kappa} + (\phi''+\mu)(\alpha+\gamma_n-\mu)\frac{(\chi-\lambda)^2}{\kappa}}{\phi'' - 2(\chi-\lambda)\zeta(\phi''-2\gamma_n) - 2(\chi-\lambda)\frac{(\phi''+\mu)}{\kappa}(\alpha+\gamma_n-\mu)}$$

$$\approx \{\lambda+(\chi-\lambda)^2\zeta(1-\frac{2\gamma_n}{\phi''}) + (\zeta+\beta_n)\frac{\mu}{\phi''}\frac{\chi^2}{\kappa} - (\gamma_n+\zeta)\frac{\chi^2}{\kappa} + (1+\frac{\mu}{\phi''})(\alpha+\gamma_n-\mu)\frac{(\chi-\lambda)^2}{\kappa}\}$$

$$\{1+2(\chi-\lambda)\zeta(1-\frac{2\gamma_n}{\phi''}) + \frac{2(\chi-\lambda)}{\kappa}(\alpha+\gamma_n-\mu)(1+\frac{\mu}{\phi''})\}$$

$$\approx \lambda + \frac{\alpha(\gamma_n+\beta_n+\zeta)}{(\gamma_n+\beta_n+\zeta-\mu)}\frac{\chi^2}{\kappa} + \zeta\chi^2\left[\frac{(\beta_n+\zeta-\gamma_n-\mu)}{(\gamma_n+\beta_n+\zeta-\mu)} - \frac{1}{\kappa}\right] \quad (4-84)$$

or

$$0.4t_L \approx -\frac{P-P_n'}{\frac{dp}{dt}} - \frac{\alpha m_1(\gamma_n+\beta_n+\zeta)\chi^2}{\kappa\dot{m}_2(\gamma_n+\beta_n+\zeta-\mu)} - \zeta\chi^2\frac{m_1}{\dot{m}_2}\left[\frac{(\beta_n+\zeta-\gamma_n-\mu)}{(\gamma_n+\beta_n+\zeta-\mu)} - \frac{1}{\kappa}\right] \quad (4-85)$$

Equation (4-85) gives the lifetime of the spray when the fuel vapour is considered as a non-ideal gas. All quantities on the right hand side of equation (4-85), except P_n', and κ are to be determined from experimental data.

4.7 Conditions during the Transition Period

We shall now consider conditions between the end of injection and complete evaporation of all droplets. We choose the end of injection as our new time origin so that during the transition period we have

$$0 < t < t_L$$

At the time t = 0, the total mass of liquid droplets present in the evaporation chamber is given by equation (4-35). These droplets, of course, are by no means of uniform size but differ in size according to their age t'. Their age distribution is given by equation (4-33)

$$dm^{(\ell)} = \dot{m}_2\left(1 - \frac{t'}{t_L}\right)^{3/2} dt' \qquad (4\text{-}33)$$

At time t after the end of injection, this amount will have decreased to

$$dm^{(\ell)} = \dot{m}_2\left[1 - \frac{(t'+t)}{t_L}\right]^{3/2} dt' \qquad (4\text{-}86)$$

and the total amount of liquid at this time will be

$$m^{(\ell)} = \int_{t'=0}^{t'=t_L-t} dm^{(\ell)} = \frac{2}{5}\,\dot{m}_2 t_L\left(1 - \frac{t}{t_L}\right)^{5/2} \qquad (4\text{-}87)$$

The rate of droplet evaporation during the transition period is therefore,

$$\frac{dm^{(\ell)}}{dt} = - \dot{m}_2 (1 - \frac{t}{t_L})^{3/2} \qquad (4\text{-}88)$$

and a corresponding amount of energy is needed to vaporize these droplets.

Making the same simplifying assumptions as outlined at the beginning of section 4.6, one can now write the energy balance for a time element, dt.

4.7.1 Case I. Fuel vapour is considered an ideal gas

From equations (4-6), (4-10) and (4-12a), the energy balance equation for an ideal gas is:

$$\{m_1' C_{v_1} + [m_{2f} - 0.4\dot{m}_2 t_L(1 - \frac{t}{t_L})^{5/2}](\bar{C}p_2 - \frac{R}{M_2})\}$$

$$dT + \dot{m}_2(1 - \frac{t}{t_L})^{3/2}(C_{v_1} T_o \beta_i + \bar{C}p_2 T - \frac{RT}{M_2})dt = HS(T_o - T)dt \qquad (4\text{-}89)$$

Here, m_{2f} is the total amount of fuel injected into the chamber.

We now introduce a new dimensionless variable

$$u = \sqrt{1 - t'/t_L} \qquad (1 > u > o) \qquad (4\text{-}90)$$

Then, equation (4-89) assumes the form

$$\frac{dT}{du} - f_{11}(u)T = - f_{12}(u)T_o \qquad (4\text{-}91)$$

where

$$f_{11}(u) = \varepsilon_i \frac{u + 5\sigma_i u^4}{1 - \varepsilon_i \sigma_i u^5} \approx \varepsilon_i(u + 5\sigma_i u^4) + \varepsilon_i^2(\sigma_i u^6 + 5\sigma_i^2 u^9) \qquad (4\text{-}92a)$$

$$f_{12}(u) = \varepsilon_i \frac{u - 5\tau_i u^4}{1 - \varepsilon_i \sigma_i u^5} \approx \varepsilon_i(u - 5\tau_i u^4) + \varepsilon_i^2(\sigma_i u^6 - 5\sigma_i \tau_i u^9) \qquad (4\text{-}92b)$$

$$\varepsilon_i = \frac{2HSt_L}{m_1 C_{v_1}(\kappa + \gamma_i \chi_f)} = \frac{10\lambda\alpha}{\kappa + \gamma_i \chi_f} \qquad (4\text{-}93a)$$

$$\sigma_i = 0.2\ \dot{m}_2(\bar{C}p_2 - \frac{R}{M_2})/HS = 0.1\ \gamma_i/\alpha \qquad (4\text{-}93b)$$

$$\tau_i = 0.2\ \beta_i \dot{m}_2 C_{v_1}/HS = 0.1\ \beta_i/\alpha \qquad (4\text{-}93c)$$

$$\chi_f = \frac{m_{2f}}{m_1} \qquad (4\text{-}93d)$$

Note that $\varepsilon_i << 1$ so that series expansion by powers of ε_i can be used. Then the solution of equation (4-91) is

$$\frac{T}{T_o} = C+[(C-1)\frac{u^2}{2} + (C\sigma_i+\tau_i)u^5]\varepsilon_i+[(C - \tfrac{1}{2})\frac{u^4}{4} + (16C\sigma_i-7\sigma_i+2\tau_i)\frac{u^7}{14}$$

$$+ (\frac{3C}{2}\ \sigma_i+\tau_i)\sigma_i u^{10}]\varepsilon_i^2 \qquad (4\text{-}94)$$

where C is an integration constant.

Equation (4-94) can be verified by substituting back into the original differential equation (4-91). It is found that the solution is accurate to the second order in ε_i.

For the corresponding pressure, by modifying equation (4-63)

$$P = P_o\{(1-\kappa) + [\kappa+\mu(\chi_f-\lambda u^5)]\frac{T}{T_o}\} \qquad (4\text{-}95)$$

Here, λu^5 is the liquid mass remaining at time t after injection and is derived from equations (4-87) and (4-90). Substituting equation (4-94) into equation (4-95) and neglecting terms with ε_i^2, one finds

$$\frac{P}{P_o} \approx (1-\kappa)+[(\kappa+\mu\chi_f)-\mu\lambda u^5]\{C+[(C-1)\frac{u^2}{2} + (C\sigma_i+\tau_i)u^5]\varepsilon_i\} \tag{4-96}$$

The constant C can be determined from the initial condition:

For $$t = o \; ; \quad u = 1 \; ; \quad P = P_f \; ,$$

where P_f is known from the experimental pressure-time curve and equals the pressure at the exact moment when fuel injection is terminated. Apply the initial condition to equation (4-96) and solve for C gives

$$C = \frac{[(\frac{P_f}{P_o} + \kappa-1)/(\kappa+\mu\chi_f-\mu\lambda)] + (\frac{1}{2} - \tau_i)\varepsilon_i}{1 + \varepsilon_i(\frac{1}{2} + \sigma_i)} \tag{4-97}$$

or

$$C \approx \left[\frac{(\frac{P_f}{P_o}) + \kappa-1}{\kappa+\mu\chi_f-\mu\lambda} + (\frac{1}{2} - \tau_i)\varepsilon_i\right][1-\varepsilon_i(\frac{1}{2} + \sigma_i)] \tag{4-98}$$

Neglecting second order terms in ε_i gives

$$C \approx \frac{(\frac{P_f}{P_o}) + \kappa-1}{\kappa+\mu\chi_f-\mu\lambda} + \varepsilon_i\left[(\frac{1}{2} - \tau_i) - (\frac{1}{2} + \sigma_i)\frac{(\frac{P_f}{P_o}) + \kappa-1}{\kappa+\mu\chi_f-\mu\lambda}\right] \tag{4-99}$$

Substituting equation (4-99) into equation (4-96) gives

$$\frac{P}{P_o} \approx (1-\kappa) + [\kappa+\mu\chi_f-\mu\lambda u^5]\left\{\frac{(\frac{P_f}{P_o}) + \kappa-1}{\kappa+\mu\chi_f-\mu\lambda} + \right.$$

$$+ \varepsilon_i\left[(\tfrac{1}{2} - \tau_i)-(\tfrac{1}{2} + \sigma_i)\frac{(\frac{P_f}{P_o}) + \kappa-1}{\kappa+\mu\chi_f-\mu\lambda}\right]$$

$$\left. + \left[\frac{(\frac{P_f}{P_o}) + \kappa-1}{\kappa+\mu\chi_f-\mu\lambda} - 1\right]\frac{u^2}{2}\,\varepsilon_i + \left[\frac{(\frac{P_f}{P_o}) + \kappa-1}{\kappa+\mu\chi_f-\mu\lambda}\,\sigma_i+\tau_i\right]u^5\varepsilon_i\right\}$$

(4-100)

In the derivation of equation (4-100), all terms containing ε_i^2 have been neglected.

Now,

$$\frac{\kappa+\mu\chi_f-\mu\lambda u^5}{\kappa+\mu\chi_f-\mu\lambda} = \frac{1-\mu\lambda u^5/(\kappa+\mu\chi_f)}{1-\mu\lambda/(\kappa+\mu\chi_f)} \approx 1 + \frac{\mu\lambda}{\kappa+\mu\chi_f}\,(1-u^5)$$

(4-101)

Making use of equation (4-101) and nelgecting terms containing $\lambda\varepsilon_i$, equation (4-100) becomes

$$\frac{P}{P_o} \approx (1-\kappa)+\left[1 + \frac{\mu\lambda(1-u^5)}{\kappa+\mu\chi_f}\right]\left[\frac{P_f}{P_o} + \kappa-1\right]-\left[\frac{P_f}{P_o} + \kappa-1\right](\tfrac{1}{2} + \sigma_i)$$

$$\varepsilon_i + (\kappa+\mu\chi_f)(\tfrac{1}{2} - \tau_i)\varepsilon_i$$

$$+ \left[\left[\frac{P_f}{P_o} + \kappa-1\right]-(\kappa+\mu\chi_f)\right]\frac{u^2}{2}\,\varepsilon_i+\left[\left[\frac{P_f}{P_o} + \kappa-1\right]\sigma_i+(\kappa+\mu\chi_f)\tau_i\right]\varepsilon_i u^5$$

(4-102)

Rearranging equation (4-102) gives

$$\frac{P}{P_o} = \frac{P_f}{P_o} - \varepsilon_i \left\{ \left[\frac{P_f}{P_o} + \kappa - 1 \right] \left[\left(\omega_i + \frac{1}{2}\right) - \left(\omega_i u^5 + \frac{u^2}{2}\right) \right] + \right.$$

$$\left. + (\kappa + \mu\chi_f) \left[\left(\tau_i - \frac{1}{2}\right) - \left(\tau_i u^5 - \frac{u^2}{2}\right) \right] \right\} \qquad (4\text{-}103)$$

where $$\omega_i = \sigma_i - \lambda\mu/\varepsilon_i(\kappa+\mu\chi_f) = 0.1(\gamma_i - \mu)\kappa/\alpha(\kappa+\mu\chi_f) \qquad (4\text{-}104)$$

Letting (dP/du) = 0 gives an equation for u_m, i.e. the value of u corresponding to the minimum pressure, P_m. At this point, the physical phenomenon is such that the heat lost by the hot gas and vapor mixture to the evaporating droplets equals the heat gained by the mixture from the chamber wall. Differentiating P in equation (4-103) with respect to u and setting dP/du = 0, one finds after simplifying

$$u_{m_i} = \left\{ \frac{1 - \frac{P_f}{P_o} + \mu\chi_f}{5\left[\omega_i\left(\frac{P_f}{P_o} + \kappa - 1\right) + \tau_i(\kappa+\mu\chi_f)\right]} \right\}^{1/3} \qquad (4\text{-}105)$$

Substituting u_m into equation (4-103) gives

$$\frac{P_m}{P_o} = \frac{P_f}{P_o} - \varepsilon_i \Bigg\{ \left(\frac{P_f}{P_o} + \kappa - 1\right)\left(\omega_i + \frac{1}{2}\right) + (\kappa + \mu\chi_f)\left(\tau_i - \frac{1}{2}\right) -$$

$$- \left(\frac{P_f}{P_o} + \kappa - 1\right)\left(\omega_i u_{m_i}^3 + \frac{1}{2}\right) u_{m_i}^2 - (\kappa + \mu\chi_f)\left(\tau_i u_{m_i}^3 - \frac{1}{2}\right) u_{m_i}^2 \Bigg\}$$

$$= \frac{P_f}{P_o} - \varepsilon_i \Bigg\{ \omega_i \left(\frac{P_f}{P_o} + \kappa - 1\right) + (\kappa + \mu\chi_f)(\tau_i) -$$

$$- \frac{1}{2}\left(1 - \frac{P_f}{P_o} + \mu\chi_f\right) + \frac{1}{2}\left(1 - \frac{P_f}{P_o} + \mu\chi_f\right) u_{m_i}^2$$

$$- u_{m_i}^2 \left[\left(\frac{P_f}{P_o} + \kappa - 1\right)\omega_i + (\kappa + \mu\chi_f)\tau_i \right] u_{m_i}^3 \Bigg\} \qquad (4\text{-}106)$$

But

$$u_{m_i}^2 \left[\left(\frac{P_f}{P_o} + \kappa - 1\right)\omega_i + (\kappa + \mu\chi_f)\tau_i \right] u_{m_i}^3 = 0.2\left(1 - \frac{P_f}{P_o} + \mu\chi_f\right) u_{m_i}^2$$

Therefore, equation (4-106) becomes

$$\frac{P_m}{P_o} = \frac{P_f}{P_o} - \varepsilon_i \left[\omega_i \left(\frac{P_f}{P_o} + \kappa - 1\right) + \tau_i (\kappa + \mu\chi_f) + \left(0.3 u_{m_i}^2 - \frac{1}{2}\right)\left(1 - \frac{P_f}{P_o} + \mu\chi_f\right) \right] \qquad (4\text{-}106a)$$

Substituting from equations (4-93's) and (4-104) and noting that

$$1 - \frac{P_f}{P_o} \ll 1 \quad , \quad \text{and} \quad \chi_f \ll 1$$

and that the product of these quantities can be neglected, one finally obtains

$$\frac{1}{\lambda} \cdot \frac{P_f - P_m}{P_o} = (\beta_i + \gamma_i - \mu) - \frac{(\gamma_i - \mu)}{\kappa} \left[(\beta_i + \gamma_i)\chi_f + (1 - \frac{P_f}{P_o} + \mu\chi_f) \right] + \\ + \frac{\alpha}{\kappa} (3u_{m_i}^2 - 5)(1 - \frac{P_f}{P_o} + \mu\chi_f) \qquad (4\text{-}107)$$

and

$$u_{m_i} = \left\{ \frac{2\alpha(1 - \frac{P_f}{P_o} + \mu\chi_f)}{(\beta_i + \gamma_i - \mu)\kappa + \beta_i \mu\chi_f - (\gamma_i - \mu)(1 - \frac{P_f}{P_o} + \mu\chi_f)} \right\}^{1/3} \qquad (4\text{-}108)$$

Equation (4-107) can be used for the calculation of λ which is proportional to t_L. It will be noted that κ only occurs in small correction terms. This means that the distribution of spray droplets has only a minor influence on the minimum pressure attained. In a first approximation, one has

$$\lambda \approx (P_f - P_m)/P_o(\beta_i + \gamma_i - \mu) \qquad (4\text{-}109)$$

The influence of heat transfer is expressed by α and it will be noted that, according to equation (4-108), $u_m \approx 0$, i.e. $t_m \approx t_L$ if $\alpha \approx 0$. (Where t_m is the time corresponding to minimum pressure; the approximate signs are used because equation (4-108) is not exact.) This is as expected because in the absence of substantial heat transfer the chamber pressure will decrease until the last droplets

have been vaporized.

Determination of the lifetime t_L from equation (4-107) will probably be less accurate and reliable than from equation (4-69d) because of the small value of the ratio between the difference of P_f and P_m to the initial chamber pressure. However, the two determinations can be compared.

Theoretically t_L could also be calculated from u_m (equation 4-108) since $u_m = \sqrt{1 - t_m/t_L}$. However, a satisfactory result cannot be expected from this because the minimum of P will be rather flat so that it is difficult to find t_m from the experimental pressure-time curve. Moreover, the fact that the droplets are not really of uniform size at the moment of injection tends to further falsify the result since a few large droplets will persist longer than the rest.

At the end of droplet evaporation, i.e. at time t_L after fuel injection is terminated, $u = 0$, and $P = P_{e_i}$ where P_{e_i} is the pressure at the end of complete droplet evaporation. Applying these conditions to equation (4-103) gives

$$\frac{P_{e_i}}{P_o} = \frac{P_f}{P_o} - \varepsilon_i\left[\left(\frac{P_f}{P_o} + \kappa - 1\right)\left(\omega_i + \frac{1}{2}\right) + (\kappa + \mu\chi_f)\left(\tau_i - \frac{1}{2}\right)\right]$$

$$= \frac{P_f}{P_o} - \varepsilon_i\left[\omega_i\left(\frac{P_f}{P_o} + \kappa - 1\right) + \tau_i(\kappa + \mu\chi_f) - \frac{1}{2}\left(1 - \frac{P_f}{P_o} + \mu\chi_f\right)\right] \qquad (4\text{-}110)$$

If equation (4-106a) is subtracted from equation (4-110), one obtains

$$\frac{P_{e_i} - P_m}{P_o} = 0.3\, u_{m_i}^2 \left(1 - \frac{P_f}{P_o} + \mu \chi_f\right) \qquad (4\text{-}111)$$

Equation (4-111) shows that the pressure at the end of droplet evaporation is higher than the minimum pressure because the right-hand side of equation (4-111) is positive. This is to be expected because of the influence of heat transfer.

4.7.2 Case II. Fuel vapour is considered a non-ideal gas

When the fuel vapour is considered a non-ideal gas, the energy balance equation, obtained from equations (4-1), (4-4), (4-22b), (4-48), (4-49), and (4-87), is:

$$\{m_1' + [m_{2f} - .4\dot{m}_2 t_L(1 - \frac{t}{t_L})^{5/2}][\gamma_n + \frac{bP_o}{C_{v_1}T_o}(\kappa+\chi_f\mu) - \frac{bP_o}{C_{v_1}T_o}\lambda\mu(1 - \frac{t}{t_L})^{5/2}]\}dT$$

$$+ \dot{m}_2(1 - \frac{t}{t_L})^{3/2}\{[\gamma_n T + \frac{bP_o}{C_{v_1}T_o}(\kappa+\chi_f\mu)T - \frac{bP_o}{C_{v_1}T_o}\lambda\mu(1 - \frac{t}{t_L})^{5/2}T] +$$

$$+ [\beta_n T_o + \frac{bP_o}{C_{v_1}T_o}(1-\kappa)T_o]\}dt = \frac{HS}{C_{v_1}}(T_o - T)dt \qquad (4\text{-}112)$$

Making use of equations (4-26b), (4-90) and divide by m_1, equation (4-112) becomes

$$\{\kappa + (\chi_f - \lambda u^5)[\gamma_n + \zeta(\kappa+\chi_f\mu) - \zeta\lambda\mu u^5]\}dT$$

$$- 5\lambda u^4[\gamma_n + \zeta(\kappa+\chi_f\mu) - \zeta\lambda\mu u^5]Tdu$$

$$- 5\lambda u^4[\beta_n+\zeta(1-\kappa)]T_o\,du = -10\lambda\alpha u(T_o - T)du \qquad (4\text{-}112a)$$

Let

$$\lambda^* = \lambda/\kappa; \quad \gamma_n'' = \gamma_n+\zeta(\kappa+\chi_f\mu); \quad \zeta'' = \zeta\lambda\mu; \quad \beta_n'' = \beta_n+\zeta(1-\kappa) \tag{4-113}$$

equation (4-112a) becomes

$$[1 + (\chi_f'-\lambda^*u^5)(\gamma_n''-\zeta''u^5)]d\left(\frac{T}{T_o}\right) - 5\lambda^*(2\alpha u+\gamma_n''u^4-\zeta''u^9)\left(\frac{T}{T_o}\right)du = 5\lambda^*(\beta_n''u^4-2\alpha u)du \tag{4-114}$$

or

$$\frac{d\left(\frac{T}{T_o}\right)}{du} - \frac{5\lambda^*(2\alpha u+\gamma_n''u^4-\zeta''u^9)}{[1 + \chi_f'\gamma_n''-(\chi_f'\zeta''+\gamma_n''\lambda^*)u^5+\lambda^*\zeta''u^{10}]}\left(\frac{T}{T_o}\right) = \frac{5\lambda^*(\beta_n''u^4-2\alpha u)}{[1 + \chi_f'\gamma_n''-(\chi_f'\zeta''+\gamma_n''\lambda^*)u^5+\lambda^*\zeta''u^{10}]} \tag{4-114a}$$

Equation (4-114a) is again a linear equation of the first order. The solution is:

$$\frac{T}{T_o} = C_n + [(C_n-1)\frac{u^2}{2} + (C_n\sigma_n+\tau_n)u^5-\alpha''C_nu^{10}]\varepsilon_n + [(C_n - \tfrac{1}{2})\frac{u^4}{4} + (16C_n\sigma_n+2\tau_n-7\sigma_n)\frac{u^7}{14} + (\tfrac{3}{2}C_n\sigma_n+\tau_n)\sigma_nu^{10}]\varepsilon_n^2 \tag{4-115}$$

where

$$\varepsilon_n = \frac{10\lambda^*\alpha}{1 + \chi_f'\gamma_n''} \tag{4-116a}$$

$$\sigma_n = \frac{0.1\ \gamma_n''}{\alpha} \qquad (4\text{-}116b)$$

$$\tau_n = \frac{0.1\ \beta_n''}{\alpha} \qquad (4\text{-}116c)$$

$$\alpha'' = \frac{\lambda\zeta\mu}{20\alpha} \qquad (4\text{-}116d)$$

and C_n is an integration constant.

The corresponding pressure is obtained by substituting equation (4-115) into equation (4-95) to give (neglecting ε_n^2 and λ^2 terms):

$$\frac{P}{P_o} \approx (1-\kappa)+[\kappa+\mu(\chi_f-\lambda u^5)]\{C_n+[(C_n-1)\frac{u^2}{2} + (C_n\sigma_n+\tau_n)u^5]\varepsilon_n\} \qquad (4\text{-}117)$$

Apply the initial conditions:

$$t = o\ ;\quad u = 1\ ;\quad P = P_f \text{ (from experimental result)} \qquad (4\text{-}118)$$

equation (4-117) gives

$$C_n = \frac{[(\frac{P_f}{P_o} + \kappa-1)/(\kappa+\mu\chi_f-\mu\lambda)]+(\frac{1}{2} - \tau_n)\varepsilon_n}{1 + \varepsilon_n(\frac{1}{2} + \sigma_n)} \qquad (4\text{-}119)$$

Neglecting second order terms in ε_n gives

$$C_n \approx \frac{(\frac{P_f}{P_o})+\kappa-1}{\kappa+\mu\chi_f-\mu\lambda} + \varepsilon_n\left[(\frac{1}{2} - \tau_n)-(\frac{1}{2} + \sigma_n)\ \frac{(\frac{P_f}{P_o})+\kappa-1}{\kappa+\mu\chi_f-\mu\lambda}\right] \qquad (4\text{-}120)$$

Substituting equation (4-120) into equation (4-117) gives (neglecting ε_n^2 terms)

$$\frac{P}{P_o} \approx (1-\kappa)+[\kappa+\mu(\chi_f-\lambda u^5)]\left\{\frac{(\frac{P_f}{P_o})+\kappa-1}{\kappa+\mu\chi_f-\mu\lambda} + \varepsilon_n\left[(\tfrac{1}{2}-\tau_n)+(\tfrac{1}{2}+\sigma_n)\frac{(\frac{P_f}{P_o})+\kappa-1}{\kappa+\mu\chi_f-\mu\lambda}\right]\right.$$

$$\left. + \left[\frac{(\frac{P_f}{P_o})+\kappa-1}{\kappa+\mu\chi_f-\mu\lambda} - 1\right]\frac{u^2}{2}\varepsilon_n + \left[\frac{(\frac{P_f}{P_o})+\kappa-1}{\kappa+\mu\chi_f-\mu\lambda}\sigma_n+\tau_n\right]u^5\varepsilon_n\right\} \quad (4\text{-}121)$$

Equation (4-121) can be seen to be identical to equation (4-100) except for the constants ε, σ, τ. Therefore, by performing the same operations as shown in section (4.7.1), one finally obtains

$$\frac{1}{\lambda}\frac{P_f-P_m}{P_o} = (\beta_n''+\gamma_n''-\mu) - \frac{(\gamma_n''-\mu)}{\kappa}[(\beta_n''+\gamma_n'')\chi_f+(1-\frac{P_f}{P_o}+\mu\chi_f)]$$

$$+ \frac{\alpha}{\kappa}(3u_{m_n}^2-5)(1-\frac{P_f}{P_o}+\mu\chi_f) \quad (4\text{-}122)$$

and

$$u_{m_n} = \left\{\frac{2\alpha(1-\frac{P_f}{P_o}+\mu\chi_f)}{(\beta_n''+\gamma_n''-\mu)\kappa+\beta_n''\mu\chi_f-(\gamma_n''-\mu)(1-\frac{P_f}{P_o}+\mu\chi_f)}\right\}^{1/3} \quad (4\text{-}123)$$

Equation (4-122) gives an alternative expression for the calculation of t_L. However, $(P_f-P_m)/P_o$ is very small and determination of t_L from equation (4-122) will not be accurate enough.

The pressure difference between the end of liquid fuel evaporation and the minimum is given by

$$\frac{P_{e_n}-P_m}{P_o} = 0.3\ u_{m_n}^2\ \left(1 - \frac{P_f}{P_o} + \mu\chi_f\right) \qquad (4\text{-}124)$$

4.8 The Warm-up Period

After all injected fuel has been vaporized, a slow warm-up period follows during which the gas temperature gradually approaches the temperature of the evaporation chamber wall which has been assumed to remain constant and equal to the initial temperature, T_o. Furthermore, it can be assumed that - at least during the later part of the period - the gas temperature will be uniform so that

$$m_1' \approx m_1 \quad \text{and} \quad \kappa \approx 1 \ .$$

4.8.1 Case I. Fuel Vapour is considered an ideal gas

One has from the energy balance

$$[m_1 C_{v_1} + m_{2f}(\bar{C}p_2 - \frac{R}{M_2})]dT = HS(T_o - T)dt \qquad (4\text{-}125)$$

The solution of equation (4-125) is

$$T_o - T = (T_o - T_r)\exp[-(t-t_r)/B_i] \qquad (4\text{-}126)$$

where the subscript r refers to a reference point and

$$B_i = [m_1 C_{v_1} + m_{2f}(\bar{C}p_2 - \frac{R}{M_2})]/HS \qquad (4\text{-}127)$$

Further, from equations (4-1) and (4-2), it follows that

$$P = P_o\,(1 + \mu\chi_f)T/T_o \qquad (4\text{-}128)$$

Using equations (4-126) and (4-128) and eliminating all temperatures gives

$$P_o(1+\mu\chi_f) - P = [P_o(1+\mu\chi_f) - P_r]\exp[-(t-t_r)/B_i] \qquad (4\text{-}129)$$

For $t \to \infty$, we have $T \to T_o$, and

$$P = P_\infty = P_o(1+\mu\chi_f) \qquad (4\text{-}130)$$

so that equation (4-129) assumes the form

$$P_\infty - P = (P_\infty - P_r)\exp[-(t-t_r)/B_i] \qquad (4\text{-}131)$$

The constant B_i can be determined from the experimental pressure-time curve and the constant α which has been used in the preceding sections is then calculated by the formula (derived from formulae 4-53a and 4-127).

$$\alpha = \frac{m_1}{2\dot{m}_2} \cdot \frac{(1+\gamma_i \chi_f)}{B_i} \qquad (4\text{-}132)$$

4.8.2 Case II. Fuel Vapour is considered a non-ideal gas

The energy balance equation is:

$$[m_1 C_{v_1} + m_{2f}(\gamma_n + \zeta + \zeta\chi_f\mu)]dT = HS(T_o - T)dt \qquad (4\text{-}133)$$

The solution of equation (4-133) is

$$T_o - T = (T_o - T_r)\exp[-(t-t_r)/B_n] \qquad (4\text{-}134)$$

where

$$B_n = \frac{[m_1 C_{v_1} + m_{2f}(\gamma_n + \zeta + \zeta\chi_f\mu)]}{HS} \qquad (4\text{-}135)$$

Expressed in terms of pressures, equation (4-134) becomes

$$P_\infty - P = (P_\infty - P_r)\exp[-(t-t_r)/B_n] \qquad (4\text{-}136)$$

where the constant B_n is to be determined from the experimental pressure vs. time curve. α is then given by

$$\alpha = \frac{m_1}{2m_2} \cdot \frac{[1 + \chi_f(\gamma_n + \zeta + \zeta\chi_f\mu)]}{B_n} \qquad (4\text{-}137)$$

CHAPTER V

SPRAY EVAPORATION.

Experimental Study, Methods and Apparatus.

5.1 Description of phenomenon and outline of study

Spray evaporation experiments were conducted by injecting a predetermined mass of liquid fuels of single molecular species into a high temperature and high pressure evaporation chamber. Only solid cone sprays* were investigated in this study. For this particular spray configuration, a temperature gradient exists during fuel evaporation. The temperature at the center core of the spray cone is a minimum and increases outward to the conic surface. Because of this temperature gradient and the inherent slow response in measuring temperatures, it is considered impractical and meaningless to measure the temperature of the mixture. On the other hand, variations in pressure propagate uniformly and rapidly throughout the system. Since pressures and temperatures can be related by expressions in the theoretical analysis (see Chapter IV), it was decided to measure pressure as a function of time and relate it to the injected mass of fuel. Consequently, analytical formulae were developed in terms of pressures.

---

*A solid cone spray is one in which the droplets forming the spray are distributed throughout the entire conical volume of the spray.

The object of the experimental investigation is to verify the validity of the concept and the soundness of the proposed method. Data required from these experiments are the pressure change as a function of time and injected fuel mass during the spray evaporation process. From these experimental data, the evaporation lag and the lifetime of the spray can be determined.

Two groups of experiments were needed for each fixed set of initial conditions in order to provide the required data. The first group provides data on pressure change during spray evaporation. The second group consists of identical experiments at much reduced sweep speed of the oscilloscope light beams. As a result, the pressure drop portion (this portion of the pressure curve is recorded in the first group of experiments) of the pressure vs. time curve is compressed. Emphasis is placed on the pressure rise portion of the curve. From the second group of experiments, heat transfer between the chamber wall and the vapour-gas mixture during spray evaporation can be estimated. This information on the heat transfer characteristics of the equipment is necessary in the determination of spray lifetime.

The remainder of this chapter is divided in the following way. In section 5-2, details on the selection of experimental parameters are given. A description of the experimental apparatus is given in section 5-3. Section 5-4

contains information on instrumentation and the calibration of various instruments. Experimental procedures are given in section 5-5. These procedures follow a definite logical sequence.

5.2 Experimental Details

Fuel: Ethyl alcohol and water (Distilled)

They were chosen for this study because their physical properties are well known. Table (5-1) in appendix G gives some selected physical properties of ethyl alcohol (refs. 4.2,5.1). Similar properties for water are readily available in the literature.

Inert gas: Nitrogen.

Nitrogen gas was chosen for pressurizing the evaporation chamber. It is relatively inexpensive, readily available, prevents combustion of the fuel and its physical properties are well known (ref.4-3).

Initial Evaporation Chamber Temperature and Pressure:

Selection of initial evaporation chamber temperature and pressure combination is limited by the strength of the material used. With a fair margin of safety, six sets of initial temperature and pressure combinations for the present investigation were chosen to be:

900°F	400 psig.
800°F	400 psig, 450 psig.
700°F	400 psig, 450 psig, 500 psig.

The maximum design temperature was 1000°F and the corresponding maximum design pressure was 600 psig. Above 1000°F, the strength of stainless steel 310 drops rapidly.

Other criteria in the selection of initial temperatures were: a). the initial evaporation chamber temperature should be well above the critical temperature of the fuel, b). the heat capacity of the nitrogen gas in the chamber at that temperature should be large enough to evaporate all the injected fuel in a reasonably short time without a large temperature drop.

Additional criteria governing the selection of initial pressures were: a). the pressure change due to fuel evaporation should be small compared to the initial evaporation chamber pressure, b). the initial evaporation chamber pressure should be as high as feasible to ensure a fairly uniform spray droplet size and a fine spray. This includes pressures near to or above the critical pressure of the fuel.

Injection Pressure: $\sim$ 200 psid.

The pressure drop across the injector-plate was chosen to be roughly 200 psid. This pressure differential has been observed to give a fine spray.

Injector-Plates: 8 and 16-hole self-impinging injector-plate and a single hole injector-plate. They all have the same opening area.

The 8 and 16-hole self-impinging injector-plate produce a fine solid spray cone of 60° angle. The size of the holes is 0.021 and 0.015 in.diameter respectively

and the holes are drilled at an angle of 30 degrees to the axis so that all liquid jets converge into an apex 1/4 in. above the injector-plate. A single hole injector-plate was also used because of its known relatively poor atomization characteristics.

Maximum total Liquid Fuel Mass injected: $\sim$ 18 and 23.4 grams.

The total liquid fuel mass injected was arbitrarily chosen to be 18 grams for ethyl alcohol and 23.4 grams for water. Calibration of the injection system has indicated that the actual quantity was 18.091 grams for ethyl alcohol. These masses should produce a pressure decrease of roughly 12 and 18 psia respectively in the evaporation chamber. This corresponds to a maximum pressure decrease of 3% to 4.5% of the initial pressure. Because the evaporation process was assumed to be quasisteady, the pressure change was kept as low as practically reasonable.

A second consideration was to keep χ (the ratio of the total liquid fuel mass injected to the mass of inert gas in the evaporation chamber) small because one of the assumptions in the analysis was that χ was small compared to unity ($\chi << 1$).

Other quantities of injected fuel masses were also used in the present study.

5.3 Description of Apparatus

Figures (5-1) to (5-6) in Appendix B show the details of the experimental apparatus. Figure (5-1) illustrates the layout of the apparatus assembly. A Blue-M electric furnace is used to heat the evaporation chamber to the predetermined temperature. The furnace is thermostatically controlled and the evaporation chamber temperature is measured by a thermometer which is inserted through an opening in the furnace wall.

The evaporation chamber is 14 inches inside diameter, 16 1/2 inches outside diameter, and 32 inches high inside. It is made of 310 stainless steel and the top and bottom pieces were welded on to the cylindrical body. It was hydrostatically tested to 1300 psig at room temperature.

Figure (5-2) shows the liquid fuel injection system. This system is connected to the evaporation chamber. The upper flange of the injector nozzle is bolted to the bottom dome of the evaporation chamber with the injector nozzle pointing upward. This configuration in effect doubled the effective evaporation chamber length. When a liquid droplet moves upward and stops short of the wall, it will fall towards the bottom of the chamber. This gives a longer available evaporation path to the droplet. A second advantage of this arrangement is that the liquid fuel reservoir can be left open to the evaporation chamber at all times.

To seal against gas leakage at the joint between the evaporation chamber and the injector nozzle, a pressurized silver-coated stainless steel metal O-ring is used. For all other metal-metal joints, precision rubber O-rings are used. Where moving parts are involved, design criteria for precision rubber O-rings as specified by the manufacturer were used.

The injector plate is fastened to the upper end of the injector nozzle by four small screws. A copper gasket is used to seal against liquid fuel leakage from the joint.

Next to the injector nozzle is the fuel reservoir. Directly below the fuel reservoir is the number 1 piston housing. The number 1 piston is connected to the number 2 piston by a square connecting rod. Fastened to the connecting rod and inside the Linear Displacement Transducer (L.D.T.) housing is the shaft of the L.D.T. The square shape prevents the connecting rod from rotating, thus protecting the L.D.T. from damage. The number 2 piston housing is below the L.D.T. mounting block and is separated from the high pressure chamber by a rupture diaphragm. A sharp plunger is incorporated in the high pressure chamber for rupturing the diaphragm. This plunger is driven by compressed air or nitrogen.

Figure (5-3) shows the two cooling systems used. Two coolant inlets and two outlets are connected to the

lower flange of the injector nozzle. One cooling system, the Lauda-Ultra Kryostats temperature bath, can be controlled to give temperatures down to -60°C. This cooling system is used before and during the experiments. The other system is a stand-by unit, which is used to protect the rubber O-rings in the fuel injection system after the experiment while the furnace is still hot. The main functions of the first system are (a). to give a fixed and known initial condition to the liquid fuel, and (b). to prevent premature evaporation of the liquid fuel.

Connected to the upper flange of the injector nozzle are two Swagelok connections (fig. 5-4). One of these connections serves for gas inlet to the evaporation chamber. In this pipe line system, a pressure reference tank, a differential pressure transducer, a pressure relief valve and a nitrogen supply cylinder are connected as shown. The other connection serves for gas outlet. Connected to this side of the piping system are: (a). a pressure gauge, and (b). an absolute pressure transducer. A cold water temperature bath is used to cool the hot gas to room temperature before the gas reaches the exit valve.

Figure (5-5) illustrates the fuel filling system together with the fuel reservoir. The top of the reservoir is connected to a calibrated burette and liquid fuel is fed into the system by gravity flow. Connected to this system is an absolute pressure transducer. At the lowest point of

the fuel reservoir is a drain for cleaning out the system and the entire system has been designed to prevent the forming of gas pockets.

Liquid fuel injection is accomplished by a displacement method. When the number 1 piston is moved into the fuel reservoir, it displaces an equal volume of fuel from the reservoir and this quantity of fuel is injected into the evaporation chamber. The total displacement volume can be varied by inserting metal blocks between the number 2 piston and the L.D.T. mounting block to change the total travel of the number one piston.

The fuel injection triggering system is shown in figure (5-6). Connected to the high pressure chamber is a nitrogen supply cylinder and a pressure relief valve which is set at 500 psig. The volume of the high pressure chamber is much larger than the change in volume which is produced by the upward movement of the number 2 piston.

There are several moving parts in the fuel injection system. They all have different hardness from the stationary parts with which they are in contact. This is necessary so that welding due to friction can be avoided. Differences in hardness between parts which are in moving contact are obtained either by the use of different metals for the moving parts or by surface hardening of the moving parts. Individual components of the fuel injection system were hydrostatically tested to 1,000 psig. All connections

in the high pressure stainless steel piping systems are stainless steel Swagelok connections. The seven solenoid valves in these systems are normally in the closed position.

This fuel injection system was designed to give:

(a). Adjustable injected liquid fuel mass.

(b). Adjustable injection pressure across the injection plate.

(c). A fairly constant injection pressure.

(d). A fairly constant fuel injection rate.

The experimental apparatus was designed to allow for the monitoring of:

(a). The fuel injection rate and the total injected liquid fuel mass as a function of time.

(b). The pressure drop due to spray evaporation as a function of the injected liquid fuel mass.

(c). The rate of pressure change as a function of time.

(d). The rate of pressure increase due to heat transfer from the chamber wall to the gaseous mixture as a function of time.

(e). The injection pressure.

(f). The pressure reference tank and evaporation chamber pressure during pressurization of this system.

(g). The evaporation chamber pressure during an experiment.

(h). The temperature of the liquid fuel in the reservoir.

5.4 Instrumentation and Calibration of Instruments

(1). Liquid fuel mass injection rate.

This quantity is monitored by a linear displacement transducer (L.D.T.) having 2 inch stroke range. The core of the L.D.T. is fixed to the square connecting rod of the numbers 1 and 2 pistons (fig. 5-2). The transducer body is fixed to a mounting block which in turn is fixed to the L.D.T. housing. This transducer requires 1.5 VDC nominal excitation. Its output is fed to the upper beam of a dual-beam oscilloscope (Type 502, #002387, Tektronix).

From the same experimental data, the total injected liquid fuel mass up to any time during fuel injection can also be determined.

The following procedure was used in the calibration of the L.D.T. (fig. 5-5).

(a). The oscilloscope which displays the L.D.T. output is switched on.

(b). The D.C. power supply to the L.D.T. is switched on.

(c). The 16-hole injector-plate at the upper end of the injector nozzle is replaced by an identical plate but without holes. It is mounted loosely to allow both air and liquid to leak out during filling of liquid fuel.

(d). The pistons are set at their lowest position.

(e). The liquid fuel reservoir system is filled with water from the calibrated burette until overflow occurs at the top of the injector nozzle. The plate is then screwed

tight to block off the overflow.

(f). Zero readings of the L.D.T. output and the corresponding liquid level in the calibrated burette are taken.

(g). The pistons are moved upward until the number 2 piston is stopped by the L.D.T. mounting block. Since the burette is the only open line in the liquid fuel system, the displaced liquid from the reservoir is forced back up the burette.

(h). Both the L.D.T. output and the liquid level in the burette are recorded.

(i). The input power supply to the L.D.T. is recorded.

(j). The number 1 piston is moved back to its initial position and its zero reading and the liquid level in the burette are recorded.

(k). Steps (g) through (j) are repeated five times.

(l). A 1/4 inch thick metal block (identified block) is inserted between the number 2 piston and the L.D.T. mounting block. This shortens the travel of both pistons by 1/4 inch but does not change the zero point (the lowest position of the pistons).

(m). Steps (d) through (l) are repeated. Each time the travel of the pistons is reduced by an additional 1/4 inch.

(n). The calibration is plotted as liquid displacement volume in c.c. vs. voltage output per volt input (graph (5-1)).

(2). Pressure drop due to spray evaporation as a function of liquid fuel mass injected and the rate of pressure drop or rise.

These quantities are monitored by a differential pressure transducer (D.P.T.) connected to the gas inlet side of the pressurization piping system (fig. 5-4). One pressure port of the D.P.T. is connected to a pressure reference tank. The other port is connected to the evaporation chamber. When the solenoid valve S.V. #2 is closed, the two ports of the D.P.T. are cut off from each other. During an experiment, this D.P.T. measures any change of pressure in the evaporation chamber with respect to the pressure reference tank pressure. A 10 VDC power supply is used to energize the D.P.T. Its output is fed to the lower-beam of oscilloscope #002387.

Calibration of the D.P.T. is done with the dead-weight tester and the calibration data are plotted in graphs (5-2) and (5-3) as psid vs. mv output per volt input.

(3). The injection pressure.

This quantity is measured by an Alinco absolute pressure transducer (A.P.T.) (P.T. #1, figure 5-4). This A.P.T. has a sensitivity of 3.000 mv/v and requires a nominal excitation voltage of 10 VAC/DC. It is connected to the liquid fuel reservoir and monitors the reservoir pressure during fuel injection. Its output is fed to the lower beam of a second dual-beam oscilloscope (Type 502A, #004261, Tektronix).

Calibration of this A.P.T. is done with the dead-weight tester and calibration data are plotted in graph (5-4) as psia vs. mv output per volt input.

(4). Evaporation chamber pressure during pressurization.

This quantity is monitored by a six inch pressure gauge. Calibration data of this gauge is shown in graph (5-5) as psig vs. gauge reading.

(5) Evaporation chamber pressure during an experiment.

A second Alinco absolute pressure transducer (P.T. #2, figure 5-5) is used to monitor this quantity. Output of this A.P.T. is fed to the upper beam of oscilloscope #004261. Calibration data of this transducer is given in graph (5-6). All calibration curves are shown in appendix B.

(6). Liquid fuel reservoir temperature.

This temperature is monitored by a mercury thermometer which is located at the coolant exit from the fuel reservoir.

Electrical circuits for the power supply to the pressure transducers and their output connections to the oscilloscopes are shown in figure (5-7). Electrical circuits for the L.D.T. and its output connections to the oscilloscope are shown in figure (5-8). Figure (5-9) shows the electrical circuits for the solenoid valves.

5.5 Experimental Procedure

The following experimental procedure is followed in the preparation for an experiment.

(1). The Lauda-Ultra Kryostat is switched on and the coolant temperature is lowered to forty degrees below zero (-40°C).

(2). Hand valve 1 is opened and hand valves 2 and 3 are closed (figure 5-3) in the coolant system. The 3-way valve is set to return the coolant back to the Kryostat. The coolant flow rate is adjusted by regulating hand valve 1 to give the fuel reservoir a temperature of 0°C.

(3). The electric furnace thermostat is set at the required temperature and the power to the furnace is switched on.

(4). Solenoid valve #2 (figure 5-4) is opened. This equalizes the pressure between the reference tank and the evaporation chamber and protects the differential pressure transducer from damage by over pressure.

(5). Solenoid valve #1 is opened to prevent a pressure build-up within the evaporation chamber.

(6). The calibrated burette is filled with pre-cooled liquid fuel. Hand valves 4 and 6 are opened to let the fuel into the fuel reservoir and the injector nozzle (figure 5-5). During filling, the liquid fuel level in the burette moves downward rapidly. When the fuel reaches the injector-plate, the small holes in the injector-plate restrict the fuel flow to a much slower rate. At this moment, the fuel injection system is full and hand valves 4 and 6 are closed.

(7). The regulator of the number 1 nitrogen supply cylinder is set at 50 psig and solenoid valve #3 is opened. The evaporation chamber is flushed with nitrogen gas.

(8). Solenoid valve #1 is closed. This prevents air from diffusing into the evaporation chamber.

(9). When the evaporation chamber temperature reaches the pre-set temperature, the two oscilloscopes are switched on. Time is allowed for the temperature of the evaporation chamber to stabilize and the oscilloscopes to warm-up.

(10). The required sensitivities of the two oscilloscopes are set.

(11). Power supplies to the transducers are switched on.

(12). Power supply to the linear displacement transducer is switched on.

(13). The evaporation chamber and the pressure reference tank are pressurized to a predetermined pressure using the number 1 nitrogen supply cylinder. The final pressure of the system is read from the 6 inch pressure gauge.

(14). Solenoid valve #7 is opened. The high pressure chamber of the fuel injection triggering system is pressurized using nitrogen supply cylinder #2 (fig. 5-6).

(15). The oscilloscope beams are positioned to their respective zero points and the oscilloscopes are set to give a single sweep from an external signal.

The system is now ready for a fuel injection experiment and the following experimental procedures are

performed.

(1). Temperature reading of the evaporation chamber is taken.

(2). Temperature reading of the coolant is taken.

(3). Evaporation chamber pressure reading is taken.

(4). Solenoid valve #3 is closed (fig. 5-4). This cuts off the number 1 nitrogen supply cylinder from the evaporation chamber and pressure reference tank system.

(5). The shutters of the two Polaroid cameras are opened.

(6). The light beams of the oscilloscopes are triggered to give their zero reference.

(7). Solenoid valve #2 is closed. This isolates the pressure reference tank from the evaporation chamber (fig. 5-4).

(8). Solenoid valve #5 is opened. This triggers the two oscilloscopes. Also, the plunger is driven into the high pressure chamber and punctures the diaphragm. The plunger is driven by either compressed air or nitrogen. (fig. 5-6).

When the mylar diaphragm is burst, compressed gas in the high pressure chamber rushes into the number 2 piston housing and acts on the lower face of the number 2 piston causing it to move upward. Because the two pistons are connected through a rigid link, the number 1 piston is forced into the fuel reservoir and liquid fuel injection takes place (fig. 5-2).

(9). For the second group experiments only, a trace of the D.P.T. output is recorded on the same film after a waiting period of 2 minutes.

(10). The shutter of the two Polaroid cameras is closed.

(11). At the end of an experiment Solenoid valve #2 is opened. This equalizes the pressure in the P.R.T. with that of the evaporation chamber (fig. 5-4).

(12). Solenoid valve #5 is closed and solenoid valve #6 is opened to vent the nitrogen gas in the system. The pressure in the high pressure chamber acts on the plunger and forces it back to its original position.

(13). Solenoid valve #7 is closed and solenoid valve #4 is opened. This vents the high pressure chamber. The piston assembly is automatically forced back to its original position (fig. 5-6).

(14). Solenoid valve #1 is opened. This vents the evaporation chamber (fig. 5-4).

(15) When the evaporation chamber pressure reaches 10 psig, solenoid valve #3 is opened. The nitrogen supply is set at 25 psig and is allowed to flush the evaporation chamber.

(16). The mylar diaphragm is replaced.

If another experiment is scheduled for the same day, the preparatory procedures are repeated. Otherwise, the following shut-down procedures are followed.

(1). The electric furnace power supply is turned off.

(2). The stand-by cooling system is started. Hand valves 2 and 3 are opened and H.V. 1 is closed. The 3-way valve is set to return the coolant back to the stand by cooling system.

So long as the evaporation chamber temperature is above 100°F, this cooling system is kept operating in order to protect the rubber "O" rings. (fig. 5-3).

CHAPTER VI

Experimental Results - Evaluations and Discussions

6.1 Experimental parameters

A total of 320 experiments were carried out with ethyl alcohol and 40 with water. the experimental parameters chosen as variables were:

(a). The initial evaporation chamber temperature.

(b). The initial evaporation chamber pressure.

(c). The total mass of liquid fuel injected.

(d). The liquid fuel injection rate.

(e). Injector-plate geometry.

In additon, two different sweep speeds of the oscilloscope beams were used for all experiments with fuel injection of 18.091 grams of ethyl alcohol and 23.4 grams of water.

Table (6-1) in appendix H gives a list of the experimental parameter combinations for ethyl alcohol using the 16-hole injector-plate. For each set listed, five experiments were conducted to provide a statistical average. Table (6-2) gives a list of the experimental parameter combinations for the remaining experiments.

In section 6.2, descriptions of the photographical experimental data are given. The variation of the total injected fuel mass over a wide range was necessary in order to provide enough data in the determination of the lifetime of the spray. This is explained further in section 6-3,which is devoted to data evaluation and to analyzing of results.Discussions on the present study are given in section 6-4 and conclusions are given in section 6.5.

6.2 Experimental Data

The four continuous data outputs of each experiment were recorded photographically. These outputs were measured as functions of time and were from:

(a). The linear displacements transducer.

(b). The differential pressure transducer.

(c). The absolute pressure transducer which measures the injection pressure.

(d). The absolute pressure transducer which measures the evaporation chamber pressure.

Photograph (6-1) in appendix C illustrates an experimental record from the first group of experiments. Only the linear displacement transducer output trace is visible. The horizontal trace at the top is the zero reference datum. The inclining trace indicates both the fuel injection rate and the total fuel mass injected up to any time. In this experiment, the liquid fuel reservoir was intentionally filled only partially. It can readily be observed that the beginning of this trace has a large step. The missing portion of this trace was due to rapid movement of the beam as a result of rapid piston motion, which can occur only when gas is displaced from the fuel reservoir. This characteristic is of significance because it shows whether the liquid fuel reservoir was full or not at the start of fuel injection. Note alsothat the end of fuel injection is well defined.

Photograph (6-2) is the experimental data obtained

from an experiment having identical initial conditions as those of photograph (6-1) except the fuel reservoir was completely filled. The beginning and end of fuel injection are well defined. The initial transient fuel injection can be seen as a step in this curve.

Photograph (6-3) shows the experimental data from another experiment. The liquid fuel reservoir was completely filled. The upper trace shows the total fuel mass injection at any time. The lower trace indicates the pressure drop in the evaporation chamber. Since the sweep speeds of the two traces were synchronized, the pressure drop at any time can be related to the total injected fuel mass up to that time. The pressure curve also indicates whether quasi-steady state spray evaporation occurred. At the beginning of fuel injection, the rate of pressure decrease in the evaporation chamber increases. This is due to droplet build-up and consequently more droplets were available for evaporation. At the end of fuel injection, due to a decrease in the number of droplets existing in the chamber, the pressure decrease curve becomes concave upward. Therefore, whenever the pressure curve shows the characteristic of a straight line, one could safely assume that quasi-steady state evaporation existed.

Photograph (6-4) is a record of the absolute pressure transducer outputs from the same experiment as photograph (6-3). The upper trace represents the absolute fuel injection pressure. This pressure jumps to a maximum

at the beginning of fuel injection and then decreases with time. At the end of fuel injection, it drops off immediately to a level slightly below its reference datum. The lower trace is the absolute pressure of the evaporation chamber. It can readily be observed that the evaporation chamber pressure decreases during fuel injection. The injection pressure is the difference between these two absolute pressures.

Photograph (6-5) shows the experimental data at a much slower recording speed. The injection portion of the record is compressed. Emphasis is placed on the pressure rise portion of the curve. This pressure rise is the result of heat transfer from the chamber wall to the gaseous mixture within the evaporation chamber. Information on the heat transfer characteristic of the equipment were obtained from similar experimental results for each set of initial conditions. It is observed that the pressure rise followed a smooth exponential curve.

Photograph (6-6) is a record of the absolute pressure transducer outputs corresponding to the experiment in photograph (6-5). Note that the sweep speed of this record differs from that of photograph (6-5). This is necessary in order to determine the total fuel injection time for comparison purpose.

6.3 Evaluation of Data and Analysis of Results

The photographic recordings were evaluated by means of a projector-comparator. These data were then used to calculate the lifetime of the sprays. Sample calculations of one such determination are given in appendices D and E for the ideal gas case and non-ideal gas case respectively.

To determine the spray lifetime corresponding to any given set of initial conditions using the ideal gas or non-ideal gas relationships, equations (4-69d) and (4-85) are used respectively. However, in either case, we have one equation with two unknowns, namely t_L and κ. Therefore, we will use the curve fitting technique to obtain a set of spray lifetimes as functions of the injected liquid fuel mass and a set of arbitrarily chosen spread coefficients. Next, we must examine the physical phenomena in order to determine the correct t_L and κ.

Following this approach, the calculated results are plotted as spray lifetime vs. the ratio of the injected liquid fuel mass to the inert gas mass for different values of κ. Next, a smooth curve is drawn through spray lifetimes having the same κ values. The resulting set of curves represent functional relations between t_L and χ for different κ. Figure (6-1) in appendix F is a typical plot of the calculated results. Clearly however, for any given set of spray conditions, there can only be one t_L. It is also clear

that t_L should be independent of χ and κ. A second physical condition is that for each value of χ, there can only be one κ and that κ increases as χ is increased. Now, in order to solve these relationships for the actual t_L and the corresponding significant κ, consider the following.

The inclining straight line in figure (6-1) represents the injection time which is required for the injection of a liquid mass as specified by the corresponding χ value. This line divides the figure into two regions. In the region to the upper left of this line, we have $t_L >$ injection time. In the region to the lower right of this line, we have $t_L <$ injection time. It is obvious that quasi-steady state spray evaporation can be established only when the injection time is equal to or greater than the lifetime of the spray.

The family of solid curves in figure (6-1) indicate the lifetime of the spray assuming the fuel vapour to be an ideal gas. They were drawn for κ values at 0.05 intervals and within the quasi-steady state region. At small values of χ, i.e. when extended into the unsteady region, this family of curves tends to converge to a narrow range of t_L. As χ increases, the curves tend to diverge and they all exhibit a concave downward characteristic. This family of curves can be divided further into two groups. The first group contains those curves having a maximum t_L at a point in the quasi-steady state region but not on the

boundary line. The second group contains those curves having their maximum t_L on the boundary line of this region. The curve, which divides the family of curves, belongs to the second group and its maximum intersects the boundary line horizontally.

Now let us consider for example, in the first group of curves in Figure (6-1), the curve for $\kappa=0.50$. This curve intersects the boundary line at $\chi=.00695$. The lifetime of the spray as determined from this curve at the intersecting point is approximately 247 milliseconds. At some later time t, say $\chi=.009$, more fuel had been injected. Since the lifetime of the spray is independent of the injection time, a point which satisfies both requirements can be identified in the quasi-steady state region. It can be seen readily that it lies between the curves for $\kappa=0.45$ and $\kappa=0.50$. This is physically impossible because κ can only increase with time. Based on this reasoning, all curves in the first group can be ruled out. The quasi-steady state region above the dotted horizontal line in Figure (6-1) is physically impossible.

The second group of curves is bounded above by the curve which divides the family of curves into two groups and below by the limiting κ curve. The lower limit of κ is fixed by the initial volume of the spray which is a function of the initial evaporation chamber conditions, the injection pressure, and the geometry of the spray. These two limiting

cases define a range of possible κ values.

In order to identify the correct κ value, one must consider the actual physical phenomenon. As injection proceeds, turbulent mixing along with mass and momentum transfer of the spray tends to increase the cooled fraction of environmental gas. A second factor, which also promotes the increase of κ, is diffusion of the fuel vapour due to the existence of a concentration gradient. Both factors favor an increase of κ from its lower limit towards its upper limit. For the 16-hole self-impinging injector plate, preliminary investigations using a transparent vessel at atmospheric pressure and room temperature supported this theory. The lower limit of κ was observed to be approximately 0.20. Since in the experiment, a sufficient time period is required for quasi-steady state to establish in the system, one may conclude that the most probable κ value would be the maximum possible in the second group of curves. This means that even though the liquid spray volume remains fairly constant, the volume of inert gas which is affected by the spread of fuel vapour keeps increasing. Given enough time, the entire inert gas mass will be affected. At that instant, κ will attain its upper limit and equals to unity. This reasoning is also in qualitative agreement with available photographical recordings on spread of a spray in a confined finite space (ref. 6-1). Therefore, the intersecting point of the dividing curve and the boundary

line of the quasi-steady state region yields the maximum possible spread of the vapour at that instant. This point specifies also the lifetime of the spray. It satisfied the physical phenomenon which requires that at constant t_L, κ increases with increasing χ. This condition is met by all other curves in this group. But κ and the lifetime of the spray determined from them are not the maximum possible and consequently have no significance in combustion chamber design.

Further indication of the variation of κ can be seen in figure (6-14). A comparison of the experimental pressure decrease to the hypothetical instantaneous pressure decreases calculated for κ = 0.20, 0.30, and 0.50, for a range of χ. Clearly, for any value of χ, physical conditions require that the rate of the hypothetical pressure decrease to be greater than the experimental value. This is true because of the presence of heat transfer effects during an experiment. Consider for example at χ = 0.015, it can be readily seen that the rate of experimental pressure decrease is greater than the hypothetical pressure decrease with κ = 0.20. However, this is physically impossible. Therefore at this instant, κ has a value greater than 0.20. On the other hand, the reverse is true with κ = 0.50. Thus one may conclude from this comparison that for this set of initial conditions, the κ value determined from figure (6-1) has the right order of magnitude.

The same reasoning applies to curves calculated from the non-ideal gas relationships. Only the dividing curve of this set of curves is shown as the broken line in Figure (6-1).

Figures (6-2) to (6-7) show the spray lifetimes determined for various initial conditions. Both ideal gas and non-ideal gas expressions were used to calculate the spray lifetimes. Results calculated by using the ideal gas relationships are shown as solid curves while results from non-ideal gas expressions are illustrated as broken curves.

Tables (6-3) to (6-7) in appendix H are lists of lifetimes of liquid fuel sprays which were subjected to the various initial and operating conditions. Results in table (6-3) were obtained from ideal gas relationships and table (6-4) from non-ideal gas expressions. These first series of results were obtained when the 16-hole injector-plate was used. The initial conditions of these experiments were 400, 450 and 500 psig and 700, 800 and 900°F. The lifetime of the sprays was found to vary between 203 and 241 milliseconds when ethyl alcohol vapour is considered an ideal gas. When it is considered a non-ideal gas, the lifetime of the sprays varied between 144 and 180 milliseconds. Table (6-5) is a list of lifetimes of ethyl alcohol sprays. The 8-hole self-impinging injector plate was used. Table (6-6) is a list of lifetimes of water sprays when the 16-hole self-impinging injector plate was used and table (6-7) is a list

of lifetimes when the 8-hole self-impinging injector plate was used.

Figures (6-8) to (6-13) show the comparison of spray lifetimes for the 8 and 16 hole self-impinging injector-plate. These include four series of results. Series two was investigation of ethyl alcohol sprays, which were produced by the 8-hole injector-plate. The initial conditions were 400 psig and 700, 800 and 900°F. Series three dealt with water sprays which were produced by the 16-hole injector-plate with the initial conditions identical to those of series two. Series four was identical to series three except that the 8-hole injector-plate was used.

No data for the one hole injector-plate is shown here because it is believed that quasi-steady state evaporation was never established. This result in itself however indicates that the injector is of poor design.

To obtain an order of magnitude of the droplet size from the average droplet lifetime, Fuch's classical formula for droplets evaporating in an infinite space will be used in the following form:

$$r^2 = \frac{2G r_d^{MD}}{\rho} t_L \qquad (6\text{-}1)$$

where D is given by $D = D_o(T/273)^{2.0} \frac{1}{P}$ (T:°K, P:atm.). For ethyl alcohol in air, $D_o = 0.102$ (cm^2/sec) (Ref. 2-10). Now consider the spray evaporation experiments having initial

conditions as listed below:

$$T_o = 900°F \ (755.2°K); \quad P_o = 400 \text{ psig } (28.2 \text{ atm.})$$

(1) Assume that the droplets evaporate at their normal boiling temperature, then

$$r = 45.4 \ \mu$$

(2) Assume that the droplets evaporate at the boiling temperature corresponding to the ambient pressure, then

$$r = 223 \ \mu$$

(3) Assume that the droplets evaporate at the temperature midway between the above two extremes, then

$$r = 112 \ \mu$$

From these droplet size calculations, it may be concluded that the average droplet lifetime determined by the use of the present analysis has the right order of magnitude.

6.4 Discussions

In the formulation of the governing equations of Chapter IV, both the liquid fuel vapour and inert gas were assumed to obey the Ideal Gas Law. For the inert gas used, this assumption is accurate even at high pressures. However, for the fuel vapour, deviation from this assumption is quite considerable at high pressures. Nevertheless, the Ideal Gas Law can still be applied in equation (4-4), because m_1' is much greater than m_2 ($m_1' >> m_2$) and a large deviation in the term containing m_2 can not affect the entire equation by any significant amount.

In solving the basic equations, the approximation technique was employed. It is based on the assumptions that the ratio of the total injected liquid fuel mass to the inert gas mass, χ, and the amount of heat transfer from the chamber wall to the gaseous mixture are small. This approach is adopted because of the complexity of the analytical mathematical model.

To obtain small values of χ, the total injected liquid fuel mass can be adjusted. This and the rate of fuel injection can be used to make the amount of heat transfer to the gaseous mixture a minimum by keeping the inert gas temperature decrease small. The influence of χ on the lifetime of the spray can be observed in figure (6-1) of appendix F. At small χ, the spray lifetime curves for different mixing coefficient, κ, tend to converge to a narrow range when extended into the unsteady state region.

As χ increases, these curves would tend to give negative t_L. This shows that the approximation method of solving the basic equation becomes less accurate as χ increases. Therefore, care must be taken in an experiment to ensure small χ values. On the other hand, one must keep the χ values large enough so that the calculated lifetime of the spray lies outside of the unsteady state region for the result to be meaningful.

Solution of the basic equations also involves the determination of the end state specific internal energy of the liquid vapours considered. During the initial four processes of the arbitrarily chosen path, the specific internal energy of the fuel vapour is allowed to vary. This applies to both the ideal gas and non-ideal gas analyses. The only difference between these two cases lies in process "e". In this process, the ideal gas theory assumes the specific internal energy to remain constant whereas the non-ideal gas theory takes into account the changes in specific internal energy of the fuel vapour.

Based on identical experimental data, lifetimes of liquid fuel sprays determined from the non-ideal gas theory are shorter than those calculated from the ideal gas expressions. This is understandable because at the temperatures and pressures investigated, the specific internal energy of the fuel vapour at the final state

deviates substantially from that of an ideal gas subjected to an identical isothermal compression process. This shows that the ideal gas theory should not be used normally. Unless there are no thermodynamic data available on the particular fuel of interest or the fuel vapour is known to behave as an ideal gas, the non-ideal gas theory should always be used. For liquid fuels which are mixtures of many components, care must be exercised in defining their boiling points and it may be necessary to resort to the ideal gas theory. In such cases, spray lifetime calculations would only give an order of magnitude. Even then, this approach can still be used to compare different injection nozzles. The more efficient nozzle will produce a larger pressure drop in the evaporation chamber when subjected to identical experimental conditions.

Three general trends on spray lifetimes can be observed from the results of figures (6-1) to (6-7). These are:

(1). For identical experimental conditions except initial evaporation chamber pressure, it was found that the spray lifetime decreases as the initial evaporation chamber pressure is increased. This phenomenon may be attributed to the fact that the spray becomes finer at higher pressures and that smaller droplets normally have shorter lifetimes. The heat transfer rate is also higher at higher ambient pressure.

(2) For different fuel injection rates while all the other experimental conditions are identical, the spray lifetime is shorter for faster injection rate. Again, this can be attributed to finer droplets existing in the spray due to higher injection velocity and subsequent greater heat transfer.

(3) If all other experimental parameters remain the same, the spray lifetime is shorter with higher initial evaporation chamber temperature. This is due to increased rate of heat transfer from the inert gas to the droplets.

Additional trends can be observed from Figures (6-8) to (6-13). These are:

(1) For identical experimental conditions, the 16-hole injector-plate produces sprays with shorter lifetime than the 8-hole injector-plate. This is due to the fact that the 16-hole injector-plate produces a finer spray.

(2) The 16-hole injector-plate gives better mixing than the 8-hole injector-plate for identical experimental conditions. This could be due to the fact that for the same length of time available, more fuel is evaporated in the case of the 16-hole injector-plate. This gives more fuel vapour available for mixing with the surrounding gas.

(3) When all experimental conditions are the same, water sprays have longer lifetime than ethyl alcohol sprays. This is expected because the internal energy change for water is much higher than ethyl alcohol between identical end states.

The above observations agree with the findings of other investigators.

For the straight jet injector-plate, experimental data indicated that poor atomization was encountered. It is suspected that quasi-steady state spray evaporation was not established during the experiments. Consequently, these data were not evaluated.

In the calculation of spray lifetimes from experimental data, increments of κ were chosen to be 0.01. This was considered accurate enough because the maximum error introduced is about ±2.0% for small values of χ. Since the solutions were approximations only, it was also considered unnecessary to computerize the calculating procedure.

A second source of error is in the evaluation of the pressure data. The maximum error introduced through the thickness of the recording traces is approximately ±3.0%, even though the projector-comparator was used.

Other sources of error that set a limit to the accuracy of the present method are introduced through the simplifying assumptions. These include the size distributions, unequal evaporation rate of same size droplets, deviations from the Ideal Gas Law and others. Though they are fairly well known, there seems to be no easy way of substantially diminishing the absolute size of the errors.

On the whole, the present analysis and equipment are great improvements over that of reference (3 - 14). In the theoretical treatment, heat transfer from the chamber wall to the gaseous mixture during fuel evaporation is considered

in the present study. In the former study (ref.3-14) it was neglected. An important characteristic of the spray, namely the spread of the vapour as a function of time can be estimated in the present analysis. The evaporation lag was mistaken for the spray lifetime in reference (3-14). It has been found in the present analysis that the evaporation lag equals approximately 40% of the spray lifetime.

The use of a much larger evaporation chamber in the present equipment has prevented the droplets from hitting the wall. This eliminated a major source of error which existed in the former investigation of Sandri and Wong. Also, any liquid fuels can be investigated with the present fuel injection system.

6.5 Conclusions

The present phenomenological approach to study the spray evaporation phenomenon has been found to have many advantages. Most important of all is the fact that it can be applied at any pressure range as long as the "d^2 law" of single droplet evaporation is valid. The method is simple and it automatically integrates an extremely complex problem to give two measurable and significant characteristics. These are:

(a). The lifetime of a spray, and

(b). The spread coefficient produced by the spray as a function of the injected liquid fuel mass.

Both characteristics are important in the design of combustion chambers. While the lifetime of the spray controls the size of the combustion chamber, the spread coefficient indicates the mixing state of the gaseous mixture. These would ultimately contribute to the understanding of spray combustion.

Another advantage of the present technique is that data acquisition does not disturb the phenomenon.

When physical and thermodynamic properties of the fuel are not known, this experimental method can still be used to compare different fuel injection nozzle designs. In such case, the fuel injection nozzle which produces a larger pressure decrease for identical operating conditions, has a higher nozzle efficiency. Full scale testing of injector

designs can be avoided by investigating scaled down models.

On the other hand, there are limitations to the application of the present method. First, it requires that certain physical properties and thermodynamic data of the liquid fuel are known before the spray lifetime and the spread coefficient can be calculated. This applies to both single component or multicomponent fuels.

Another limitation is that the method also depends on the validity of applying physical properties of a liquid fuel obtained from a single component system to a binary system.

However, the advantages of the present techniques outweigh by far all the limitations and should certainly be useful in future studies.

References

2.1 Maxwell, J.C. Diffusion. Scient. Papers II. 1890, p. 639.

2.2 Stefan, M.J. On the Dynamic Theory of Diffusion of Gases. IN Mathematisch-Naturwissen - Schaftliche Klasse, Wiener Akademie der Wissenschaften, Vol. 65-66, 1872, p. 323.

Experiments on Evaporation. IN Mathematisch-Naturwissen - Schaftliche Klasse, Wiener Akademie der Wissenschaften, Vol. 67-68, 1873, p. 385.

On the Equilibrium of a Solid Elastic Body of Non-Homogenous or Variable Temperature. IN Mathematisch-Naturwissen - Schaftliche Klasse, Wiener Akademie der Wissenschaften, Vol. 83 1881, p. 549.

2.3 Fuchs, N. Concerning the Velocity of Evaporation of Small Droplets in a Gas Atmosphere. Physikalische Zeitschrift der Sowjet Union, Vol. 6, 1934, pp. 224-243,

Translated: NACA TM 1160, August 1947.

2.4 Frössling, N. The evaporation of falling drops. Gerlands Beitrage zur Geophysik. Vol. 52, pp. 170-216, 1938. Translated: Power Jet (R. and D.) Ltd.

2.5 Ranz, W.E. On the evaporation of a drop of volatile liquid in high temperature surroundings. A.S.M.E. 54-A-143.

2.6 Kirkaldy, J.S. The Time-Dependent Diffusion Theory for Condensation of Spherical and Plane Surfaces. Can. J. Phys. 36, 1958, p. 446.

2.7 Weiber, P.R. Calculated Temperature Histories of Vaporizing Droplets to the Critical Point. AIAA Journ. Vol. 1, No. 12, Dec. 1963, pp. 2764-70.

2.8 Manrique, J.A. Borman, G.L. Calculations of Steady State Droplet Vaporization at High Ambient Pressures. Int. Jour. Heat Mass Transfer. Vol. 12, 1969, pp. 1081-1095.

2-9 Brzustowski, T.A. Chemical and Physical Limits on Vapour-phase Diffusion Flames of droplets. Can. J. Chem. Eng., 43, 1965, p. 30.

2-10 Kotake, S. Okazaki, T. Evaporation and Combustion of a fuel droplet. Int. J. Heat and Mass Transfer. Vol. 12, 1969, pp. 595-609.

2-11 Injection and Combusion of Liquid Fuels. WADC Technical Report 56-344, ASTIA Document No. AD 118142, March 1957. Battelle Memorial Institute. pp. 1-1 - 1-30; 4-50 - 4-93; 4-93 - 4-101.

2-12 Probert, R.P. The Influence of Spray Particle Size and Distribution in the Combustion of Oil Droplets. Philosophical Magazine, London, Vol. 37, 7th Series, 1946, p. 94.

2-13 Sacks, W. The Rate of Evaporation of a Kerosine Spray. NAE Note 7, 1951 Canada.

2-14 Fledderman, R.G. Hanson, A.R. The effects of turbulence and wind speed on the rate of evaporation of a fuel spray. University of Michigan, Engineering

Research Institute, Ann Arbor, Report No. CM 667, June 1951.

2-15 Benson, G.W. The Evaporation of Fuel Sprays. I - Theoretical Treatment. NAE LR-181, 1956, Canada.

2-16 Hoffman, T.W. Gauvin, W.H. An Analysis of Spray Evaporation in a high temperature environment I - Radiant Heat Transfer to Clouds of Droplets and Particles. The Canadian Journal of Chem. Engineering. Oct. 1961, pp. 179-188.

2-17 Hoffman, T.W. Gauvin, W.H. An Analysis of Spray Evaporation in a high temperature environment. II - Calculation of the Evaporative Load Distribution. The Canadian Jour. of Chem. Eng. June 1962, pp. 110-118.

2-18 Hoffman, T.W. Gauvin, W.H. An Analysis of Spray Evaporation in a high temperature environment III - Calculation of the Heat Flux Distribution in a Cylindrical Column containing a Cloud of Evaporating Droplets. The Can. Jour. Chem. Eng. Vol. 43, No. 6, Dec. 1965, pp. 325-33.

2-19	Dickinson, D.R. Marshall, Jr. W.R.	The Rates of Evaporation of Sprays. A.I. Ch. E. Jour. Vol. 14, No. 4, July 1968, pp. 541-552.
3-1	Bradley, R.S. Evans, M.G. Whytlaw-Gray, R.W.	The rate of evaporation of droplets. Evaporation and diffusion coefficients and vapour pressures of dibutyl phthalate and butyl stearate. Procs. Royal Society of London, Series A, 186; 368 (1946).
3-2	Ranz, W.E. Marshall, Jr. W.R.	Evaporation from drops. Parts I and II. Chemical Engineering Progress, Vol. 48, No. 3, March 1952. pp. 141-146. Vol. 48, No. 4, April 1952, pp. 173-180.
3-3	Hoffman, T.W. Gauvin, W.H.	Evaporation of Stationary Droplets in High Temperature Surroundings. Canadian Jour. Chem. Eng. Vol. 38, Oct. 1960, pp. 129-137.
3-4	Priem, R.J. Borman, G.L. El Wakil, M.M. Uyehara, O.A. Myers, P.S.	Experimental and Calculated Histories of Vaporizing Fuel Drops. NACA TN 3988, August 1957.

3-5	Savery, W. Borman, G.L.	Experiments on Droplet Vaporization at supercritical pressures. AIAA Paper No. 70-6 AIAA 8th Aerospace Sciences Meeting, N.Y. Jan. 1970.
3-6	Wollers, Ehmcke	The Process of Evaporation of Fuels, the Formation of Oil Vapour and the Behaviour of Oil Vapours and Oil Gases During Combustion in the Diesel Engine. Kruppsche Monats. Vol. 2, 1921, p. 1.
3-7	Rothrock, A.M. Waldron, C.D.	Fuel Vaporization and its Effect on Combustion in a High-Speed Compression-Ignition Engine. NACA Report No. 435, 1932.
3-8	Selden, R.F. Spencer, R.C.	Heat Transfer to Fuel Sprays Injected into Heated Gases. NACA Report No. 580, 1937.
3-9	Godsave, G.A.E.	The Combustion of Drops in a Fuel Spray. National Gas Turbine Establishment Memorandum No. M95, October, 1950
3-10	Bahr, D.W.	Evaporation and Spreading of iso-octane sprays in high-velocity air streams. NACA RME 53I14, 1953.

3-11	Ingebo, R.D.	Vaporization rates and drag coefficients for isooctane sprays in turbulent air streams. NACA TN 3265, Oct. 1954.
3-12	Benson, G.W.	Evaporation of Fuel Sprays. II - Experimental work. NAE LR-182, 1956, Canada.
3-13	Sjenitzer, F.	Evaporation of Liquid Spray Injected into Stream of Gas. Chem. Eng. Science, Vol. 17, May 1962, pp. 309-22.
3-14	Sandri, R. Wong, J.K.S.	On the evaporation of Fuel Sprays at High Temperatures and Pressures. National Research Council of Canada. No. 8677 (MP-36) August 1965.
3-15	Newman, J.A. Brzustowski, T.A.	Behaviour of Liquid Sprays at High Pressures. AIAA 8th Aerospace Sciences Meeting in New York, Jan. 1970, paper No. 70-8.
3-16	De Juhasz, K.J.	Spray Literature Abstracts, ASME, 1959, and subsequent editions.
4-1	Giffin, E. and Lamb, T.A.J.	The effect of Air Density on Spray Atomization. Motor Ind. Res. Assn. Report # 1953/5 (1953).

4-2 Spencer, H.M. Empirical Heat Capacity Equations of Gases and Graphite. Industrial and Engineering Chemistry. Vol.40, 2152-2154 (1948).

4-3 JANAF Thermochemical Data. Compiled and Calculated by the Dow Chemical Company, Thermal Laboratory, Midland, Michigan.

4-4 Godsave, G.A. "Studies of the Combustion of Drops in a Fuel Spray - The burning of Single Drops of Fuel" Fourth Symposium on Combustion The Combustion Institute 1952, pp.818-829.

4-5 Wronkiewicz,J.A. Combustion of Single Drops of Fuel. AIAA Paper No.71-989. AIAA 8th Annual Meeting and Technical Display.Oct.1971. 1290 Ave of the Americas, N.Y.

4-6 Natarajan,R. An experimental investigation of Droplet Combustion at high pressures. Ph.D.Thesis, Department of Mechanical Engineering, University of Waterloo,1971.

5-1 Hatch, L.F. Ethyl Alcohol. Enjay Chemical Company, 1962. Library of Congress Catalog Card Number: 62-18655. pp.122-126.

5-2 Papini, G. and Cuomo,S. Anticendio, 8,338-344 (1956).

6-1 Scott, W.M. Looking in on diesel combustion. SAE SP 345, Dec. 1968.

Appendix A

Figure 4-1 Ethyl alcohol pressure vs. enthalpy graph

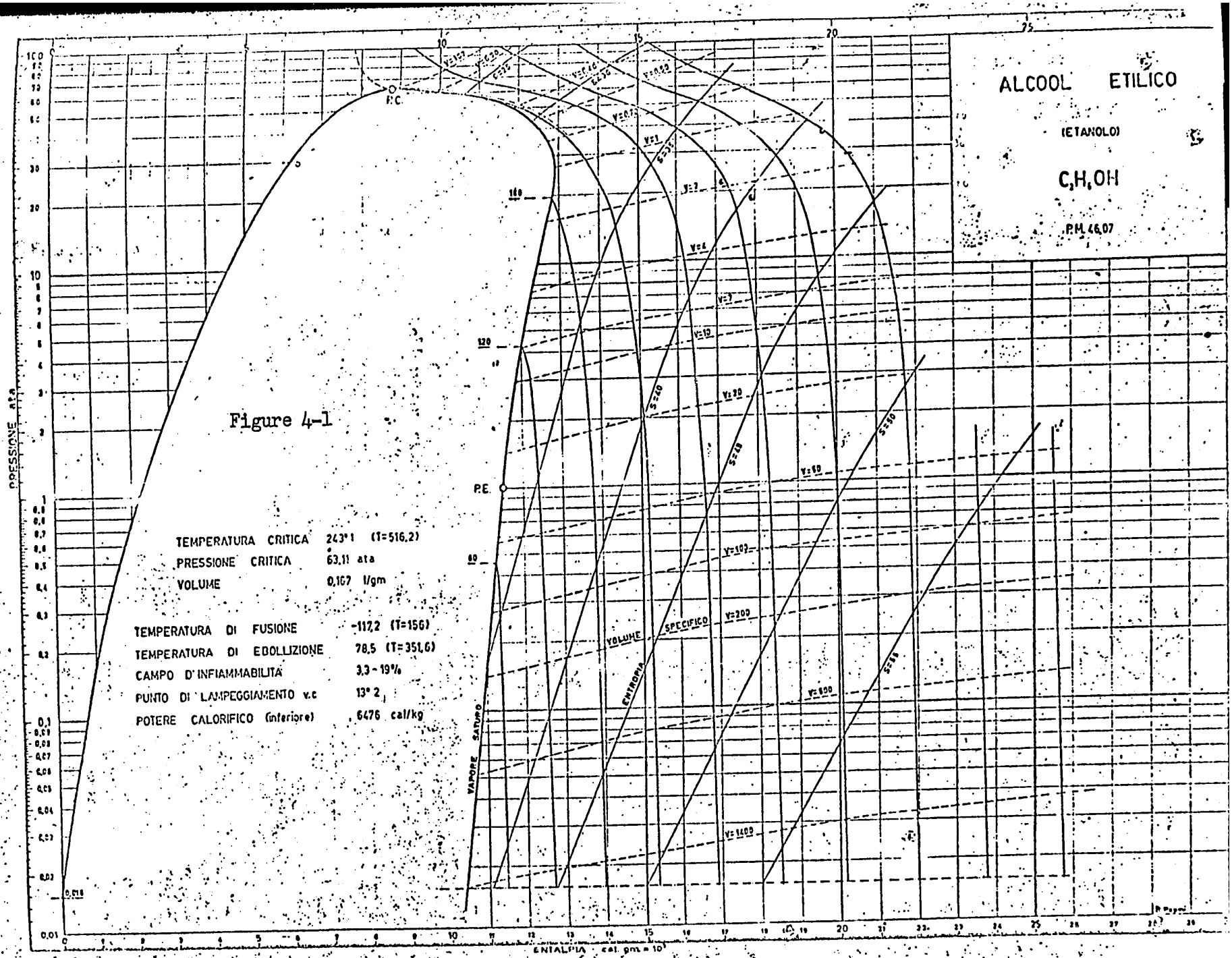

Figure 4-1

Volume specifico (l/gr. mol)

Appendix B

Figures of experimental apparatus and instrument calibration

Figure 5-1	Apparatus layout
5-2	Liquid Fuel Injection System
5-3	Injection nozzle cooling system.
5-4	Evaporation chamber pressurizing and depressurizing system.
5-5	Liquid Fuel filling system
5-6	Fuel Injection Triggering system.
5-7	Instrumentation. Electrical circuit.
5-8	Electrical circuit for power supply to the linear displacement transducer and output.
5-9	Electrical circuit for solenoid values.
Graph 5-1	Linear Displacement Transducer Calibration.
5-2	Differential Pressure Transducer Calibration.
5-3	Differential Pressure Transducer Calibration.
5-4	Absolute Pressure Transducer Calibration.

Appendix B

Graph 5-5 Pressure Gauge Calibration

5-6 Absolute Pressure Transducer Calibration. Alinco Pressure Cell: Serial #33121.

FIGURE 5-1. APPARATUS LAYOUT

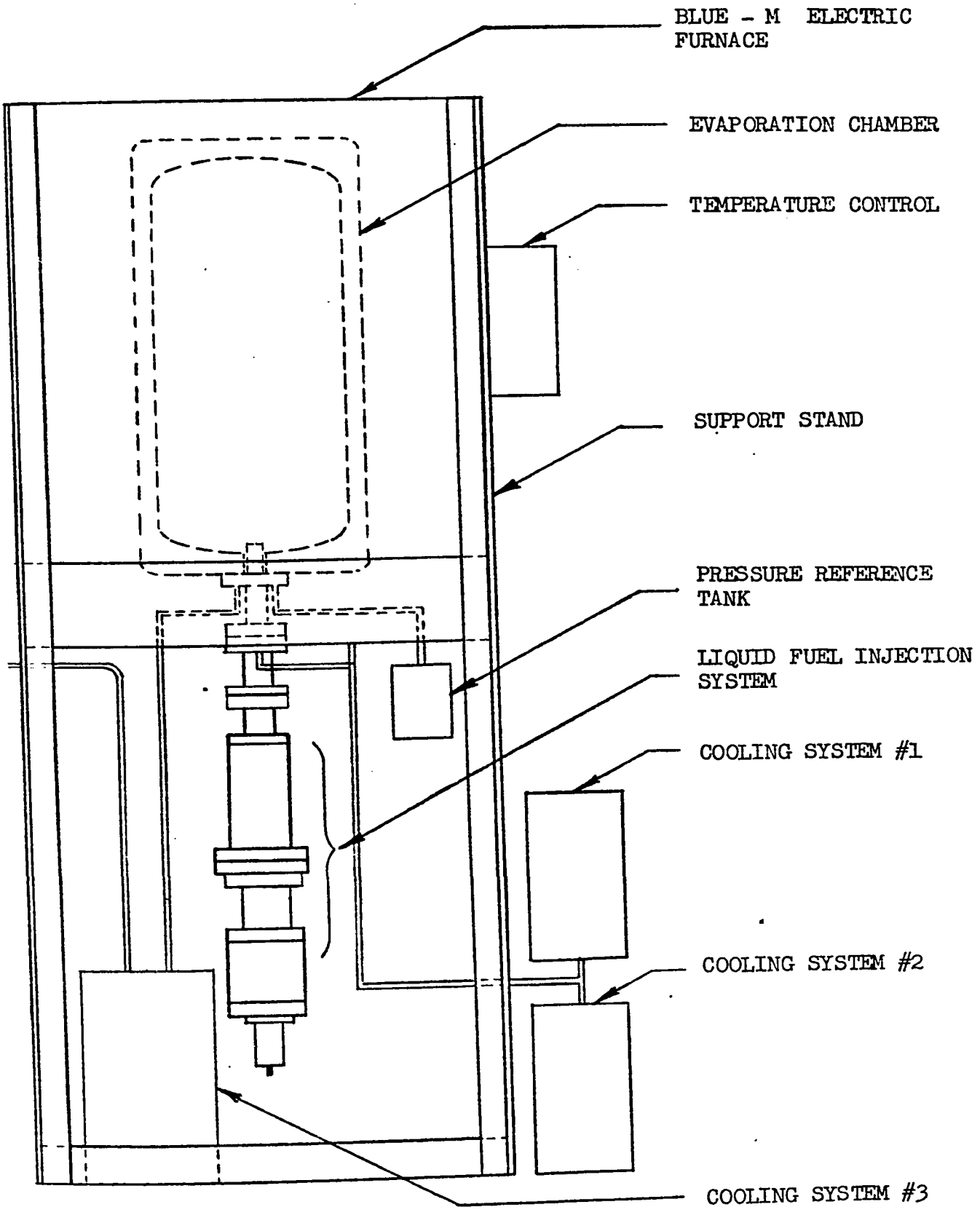

FIGURE 5-2. LIQUID FUEL INJECTION SYSTEM

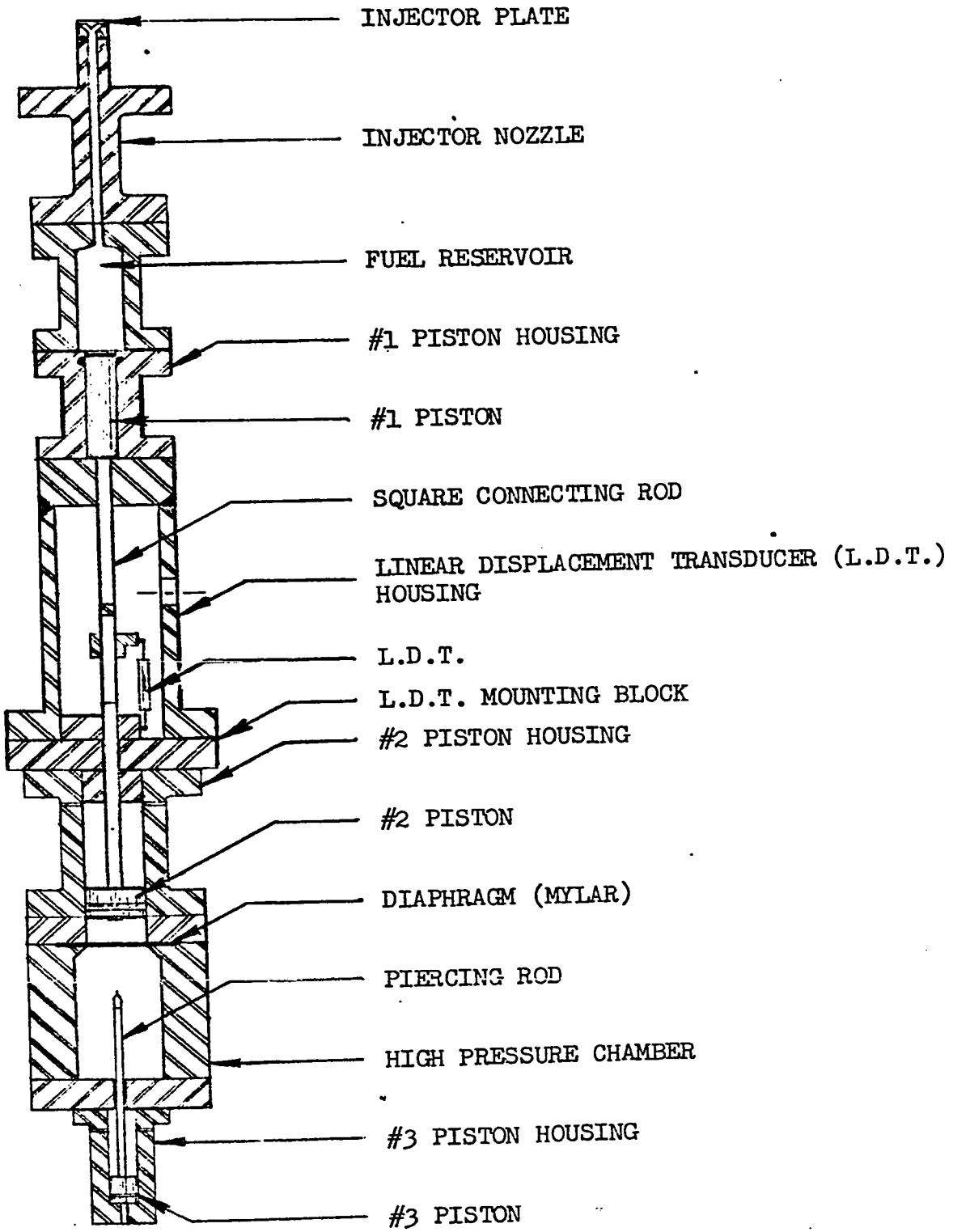

FIGURE 5-3. INJECTION NOZZLE COOLING SYSTEM

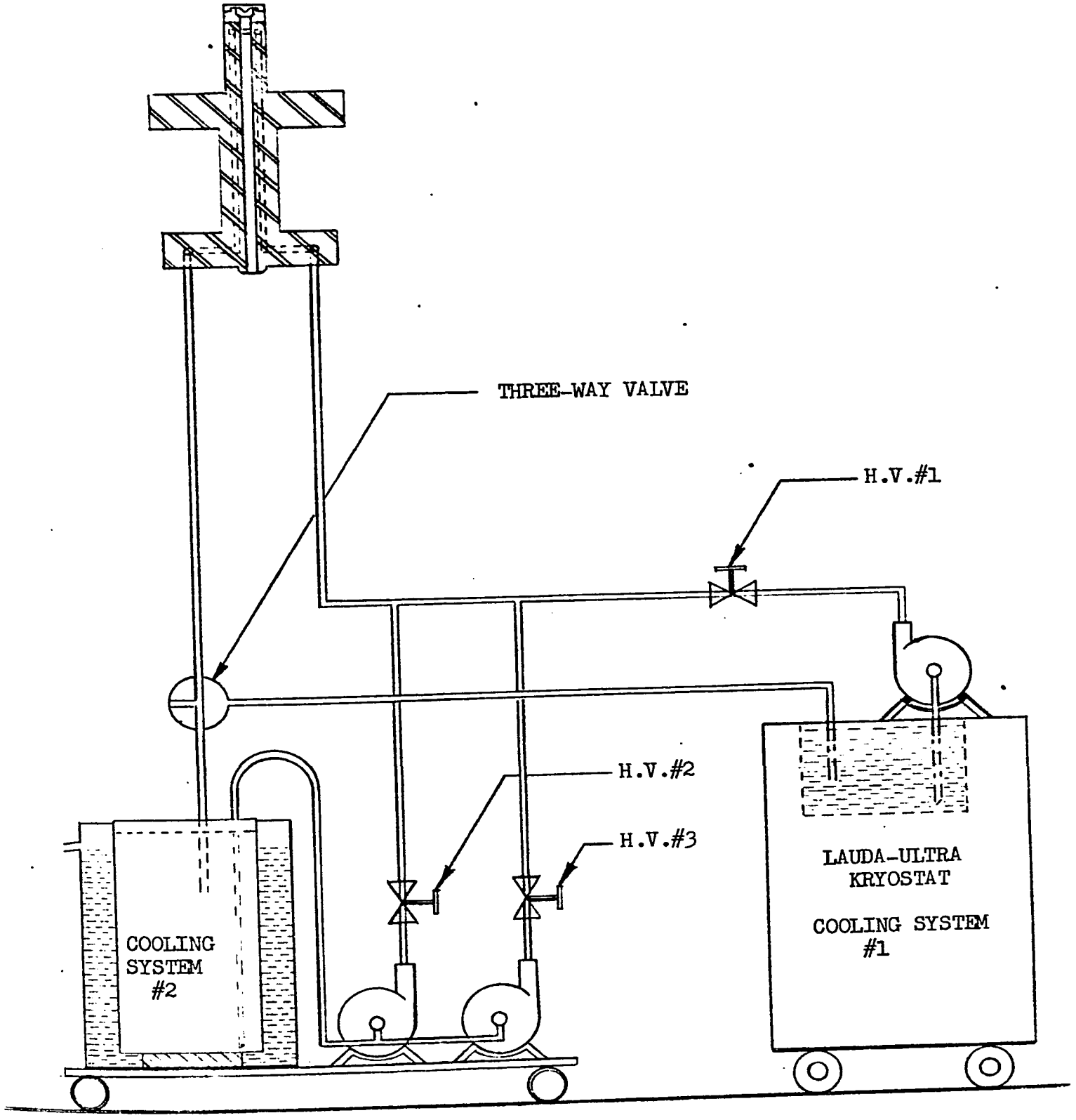

FIGURE 5-4. EVAPORATION CHAMBER PRESSURIZING AND DEPRESSURIZING SYSTEM

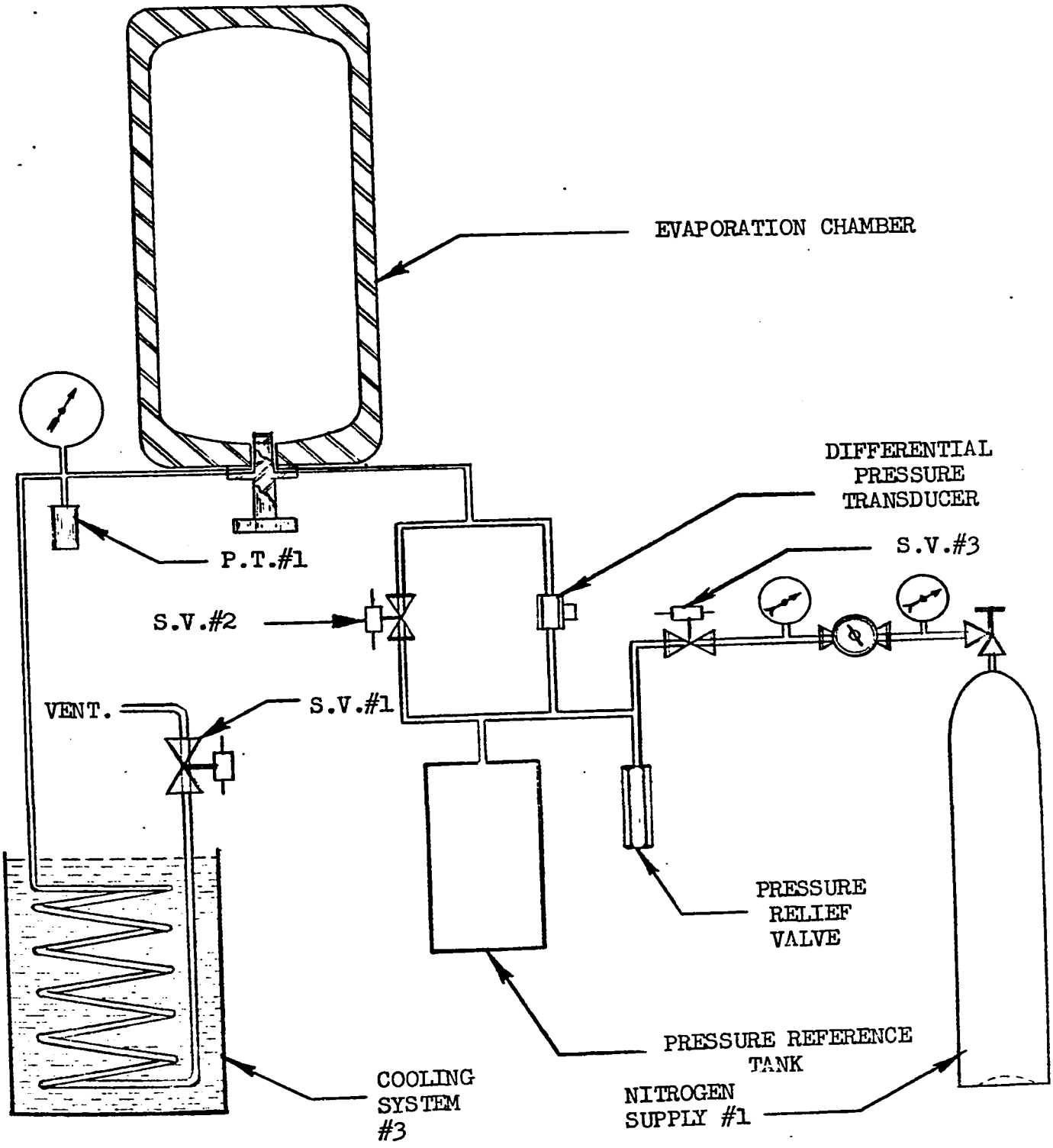

FIGURE 5-5. LIQUID FUEL FILLING SYSTEM

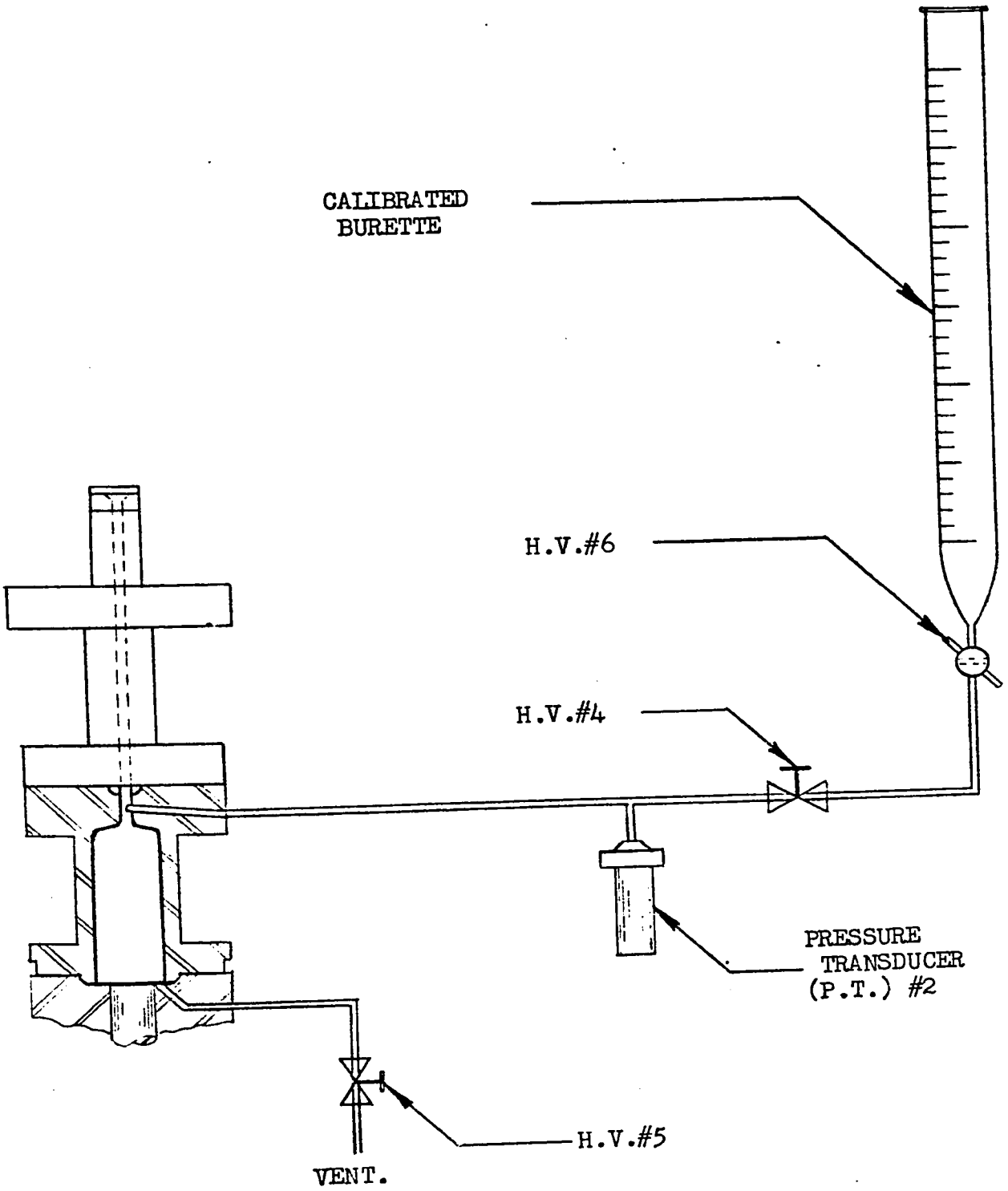

FIGURE 5-6. FUEL INJECTION TRIGGERING SYSTEM

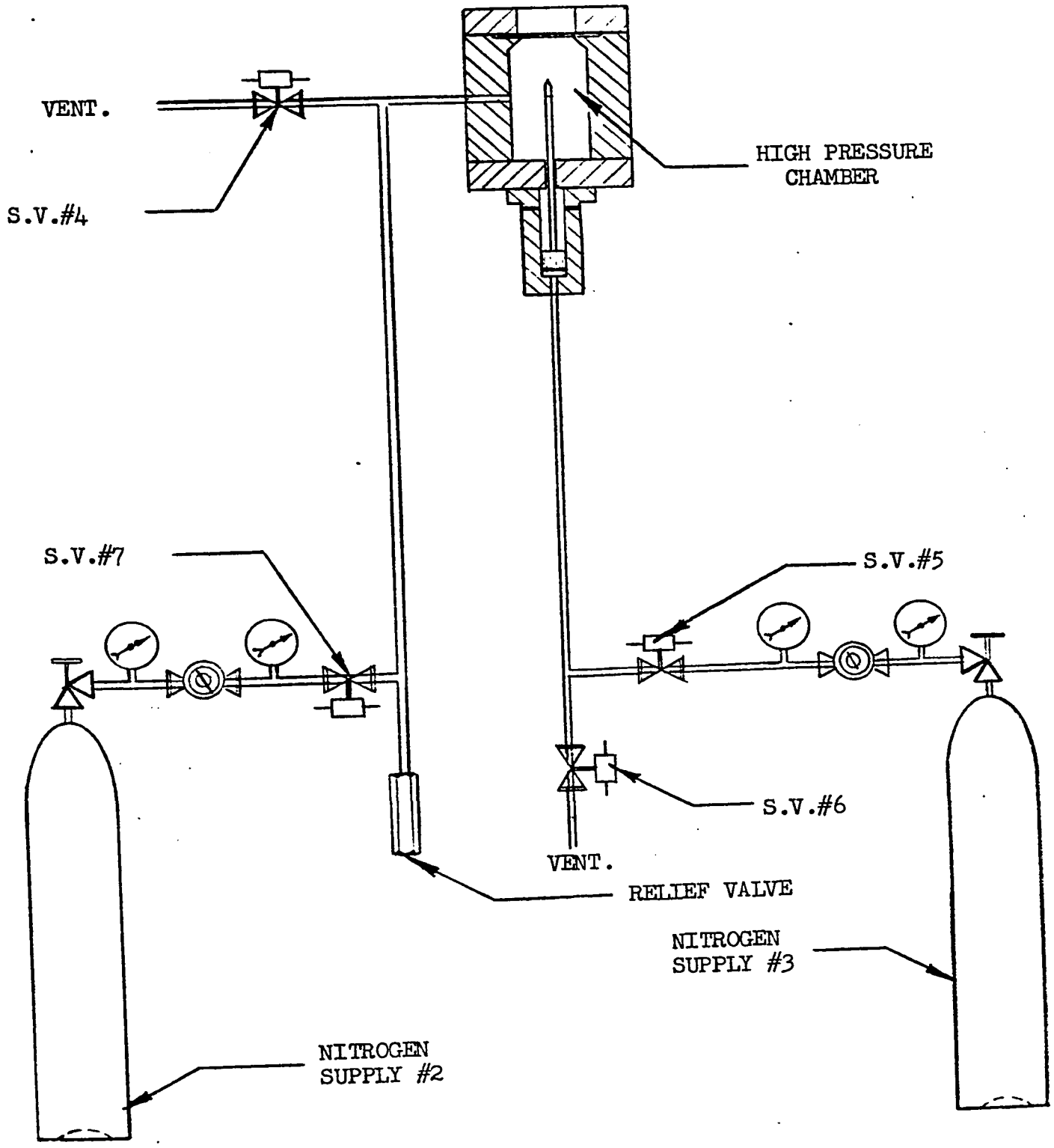

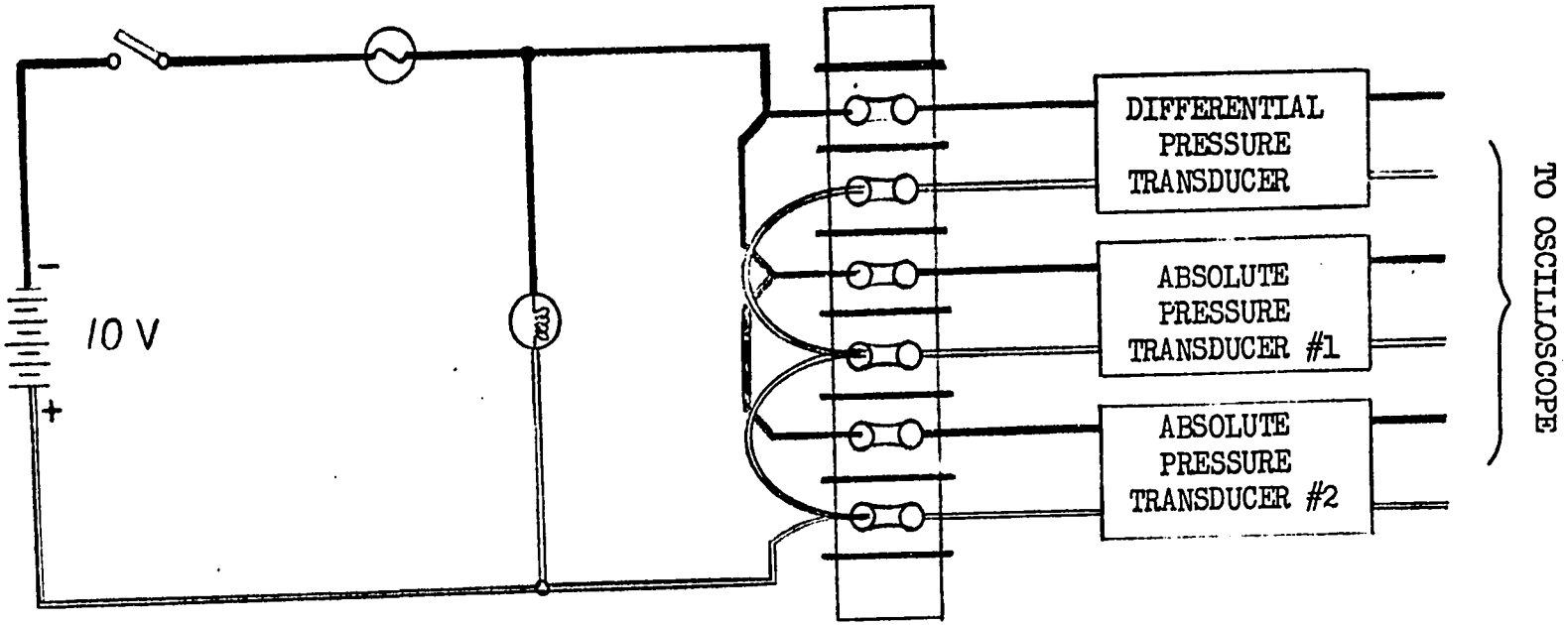

FIGURE 5-7. INSTRUMENTATION ELECTRICAL CIRCUIT

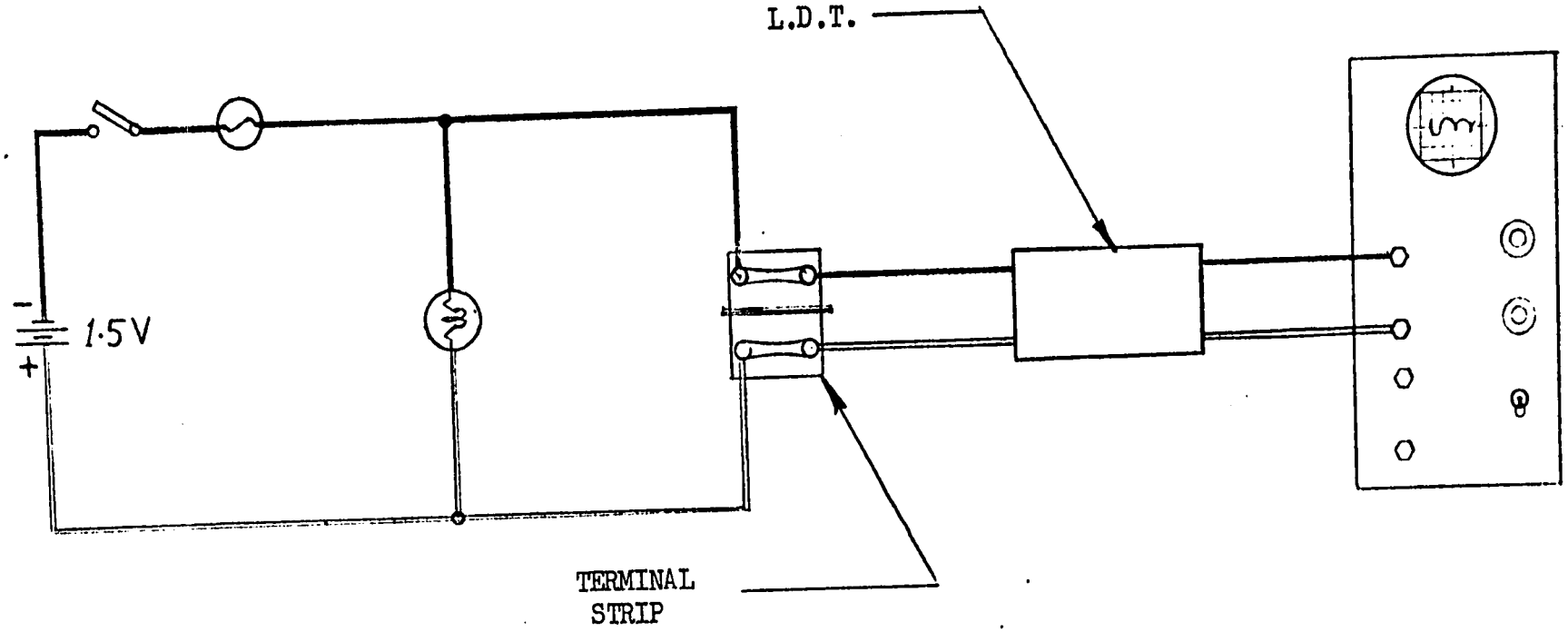

FIGURE 5-8. ELECTRICAL CIRCUIT FOR POWER SUPPLY TO LINEAR DISPLACEMENT TRANSDUCER & OUTPUT

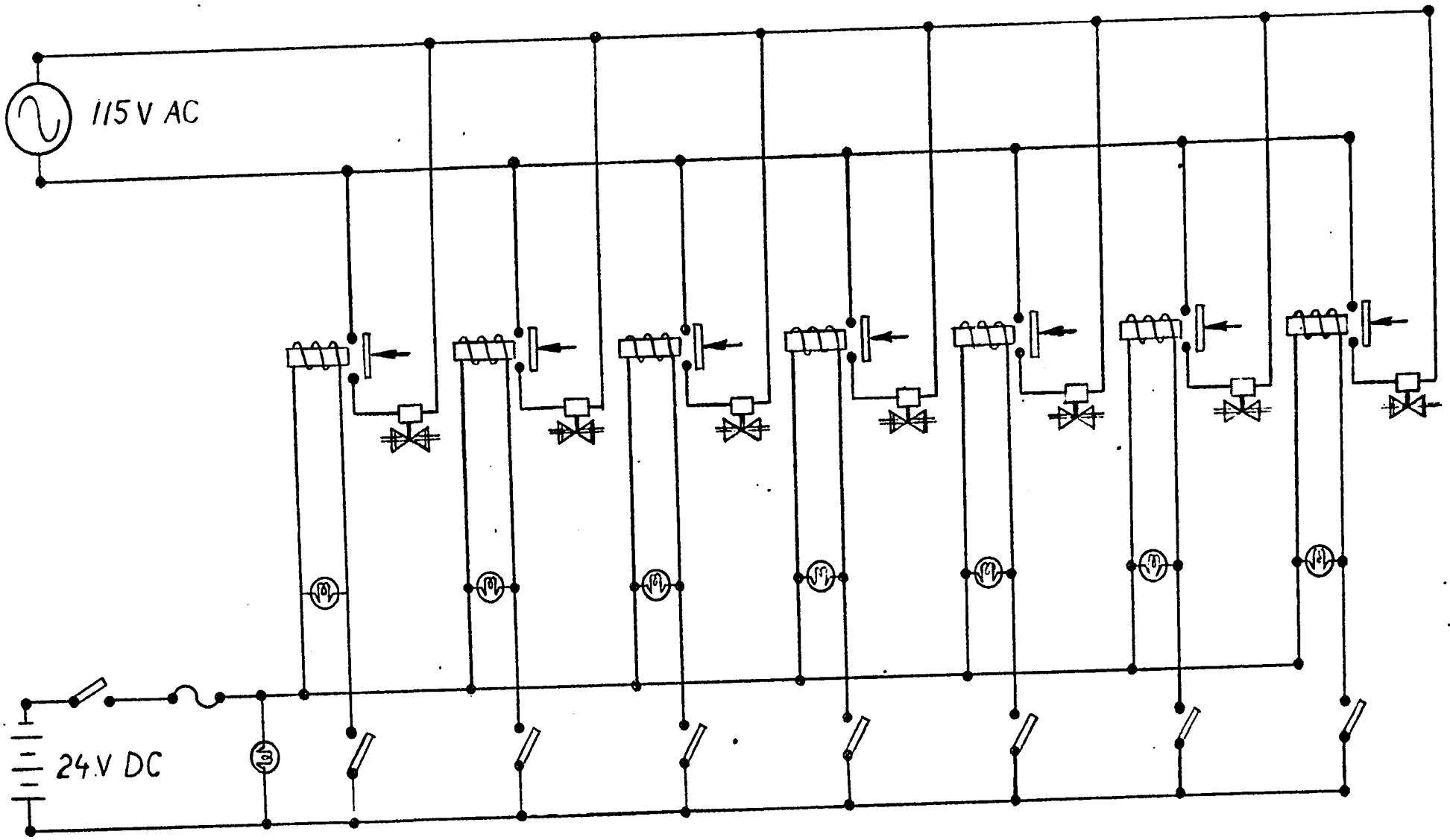

FIGURE 5-9. ELECTRICAL CIRCUIT FOR SOLENOID VALVES

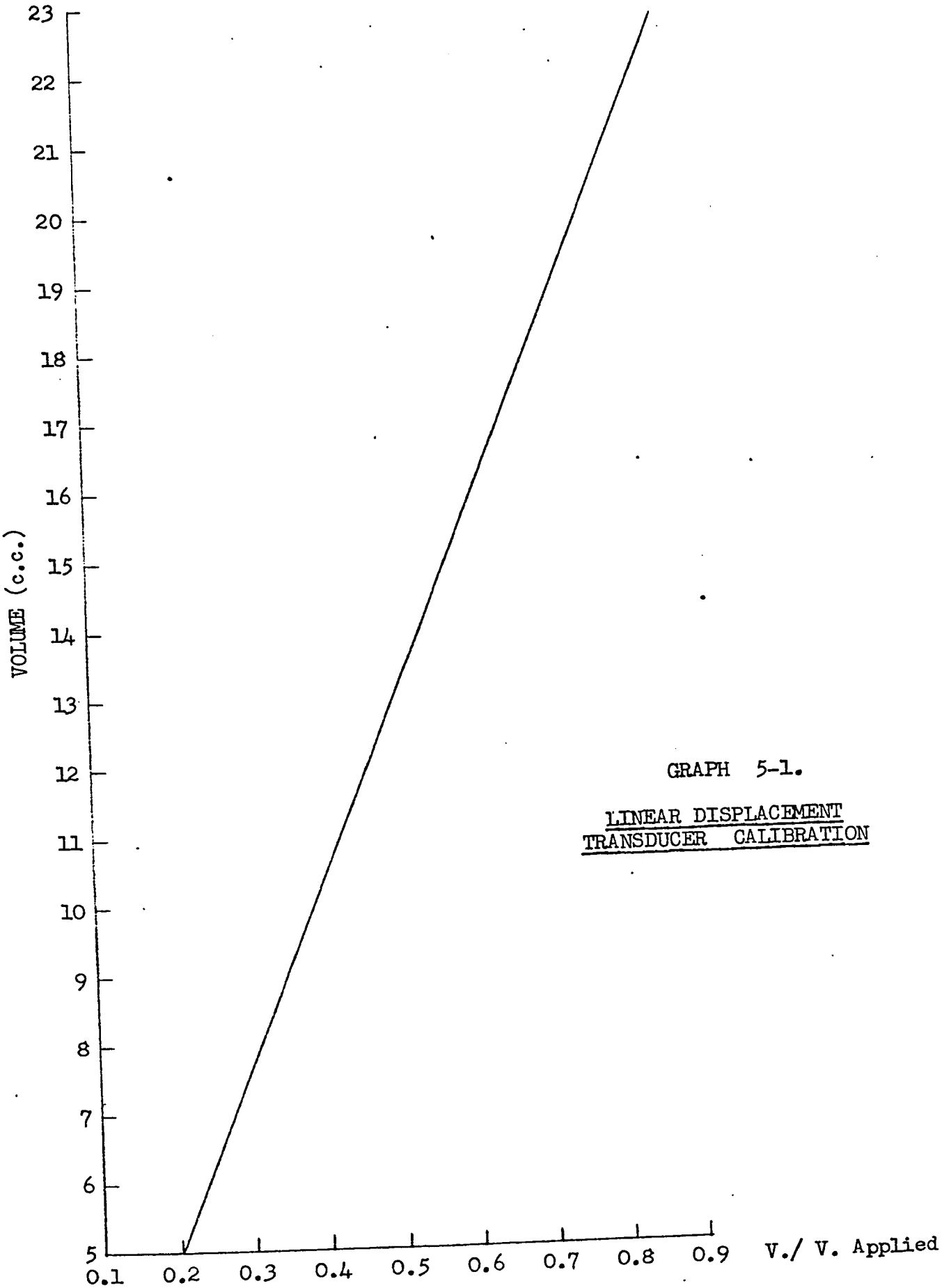

GRAPH 5-1.

LINEAR DISPLACEMENT
TRANSDUCER CALIBRATION

GRAPH 5-2. DIFFERENTIAL PRESSURE TRANSDUCER CALIBRATION

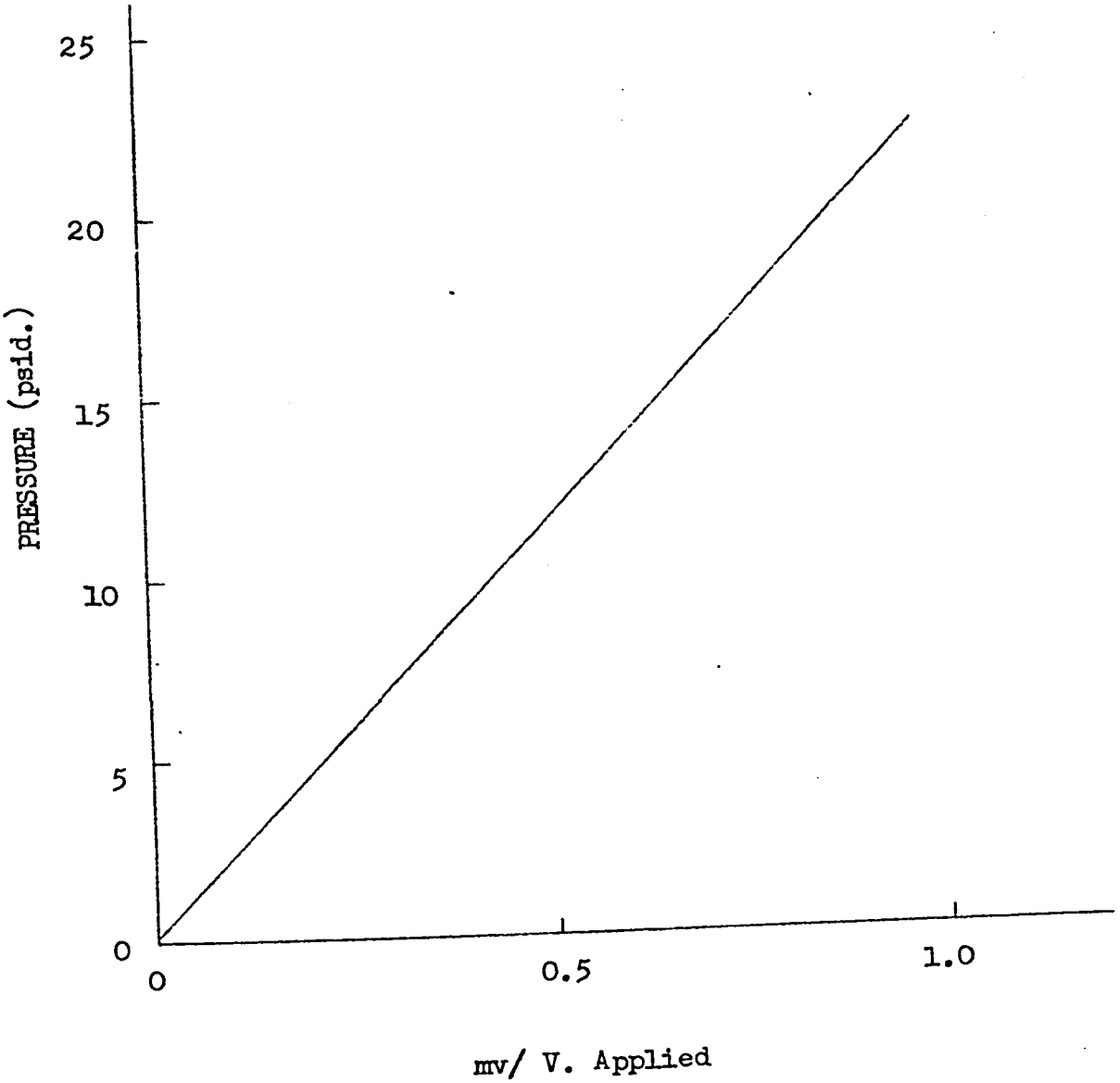

GRAPH 5-3. DIFFERENTIAL PRESSURE TRANSDUCER CALIBRATION

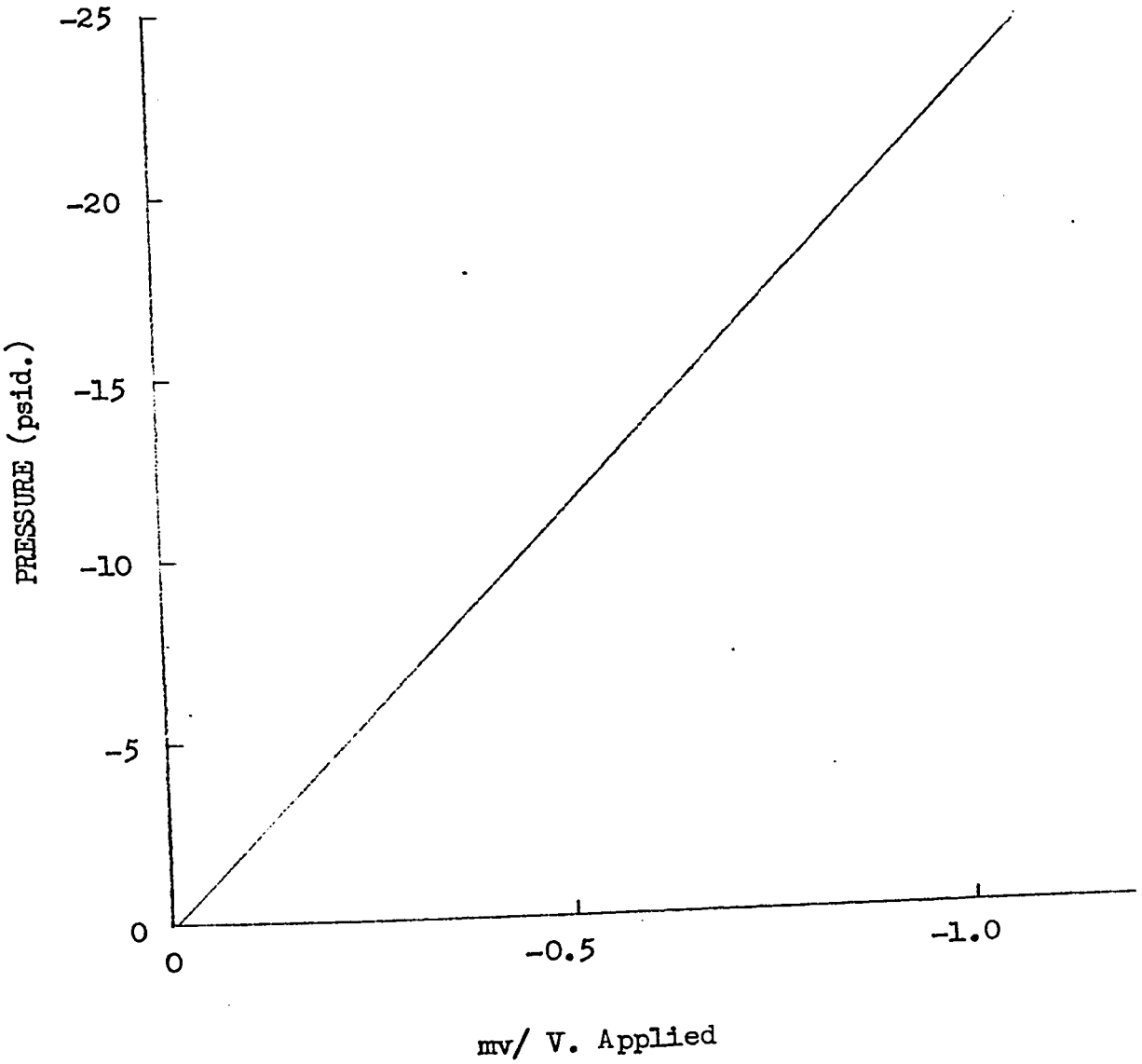

GRAPH 5-4. ABSOLUTE PRESSURE TRANSDUCER CALIBRATION
ALINCO PRESSURE CELL:SERIAL #33120

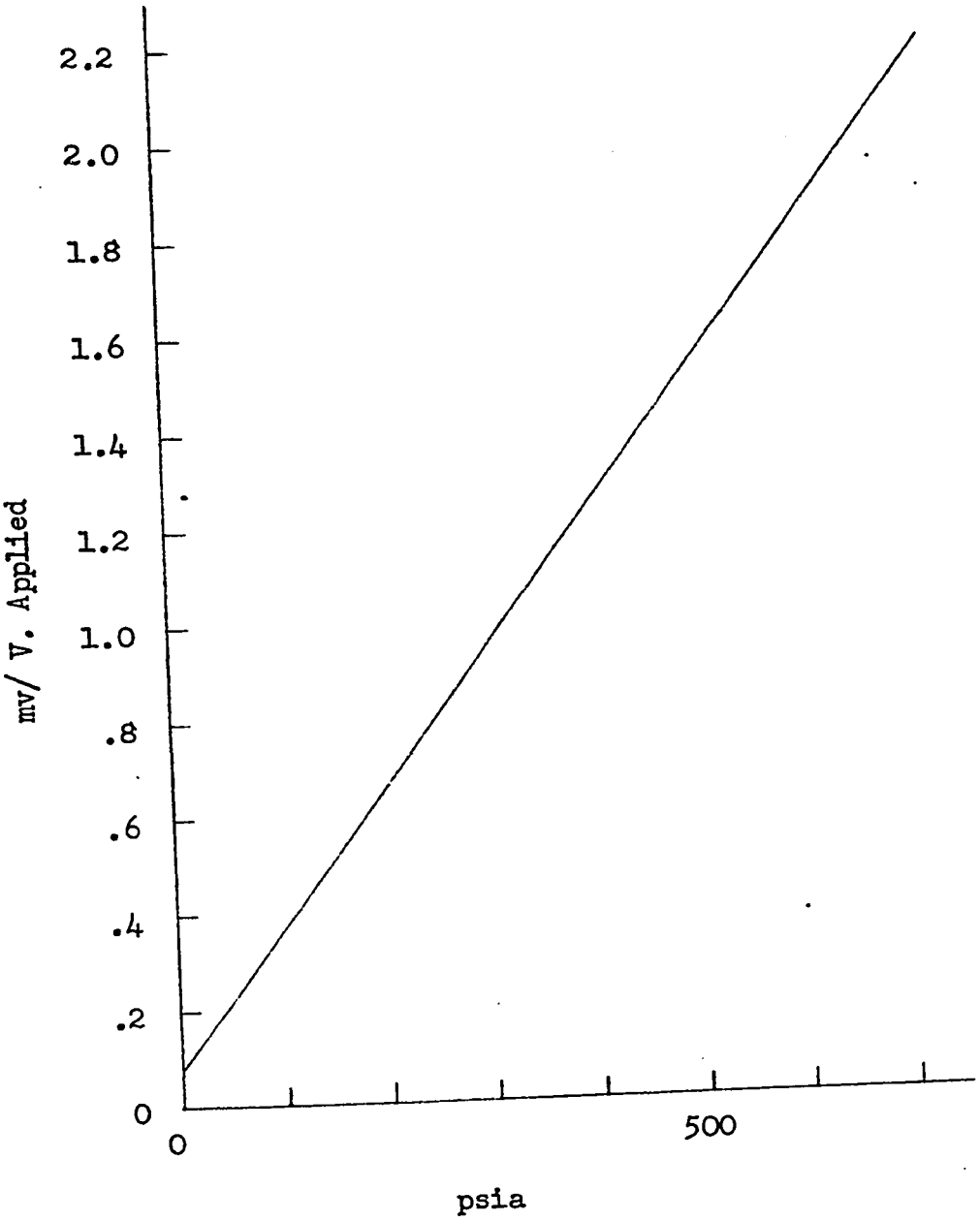

GRAPH 5-5. PRESSURE GAUGE CALIBRATION

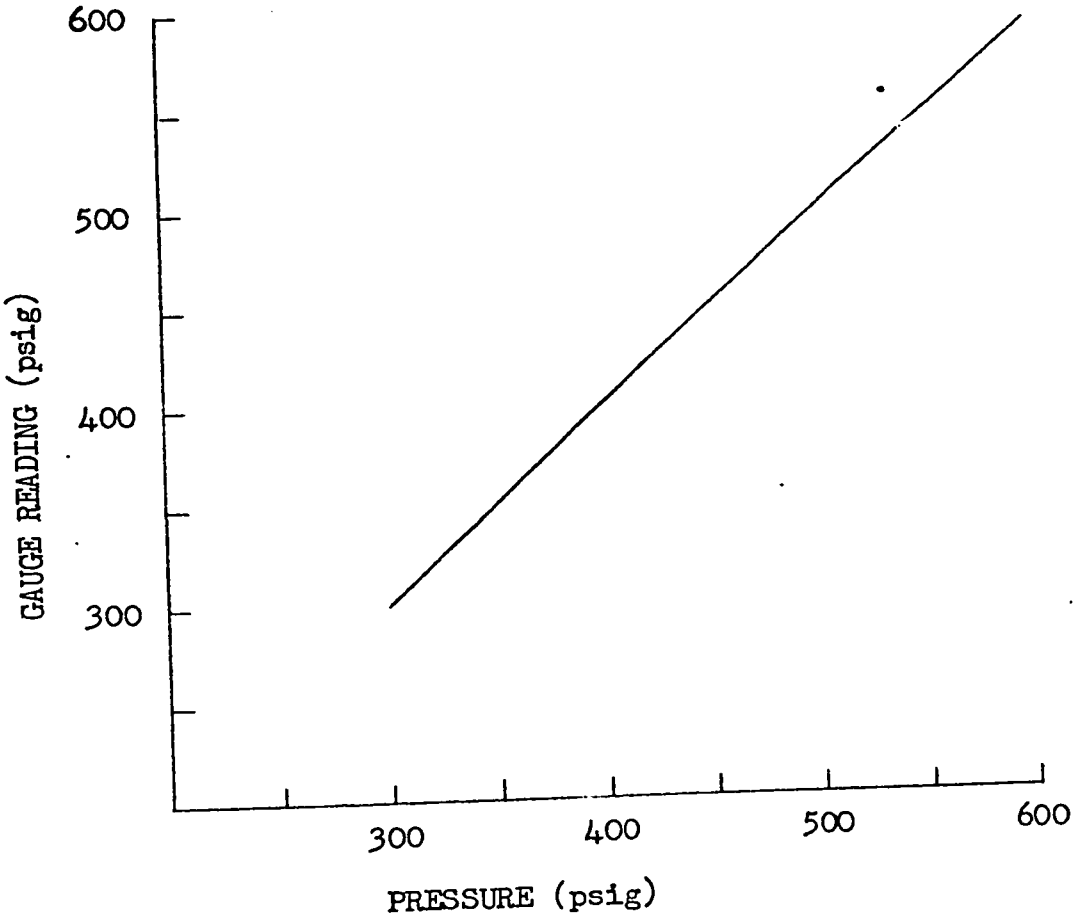

GRAPH 5-6. ABSOLUTE PRESSURE TRANSDUCER CALIBRATION
ALINCO PRESSURE CELL:SERIAL #33121

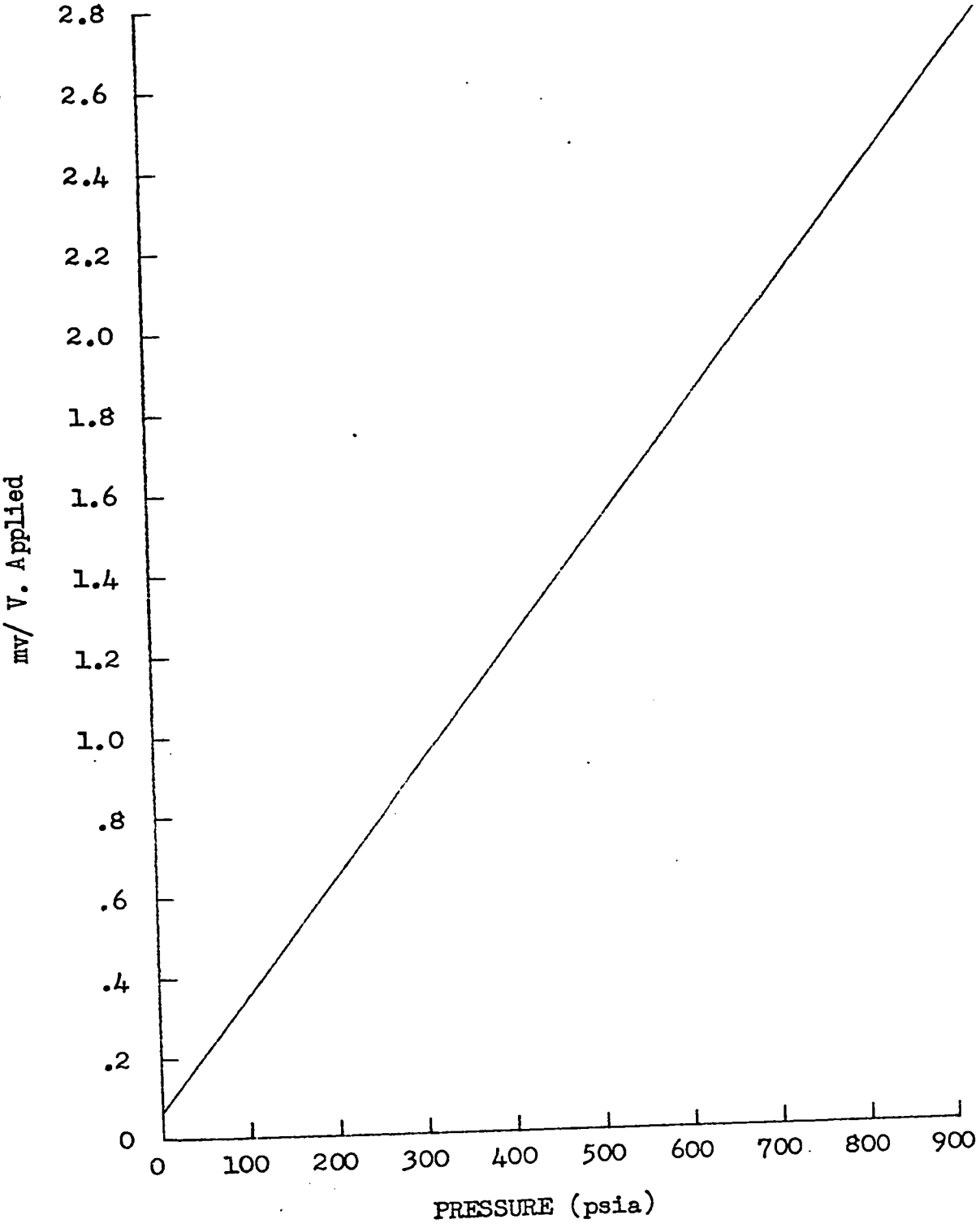

Appendix C

Photographic recordings

Photograph 6-1	Linear Displacement Transducer output. Liquid fuel reservoir partly filled.
6-2	Linear Displacement Transducer output. Liquid fuel reservoir completely filled.
6-3	Camera recording
6-4	Absolute Pressure Transducer outputs.
6-5	Camera recording
6-6	Absolute Pressure Transducer outputs.

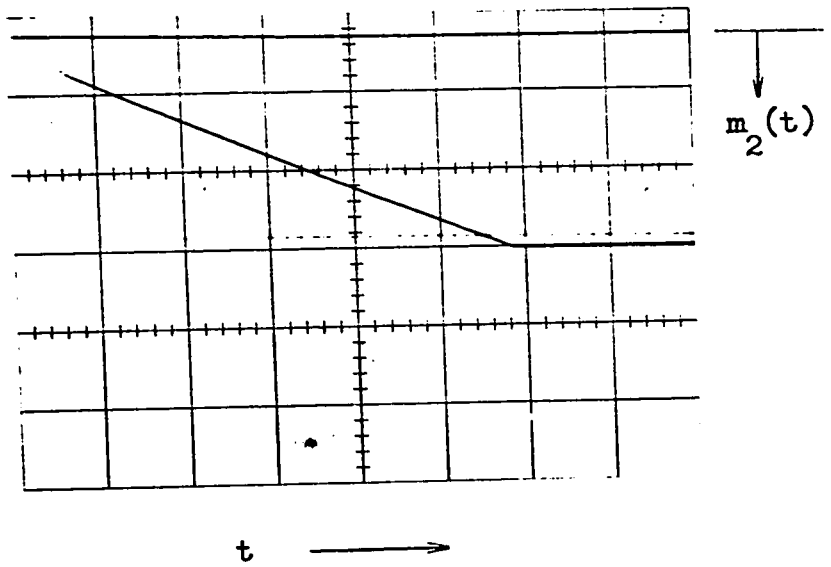

Photograph 6-1

Linear Displacement Transducer Output, $m_2(t)$

Liquid Fuel Reservoir Partly Filled.

Fuel: Ethyl Alcohol

$M_{2f} < 18.091$ g

Sweep speed: 0.1 sec/cm

$T_o = 900°F$

$P_o = 400$ psig

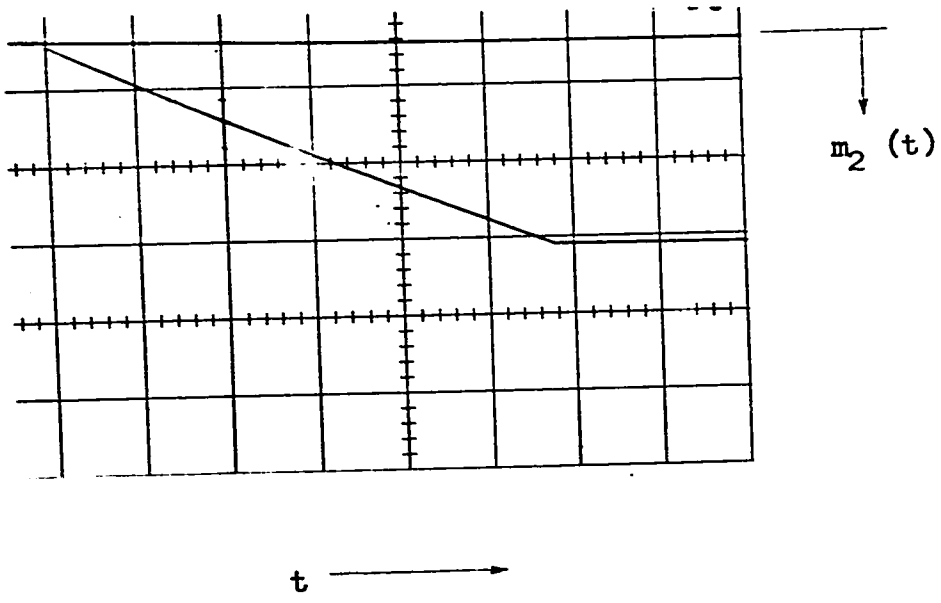

Photograph 6-2

Linear Displacement Transducer Output, $m_2(t)$

Liquid Fuel Reservoir Completely filled.

Fuel: Ethyl Alcohol.

M_{2f} = 18.091 g

T_o = 900°F

P_o = 400 psig

Sweep speed: 0.1 sec/cm

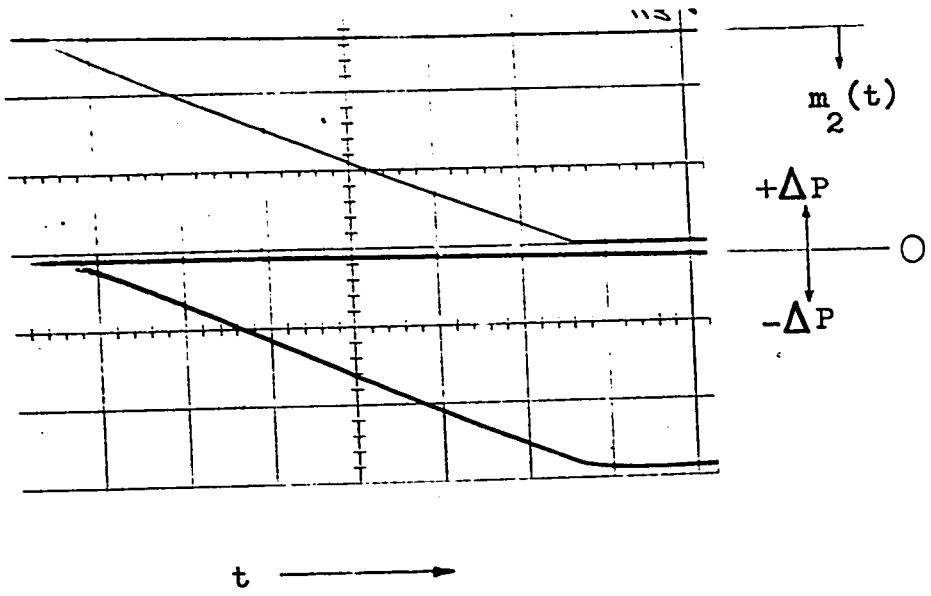

Photograph 6-3 Camera Recording

Upper trace: Linear Displacement Transducer output.

Lower trace: Differential Pressure Transducer output.

Fuel: Ethyl alcohol

M_{2f} = 18.091 g

T_o = 900°F

P_o = 400 psig

Sweep speed: 0.1 sec/cm

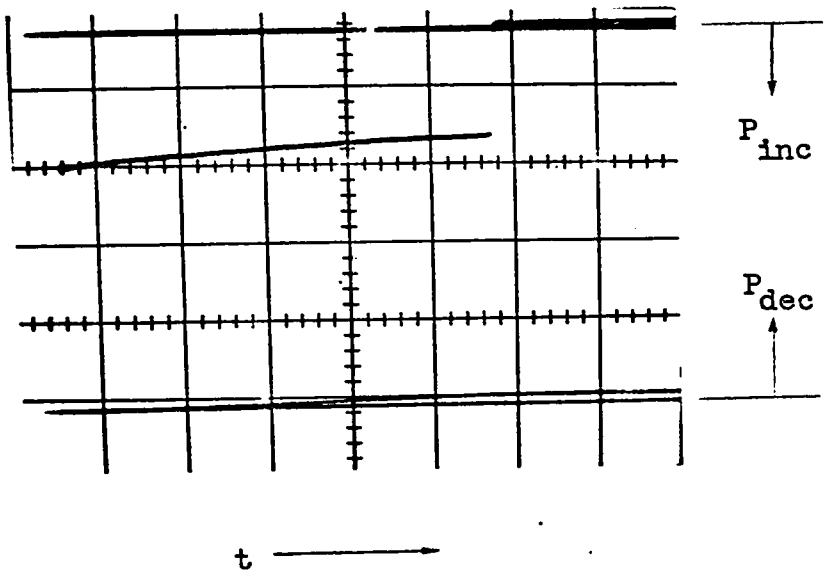

Photograph 6-4 Absolute Pressure Transducer outputs

Upper trace: Absolute Injection pressure.

Lower Trace: Absolute evaporation chamber pressure.

T_o = 900°F

P_o = 400 psig

Sweep speed: 0.1 sec/cm

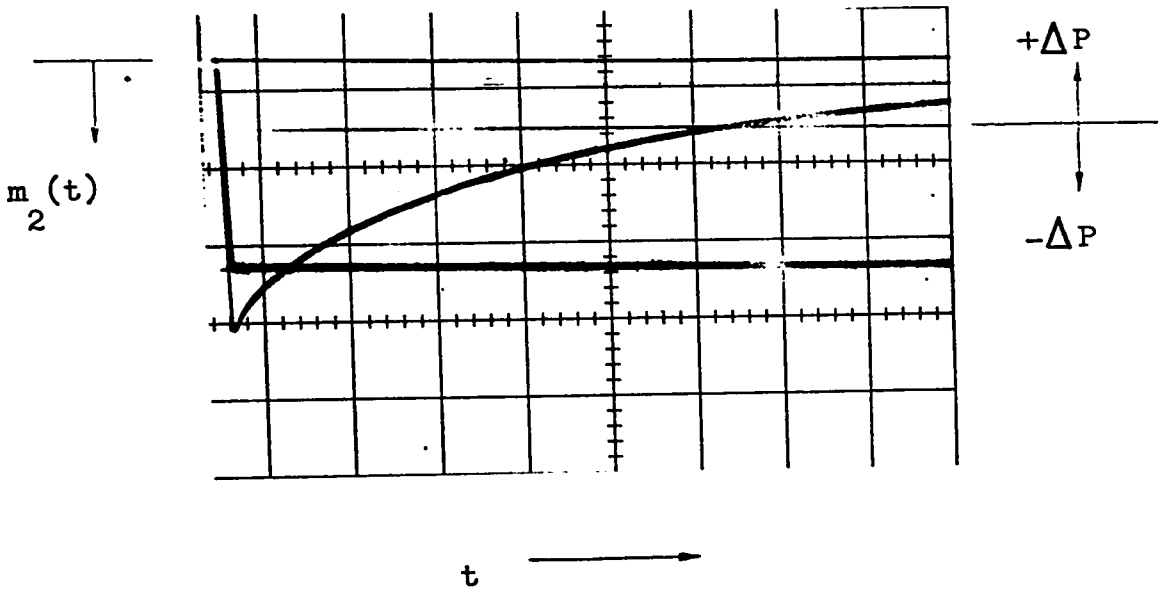

Photograph 6-5 Camera Recording

Upper beam: Linear Displacement Transducer output.

Lower beam: Differential Pressure Transducer output.

M_{2f} = 18.091 g

T_o = 900°F

P_o = 400 psig

Sweep speed: 5.0 sec/cm

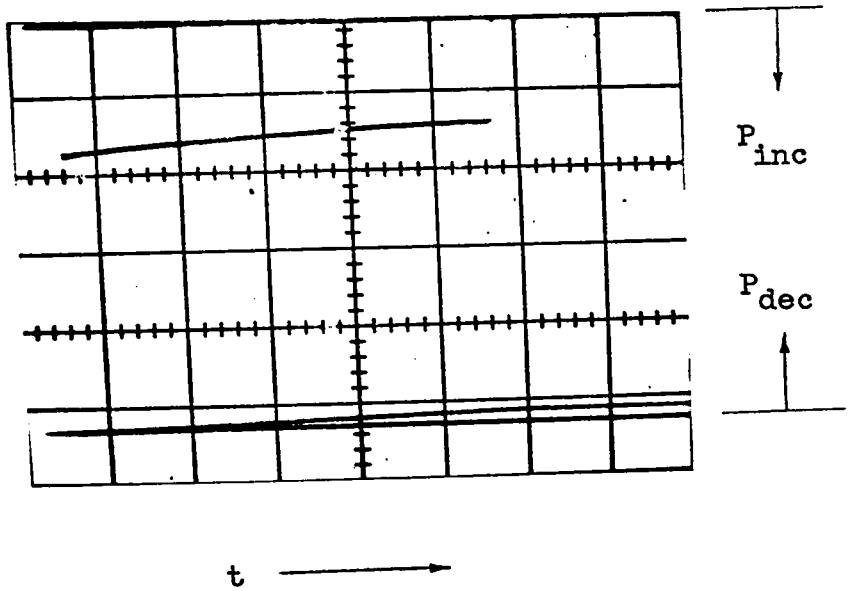

Photograph 6-6 Absolute Pressure Transducer outputs

Upper trace: Absolute injection pressure.

Lower trace: absolute evaporation chamber pressure

T_o = 900°F

P_o = 400 psig

Sweep speed: 0.10 sec/cm

Appendix D

Sample Evaluation of Experimental Data-Ideal Gas Expressions.

Fuel: Ethyl alcohol

Inert gas: Nitrogen

T_o (Initial evaporation chamber temperature): 900°F (755.2°K)

P_o (Initial evaporation chamber pressure): 414.7 psia

M_1 (Molecular weight of N_2): 28.016

M_2 (Molecular weight of C_2H_5OH): 46.07

m_{2f} (Maximum injected liquid fuel mass, g): 18.091

L_2 (Latent heat of vaporization): 204 cal/g

(1). Calculation of the mass of nitrogen gas in the evaporation chamber from the Ideal Gas Law.

$$m_1 = \frac{P_o V M_1}{R T_o} = \frac{414.7}{14.7} \times \frac{82.36}{.082054} \times \frac{28.016}{755.2} = 1050.42 \text{ g.}$$

From Van der Waal's equation:

$$(P+\frac{a}{v^2})(v-b) = RT$$

where a = 1.390 (liters^2 × atm)/mole^2

and, b = 0.03913 liters/mole

For T_o = 755.2°K and P_o = 414.7 psig, v = 2.213902 liters/g mole. Therefore

$$m_1 = \frac{82.36 \times 28.016}{2.213902} \text{ (g)} = 1{,}042.231 \text{ g.}$$

The difference between the two calculated masses is

$$\frac{1050.42 - 1042.23}{1042.23} \times 100\% = 0.79\%$$

(2). $$X_f = \frac{m_{2f}}{m_1} = \frac{18.091}{1042.231} = 0.017,358$$

(3). $$\mu = \frac{M_1}{M_2} = \frac{18.091}{46.07} = .608,118$$

(4). Calculation of maximum temperature drop in the evaporation chamber from measured maximum pressure drop:

$$\Delta P \text{ (max)} = 12.3 \text{ psia}$$

From equation (4-14)

$$T_i = \frac{P_i}{P_o} T_o \left(\frac{1}{1+X_f \mu}\right)$$

Therefore,

$$T \text{ min} = \frac{402.4}{414.7} \times 755.\dot{2} \quad \frac{1}{(1+.017,357,9 \times .608,118)}$$

$$= 725.167,7°K$$

(5). Calculation of average C_{v_1} (cal/g.°K)

C_{p_1} (at 800°K) = 7.512 (ref. 4-3)

C_{p_1} (at 700°K) = 7.350

By linear interpretation:

C_{p_1} (at 755.$\dot{2}$°K) = 7.439,46

C_{p_1} (at 725.167,7°K) = 7.390,771,7

$\bar{C}_{p_1}$ = 7.415,115,8

$$\bar{C}_{v_1} = \frac{\bar{C}_{p_1} - AR}{M_1} = \frac{7.415,115,8-1.987}{28.016} = 0.193,75$$

(6). Calculation of $\bar{C}_{p_2}$ (cal/g.°K)

$$\bar{C}_{p_2} = \frac{1}{(T_o-T)M_2} \int_T^{T_o} (4.946+0.049087T-0.000,023,855T^2 + .000,000,004,5T^3)\, dT$$

$$= \frac{1}{46.07} [4.946+0.024,543,5(T_o+T) - .000,007,952(T_o^2+T_oT+T^2) + .000,000,001,125(T_o^3+T_o^2T+T_oT^2+T^3)]$$

$$= 0.651,922,2 \text{ cal/g.°K}$$

(7). Calculation of γ_i from equation (4-12c)

$$\gamma_i = \frac{\bar{C}_{p_2} - AR/M_2}{\bar{C}_{v_1}} = 3.142,086$$

(8). Calculation of β_i from equation (4-12a)

$$\beta_i = \frac{1}{\bar{C}_{v_1} T_o} [L_2 + \int_{T_{2,o}}^{T_s} C_2 dT + \int_{T_s}^{T_o} C_{p_2} dT - \bar{C}_{p_2} T_o]$$

$$\int_{T_{2,o}}^{T_s} C_2 dT = \int_{T_{2,o}}^{T_s} (19.02967-.004,812T+.000,091,3T^2) dT$$

$$= (T_s-T_{2,o})[19.029,67-.002406(T_s+T_{2,o}) + .000,030\dot{4}3(T_s^2+T_sT_{2,o}+T_{2,o}^2)]$$

$T_s = 351.3°K$; $T_{2,o} = 273°K$

$= 44.989$ cal/g.

$$\int_{T_s}^{T_o} C_{p_2}\, dT = \int_{T_s}^{T_o} (4.946 + .049087T - .000,023,855T^2 + .000,000,004,5T^3)\, dT$$

$$= \frac{(T_o - T_s)}{M_2} [4.946 + .024,543,5(T_o + T_s) - .000,007,952\ (T_o^2 + T_o T_s + T_s^2) + .112,5 \times 10^{-8}\ (T_o^3 + T_o^2 T_s + T_o T_s^2 + T_s^3)]$$

$$= 222.18 \text{ cal/g.}$$

$$\beta_i = -0.144,735$$

(9). Calculation of P_∞

$$P_\infty = P_o(1 + \mu X_f)$$

$$= 414.7\ (1 + .608,118 \times .017,358)$$

$$= 419.077,45 \text{ psia}$$

$$P_\infty - P_o = 4.377,45 \text{ psia}$$

(10). Calculation of B_i

$$\frac{P_\infty - P}{P_\infty - P_r} = \exp\ \{-\frac{(t - t_r)}{B_i}\}$$

From experimental data

$$P_\infty - P_r = 10,377,45$$

$$P_\infty - P = 6.677,45$$

$$B_i = 5/\ell n\left(\frac{10.377,45}{6.677,45}\right) = \frac{5}{.440,892,7} = 11.340,628$$

(11). Calculation of $\dot{m}_2$ from experimental data

$$\dot{m}_2 = \frac{18.091}{.61} = 29.657 \text{ g/sec}$$

(12). Calculation of K

$$K = \frac{1}{\kappa}\left(\frac{m_1}{\dot{m}_2}\right)^2\left(\frac{1+\gamma_i\chi_f}{B_i}\right)\frac{(\beta_i+\gamma_i)}{(\beta_i+\gamma_i-\mu)}$$

$$= 146.892/\kappa$$

(13). From experimental data

$$\frac{dp}{dt} = 21.742 \text{ psia/sec}$$

(14). $$\Delta P_i' = P_o\chi\,\frac{(\beta_i+\gamma_i-\mu)+\beta_i\mu\chi'}{1+\gamma_i\chi'} = P_o\chi\,\frac{2.389,233-.088,0159\chi'}{1+3.142,086\chi'}$$

$$t_L = 2.5\left[-\frac{P-P_i'}{\frac{dp}{dt}} - K\chi^2\right]$$

m_2	18.091
χ_f	0.017,358
χ^2	$0.301,3 \times 10^{-3}$
$P_o\chi$	7.198,363
ΔP	12.05±.05

κ	K	t_L (m sec)
.30	489.64	-84.600
.35	419.69	6.133
.40	367.23	75.320
.45	326.43	129.844
.50	293.78	173.938

(15). Repeat steps (1) to (14) with different values of injected liquid fuel mass and for the same κ values listed in step (14).

(16). Draw a smooth curve through the points having the same κ value to obtain the κ curves.

(17). Draw in the boundary line of the quasi-steady state region to intersect the κ curves.

(18). Determine the upper limiting κ curve by observation. This curve intersects the boundary line of step (17) horizontally.

Appendix E

Sample Evaluation of Experimental Data-non-Ideal Gas Expression.

Fuel: Ethyl Alcohol

T_o : 900°F (755.2°K)

P_o : 414.7 psia

(1). Calculation of the mass of nitrogen gas in the evaporation chamber from the Ideal Gas Law.

$$m_1 = \frac{P_o V M_1}{R T_o} = 1050.42 \text{ g.}$$

(2). $$X_f = \frac{18.091}{1050.42} = 0.017,222,5$$

(3). Calculation of maximum temperature drop in the evaporation chamber from measured maximum pressure drop. Equation (4-128).

ΔP (max) = 12.3 psia

$$T \text{ min} = \frac{402.4}{414.7} \times 755.2 \times \frac{1}{(1+.017,222,5 \times .608,118)}$$

$$\simeq 725°K$$

(4). Calculation of C_{v_1} (cal/g.°K)

Same as in the ideal gas case.

$$\bar{C}_{v_1} = .193,75$$

(5). $\mu = 0.608,118$

(6). Calculation of $\bar{C}_{p_2}$ (cal/g°K)

Same as in the ideal gas case

$$\bar{C}_{p_2} = 0.651,922$$

(7). Calculation of γ_n from equation (4-23b).

From figure (4-1) appendix A.

$$e_2(T_o,P_o) = h(T_o,P_o)-P_o v = 415.1 \text{ cal/g.}$$

$$e_2(T_o,1) = h(T_o,1)-v = 444.5 \text{ cal/g.}$$

$$e_2(480°C,1) = 442.7 \text{ cal/g.}$$

$$e_2(420°C,1) = 405.2 \text{ cal/g.}$$

$$e_2(480°C,30 \text{ atm}) = 411.7 \text{ cal/g.}$$

$$e_2(420°C,30 \text{ atm}) = 375.1 \text{ cal/g.}$$

$$e_2(480°C,20 \text{ atm}) = 426.3 \text{ cal/g.}$$

$$\left.\frac{\partial e_2(T,1)}{\partial T}\right]_p = \frac{e_2(480°C,1 \text{ atm})-e_2(420°C,1 \text{ atm})}{480°C-420°C} = .612.0$$

$$\left.\frac{\partial e_2(T,30)}{\partial T}\right]_p = \frac{e_2(480°C,30)-e_2(420°C,30)}{480°C-420°C} = .597.6$$

$$a = \left.\frac{\partial e_2(T,30)}{\partial T}\right]_p - \left.\frac{\partial e_2(T,1)}{\partial T}\right]_p = -0.015,433,3$$

$$b = \left.\frac{\partial e_2(480,P)}{\partial P}\right]_T = \frac{e_2(480,30)-e_2(480,20)}{30 - 20} = -1.460$$

$$\zeta = \frac{bP_o}{C_{v_1} T_o} = -.281,443$$

$$\gamma_n = 3.062,431$$

(8). Calculation of β_n from equation (4-23a)

$$\beta_n = .020,04$$

(9). $P_\infty = 419.077$ psia (Same as in ideal gas case)
$P_\infty - P_o = 4.377$ psia

(10). From experimental Data (same as in ideal gas case)

$$B_n = 11.34$$

(11). Calculation of $\dot{m}_2$ from experimental data

$$\dot{m}_2 = 29.66 \text{ g/sec}$$

(12).
$$\frac{dp}{dt} = 21.74 \text{ psia/sec}$$

(13).
$$\Delta P_n' = 414.7\chi \frac{[2.192,91 - 0.158,963,8\ \chi']}{[1+\chi'(3.062,43-.281,44\kappa)-.171,15\chi\chi']}$$

(14).
$$0.4t_L \simeq -\frac{P-P_n'}{21.74} - 88.459,23\ \frac{\chi^2}{\kappa} - 9.968,33(1.793,03+\frac{1}{\kappa})\chi^2$$

Appendix F

Lifetime of ethyl alcohol and water sprays at various initial evaporation chamber temperatures and pressures.

Figure 6-1	T_o = 900°F;	P_o = 400 psig.	$\dot{m}_2$ = 29.7 g/sec
Figure 6-2	T_o = 800°F;	P_o = 450 ;	$\dot{m}_2$ = 32.6 g/sec
Figure 6-3	T_o = 800°F;	P_o = 400 ;	$\dot{m}_2$ = 32.3 "
Figure 6-4	T_o = 800°F;	P_o = 400 ;	$\dot{m}_2$ = 29.9 "
Figure 6-5	T_o = 700°F;	P_o = 500 ;	$\dot{m}_2$ = 32.4 "
Figure 6-6	T_o = 700°F;	P_o = 450 ;	$\dot{m}_2$ = 32.0 "
Figure 6-7	T_o = 700°F;	P_o = 400 ;	$\dot{m}_2$ = 32.5 "

Figure 6-8 Comparison of 16-hole (A) and 8-hole (B) nozzles. Fuel: Ethyl alcohol; T_o = 700°F; P_o = 400 psig.

Figure 6-9 Comparison of 16-hole (A) and 8-hole (B) nozzles. Fuel: Ethyl alcohol; T_o = 800°F; P_o = 400 psig.

Figure 6-10 Comparison of 16-hole (A) and 8-hole (B) nozzles. Fuel: Ethyl alcohol; T_o = 900°F; P_o = 400 psig.

Figure 6-11 Comparison of 16-hole (A) and 8-hole (B) nozzles. Fuel: Water; T_o = 700°F; P_o = 400 psig.

Figure 6-12 Comparison of 16-hole (A) and 8-hole (B) nozzles. Fuel: Water; T_o = 800°F; P_o = 400 psig.

Figure 6-13 Comparison of 16-hole (A) and 8-hole (B) nozzles. Fuel: Water; T_o = 900°F; P_o = 400 psig.

Figure 6-14 Comparison of experimental and calculated pressure decreases. Fuel: Ethyl alcohol; T_o = 900°F; P_o = 400 psig.

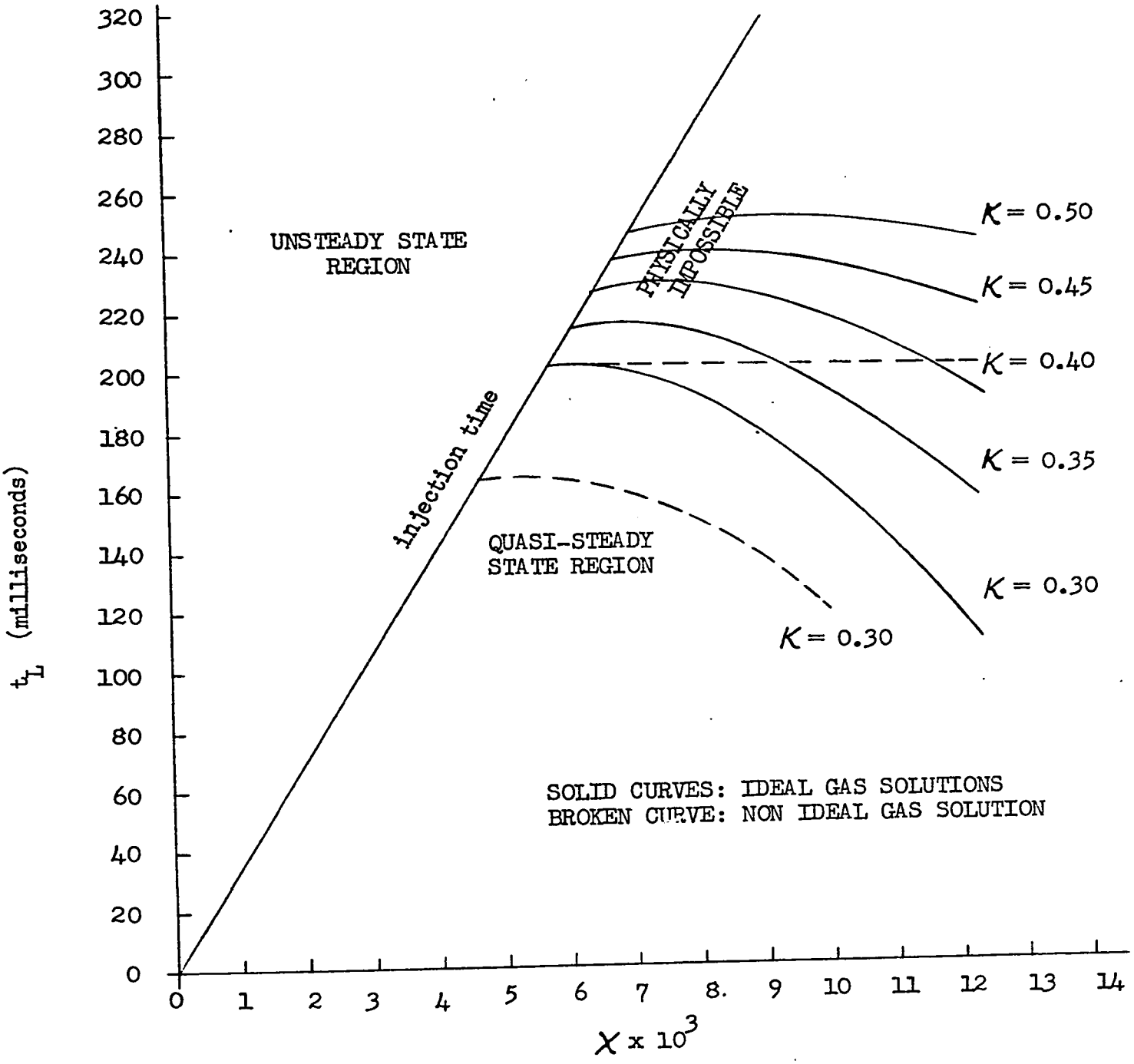

FIGURE. 6-1 LIFETIME OF SPRAY

Fuel: Ethyl alcohol
T_o = 900°F.

P_o = 400 psig.

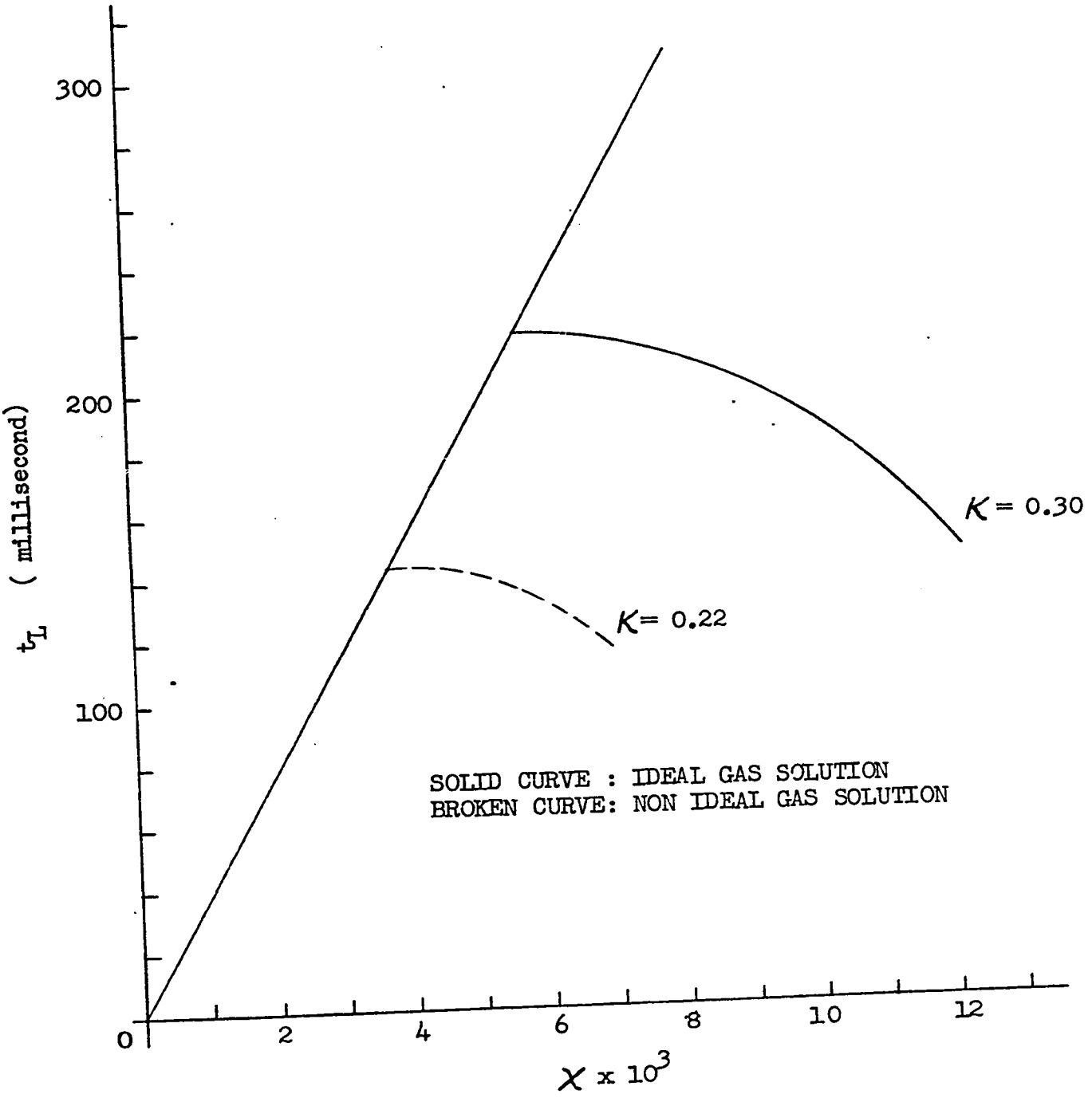

FIGURE. 6-2

LIFETIME OF SPRAY

Fuel: Ethyl alcohol

$T_o = 800^oF$

$P_o = 450$ psig.

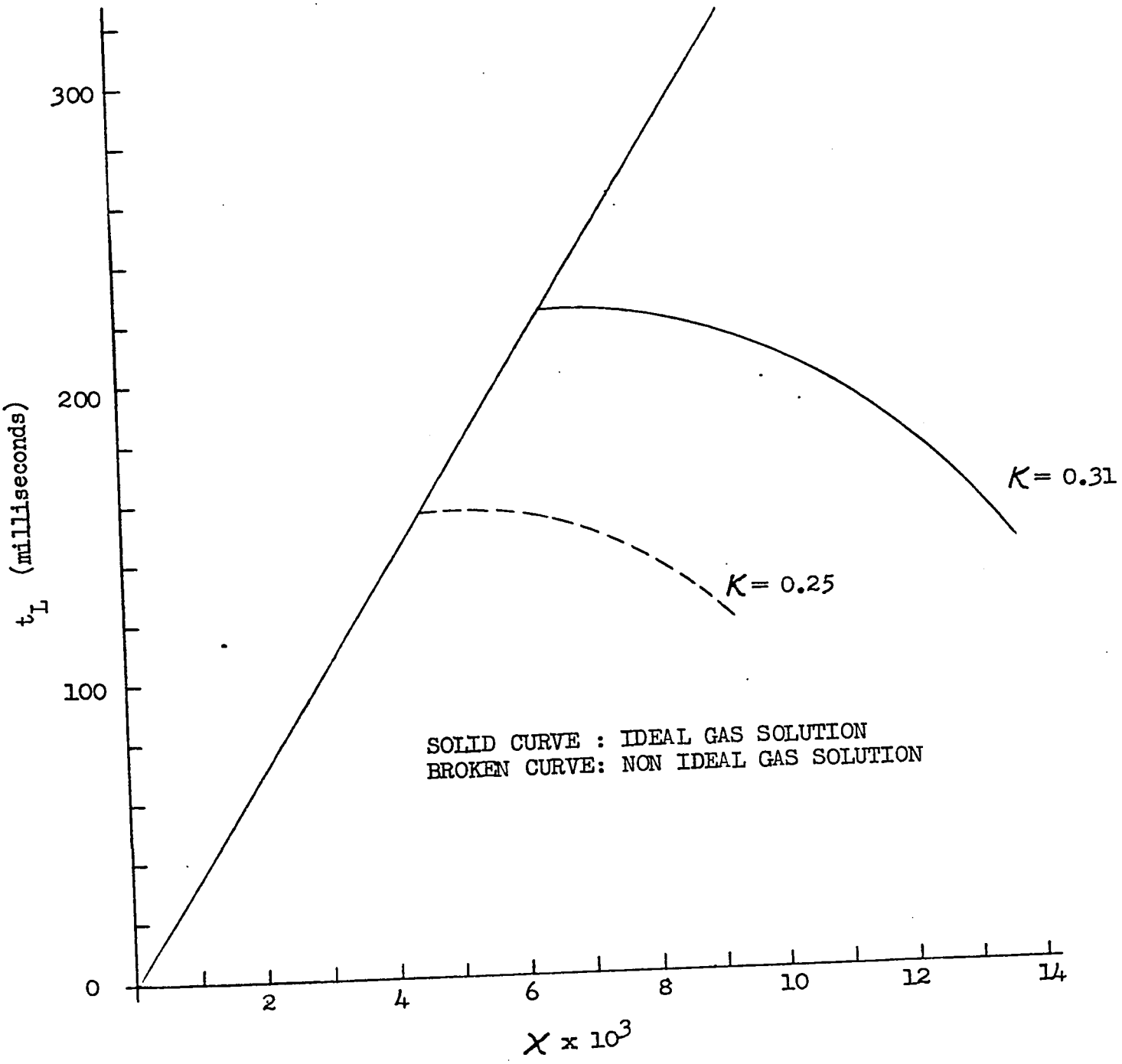

FIGURE. 6-3 LIFETIME OF SPRAY

Fuel: Ethyl alcohol

T_o = 800°F

P_o = 400 psig.

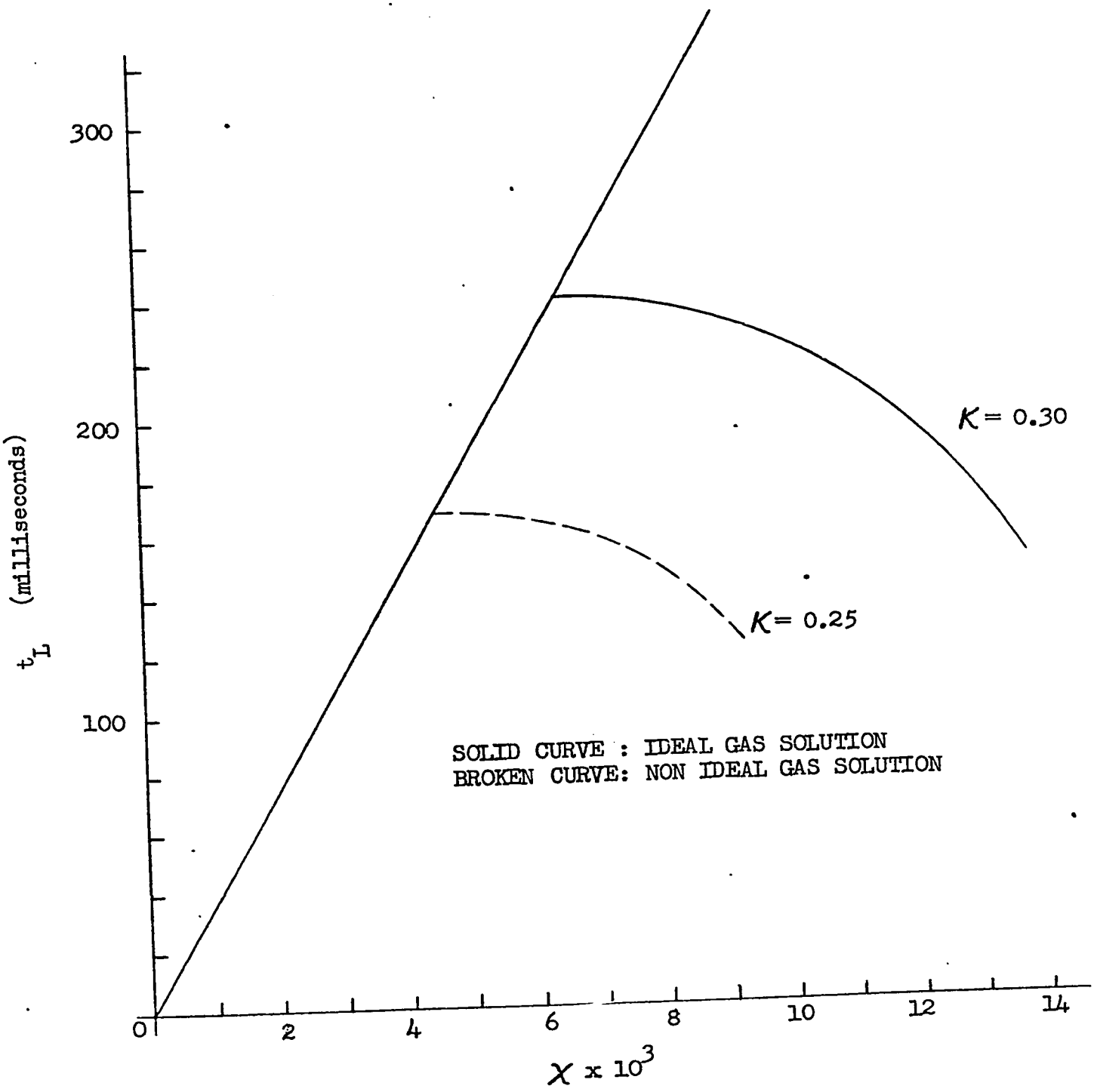

FIGURE. 6-4 LIFETIME OF SPRAY

Fuel: Ethyl alcohol
T_o = 800°F
P_o = 400 psig.

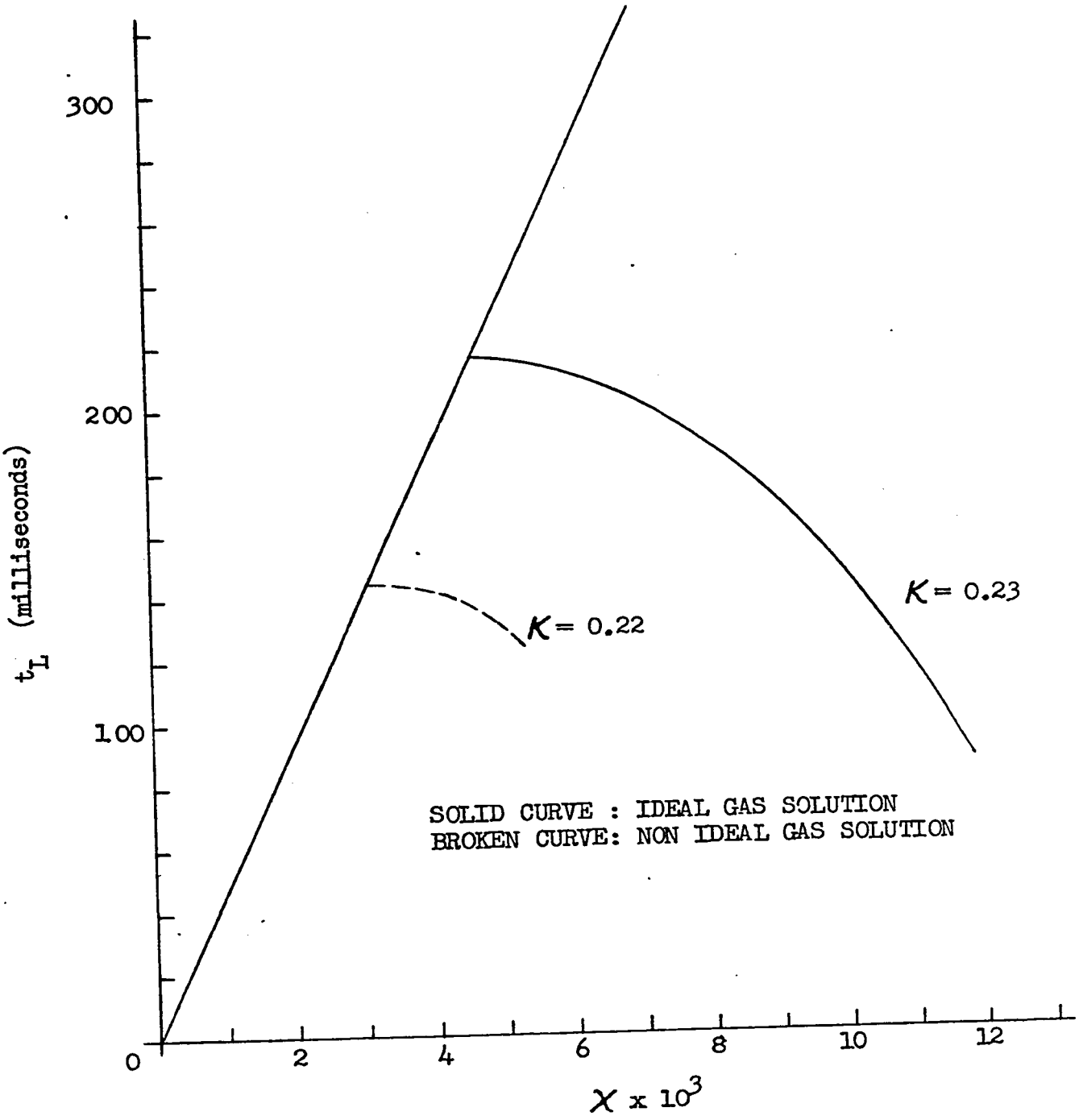

FIGURE. 6-5 LIFETIME OF SPRAY

Fuel: Ethyl alcohol
T_o = 700°F
P_o = 500 psig.

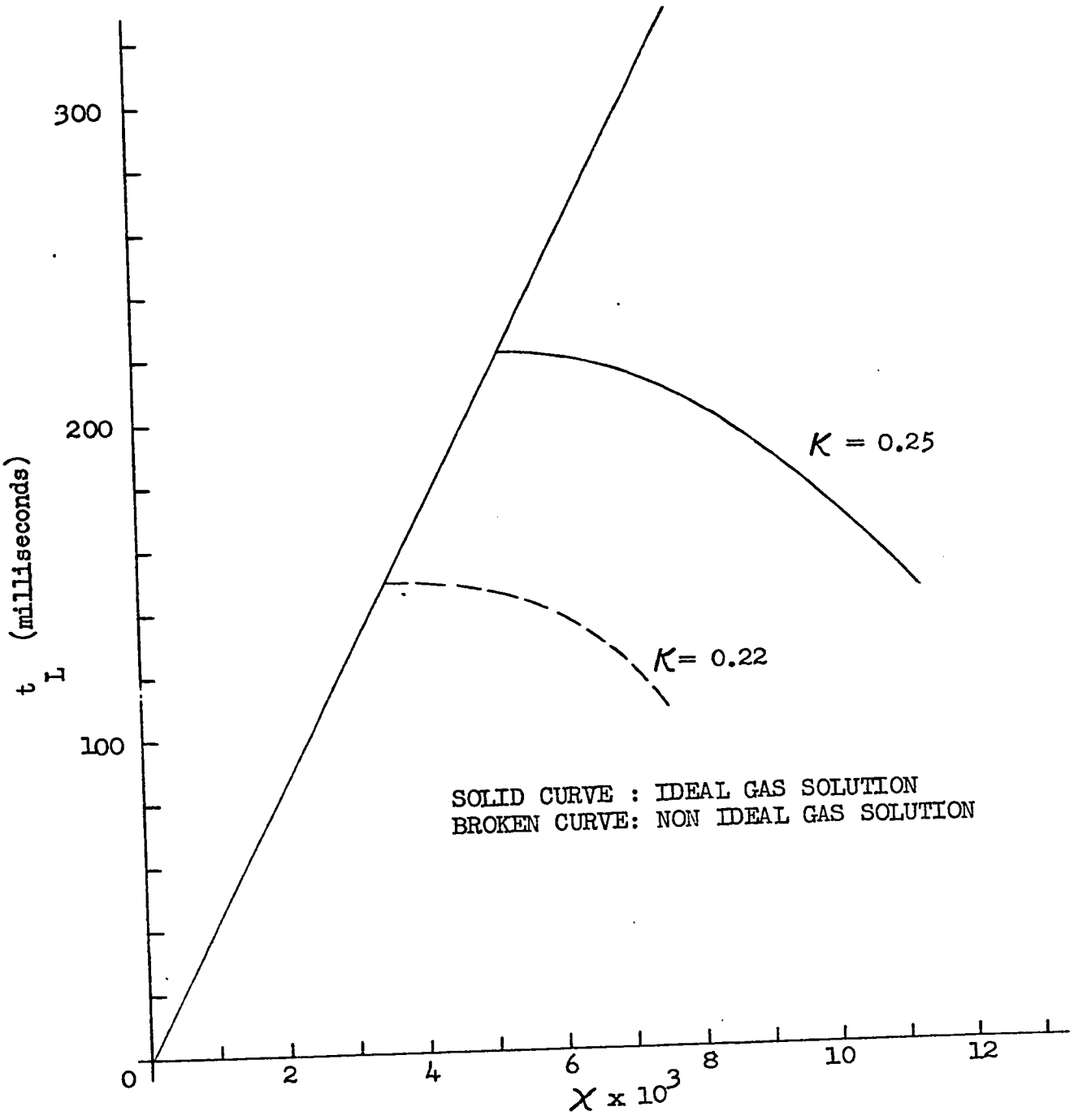

FIGURE. 6-6 LIFETIME OF SPRAY

Fuel: Ethyl alcohol
T_o = 700°F
P_o = 450 psig.

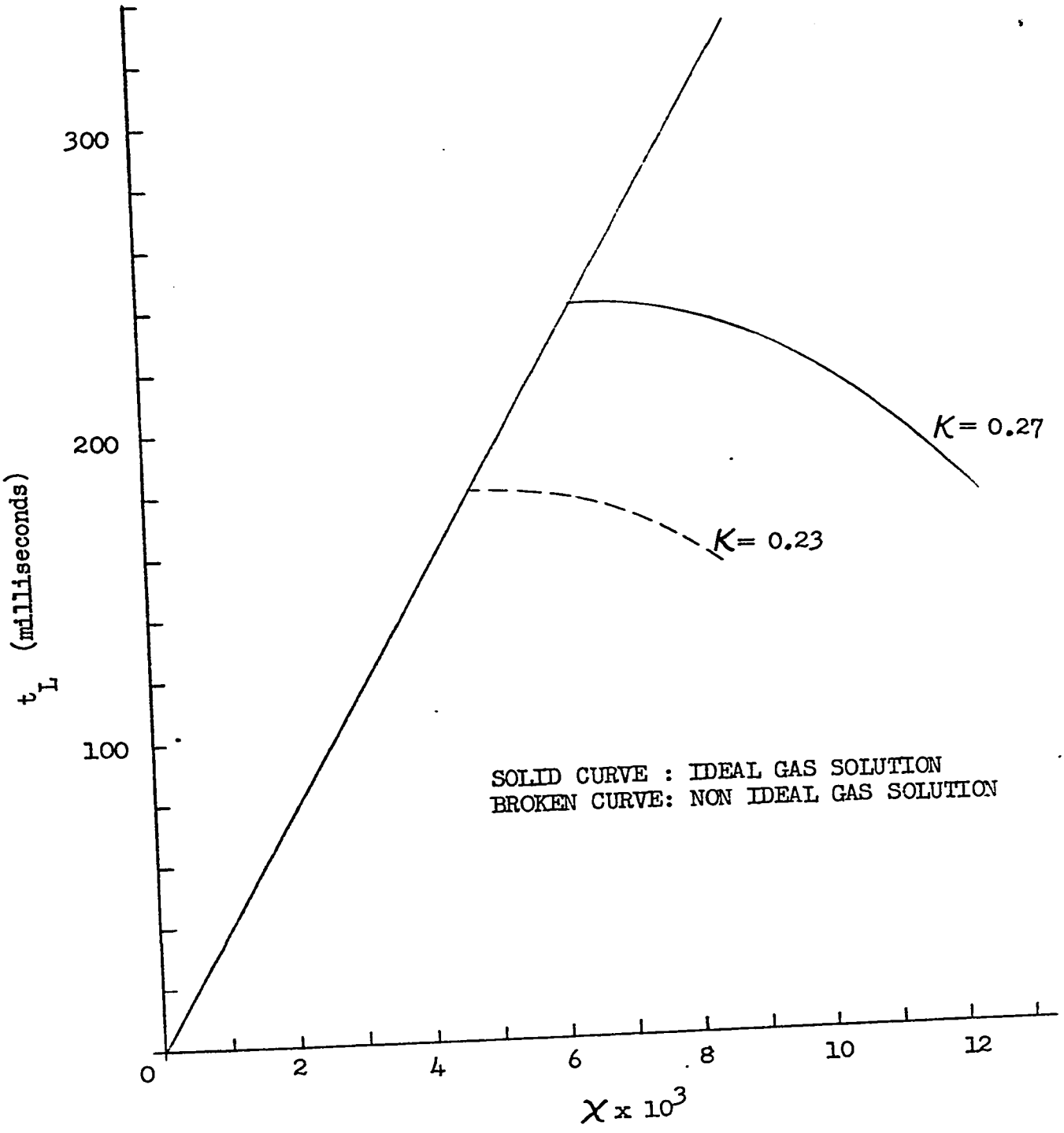

FIGURE. 6-7 LIFETIME OF SPRAY

Fuel: Ethyl alcohol

$T_o = 700^oF$

$P_o = 400$ psig.

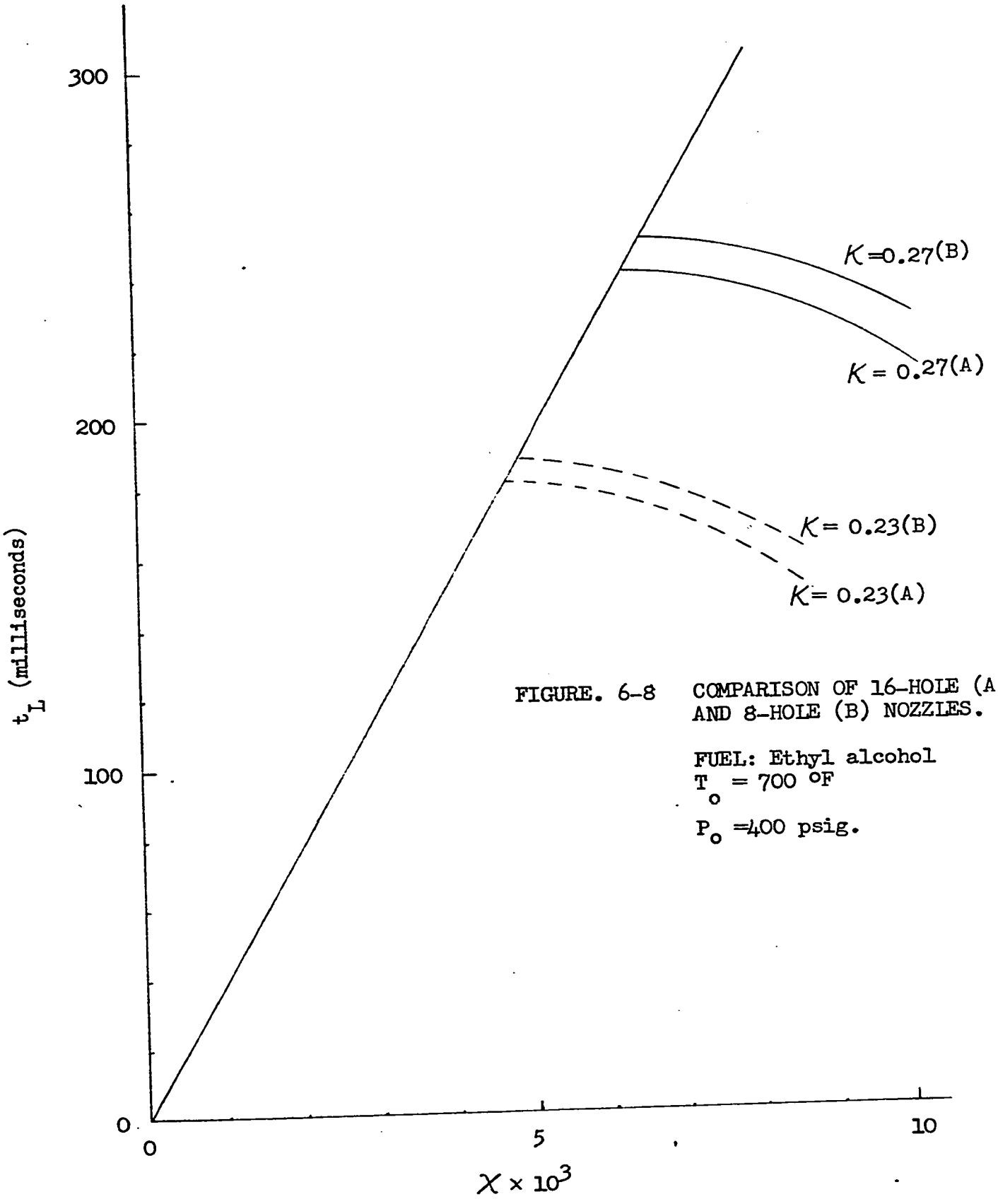

FIGURE. 6-8 COMPARISON OF 16-HOLE (A) AND 8-HOLE (B) NOZZLES.

FUEL: Ethyl alcohol
T_o = 700 °F
P_o =400 psig.

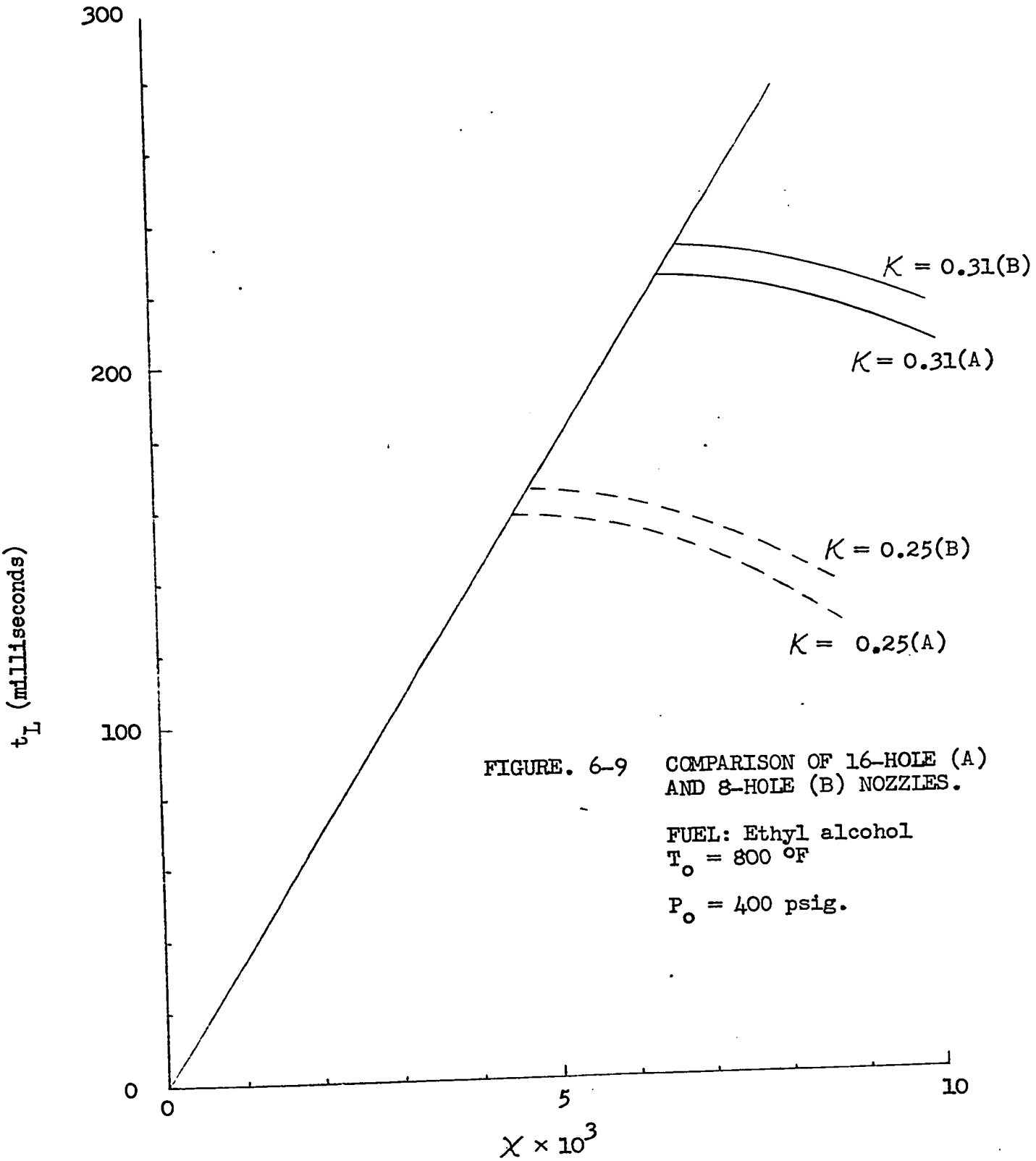

FIGURE. 6-9 COMPARISON OF 16-HOLE (A) AND 8-HOLE (B) NOZZLES.

FUEL: Ethyl alcohol
T_o = 800 °F

P_o = 400 psig.

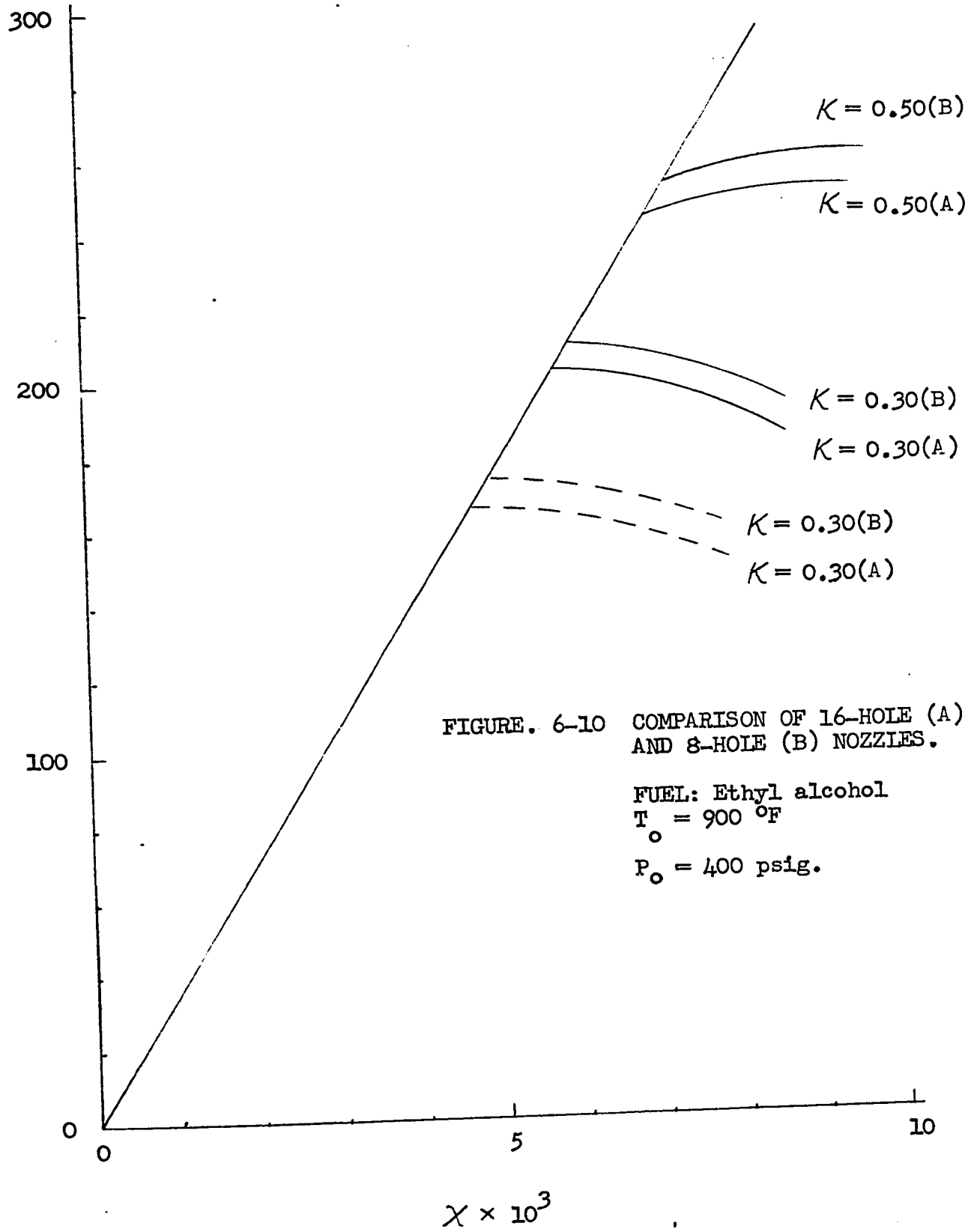

FIGURE. 6-10 COMPARISON OF 16-HOLE (A) AND 8-HOLE (B) NOZZLES.

FUEL: Ethyl alcohol
T_o = 900 °F
P_o = 400 psig.

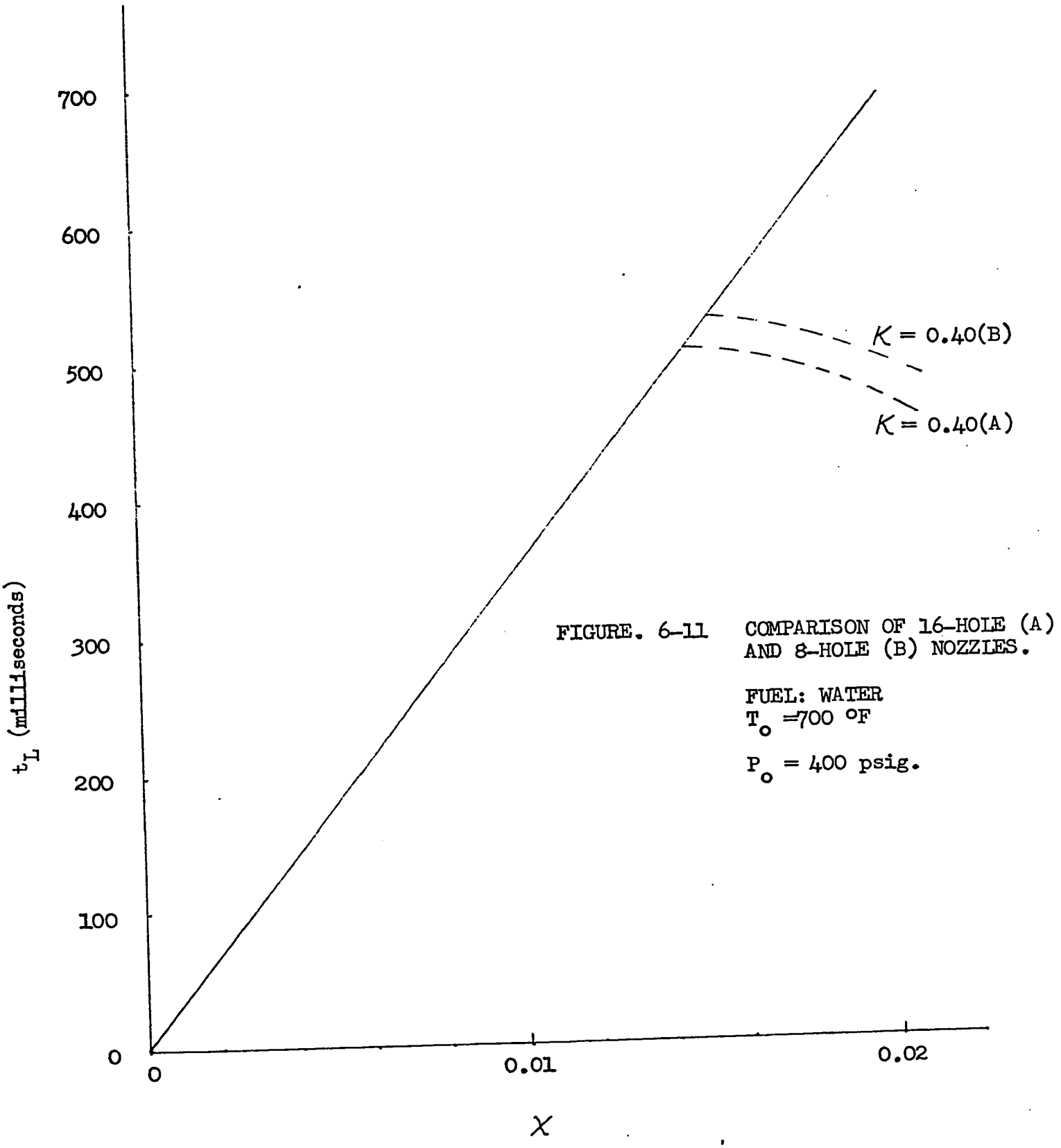

FIGURE. 6-11 COMPARISON OF 16-HOLE (A) AND 8-HOLE (B) NOZZLES.

FUEL: WATER
T_o =700 °F

P_o = 400 psig.

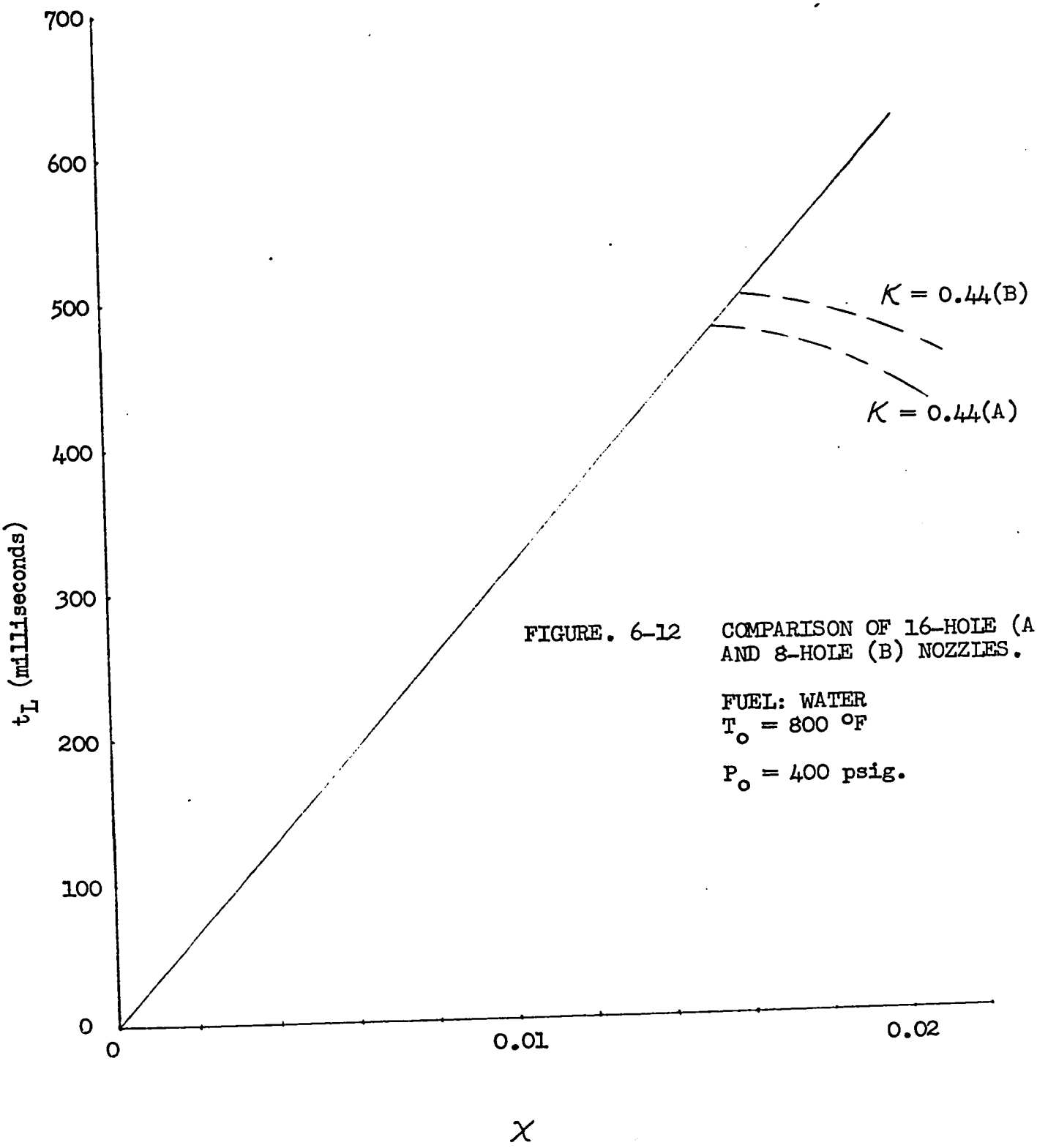

FIGURE. 6-12 COMPARISON OF 16-HOLE (A) AND 8-HOLE (B) NOZZLES.

FUEL: WATER
T_o = 800 °F

P_o = 400 psig.

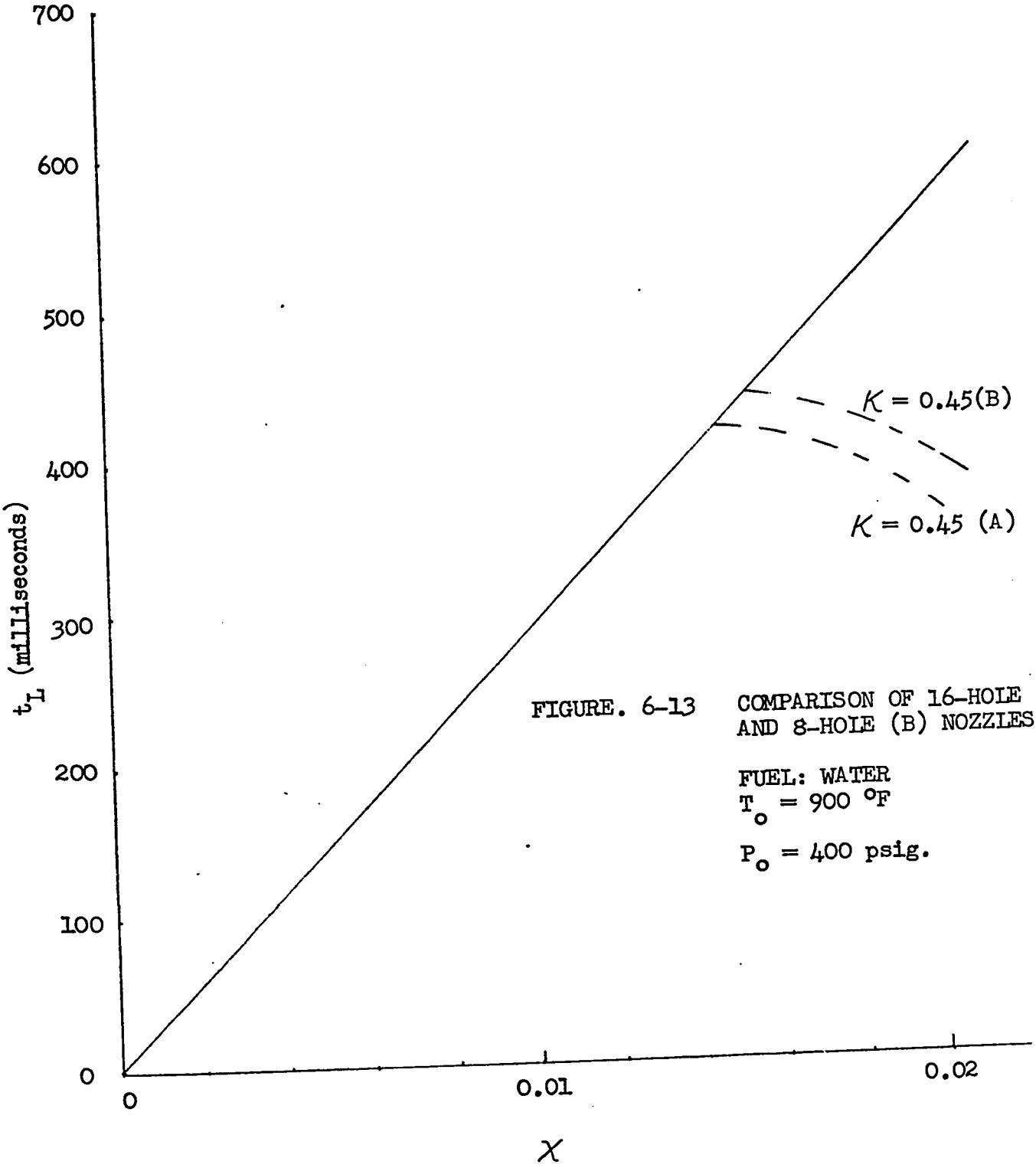

FIGURE. 6-13 COMPARISON OF 16-HOLE (A) AND 8-HOLE (B) NOZZLES.

FUEL: WATER
$T_o = 900\ ^oF$
$P_o = 400$ psig.

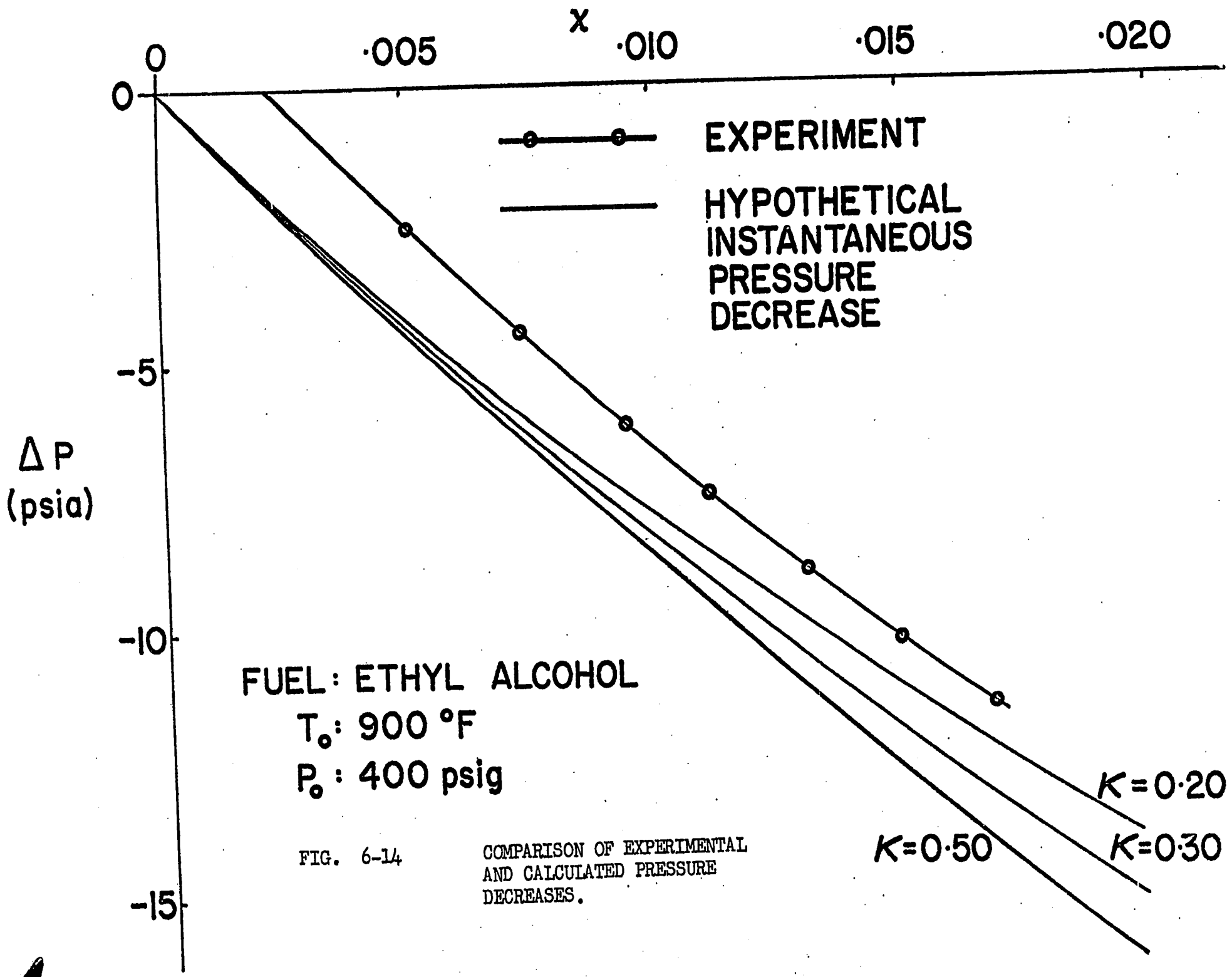

FIG. 6-14 COMPARISON OF EXPERIMENTAL AND CALCULATED PRESSURE DECREASES.

Appendix G

Table 5-1. Selected Physical Properties of ethyl alcohol.

TABLE 5-1

Selected Physical Properties of Pure Ethanol (Ref. 5.1).

Molecular weight, C_2H_5OH	46.07
Boiling point, 760 mm, °C	78.3
Critical temperature, °C	243.1
Critical Pressure, mm Hg	47,850
atms.	63.11
Specific gravity 20/20°C	0.7905
Heat of vaporization cal/g.	204.3
Specific heat, C_p 25°C	0.588

Density, g/ml

Temp. °C	Density
0	.806,306
5	.802,09
10	.797,87
15	.793,60
20	.789,34
25	.785,12
30	.780,75
35	.776,41
40	.772,03
50	.763,14

Coefficient of cubic expansion, 20°C. .001,8

Liquid up to 130°C (Ref. 5-2)

$C_p = 19.029,67 - 0.004,812T + .000,091,3\ T^2$ (cal/g mole °K)

Gas up to 1500°K (Ref. 4-2)

$C_p = 4.946 + 0.049,087\ T - .000,023,855\ T^2 + .000,000,004,5T^3$

(cal/g.mole °K)

Appendix H

Experimental Parameter Combinations and Lifetime of Sprays

Table 6-1 Experimental Parameter Combinations

Table 6-2 Experimental Parameter Combinations

Table 6-3 Lifetime of ethyl alcohol sprays. Ideal gas solutions.

Table 6-4 Lifetime of ethyl alcohol sprays. Non-ideal gas solutions.

Table 6-5 Lifetime of ethyl alcohol sprays. Non-ideal gas solutions. 8-hole self-impinging injector plate.

Table 6-6 Lifetime of water sprays. Non-ideal gas solutions. 16-hole self-impinging injector plate.

Table 6-7 Lifetime of water sprays. Non-ideal gas solutions. 8-hole self-impinging injector plate.

TABLE 6-1 EXPERIMENTAL PARAMETER COMBINATIONS

Fuel: Ethyl alcohol, 16-hole injector-plate

Initial Evaporation Chamber T. (°F)	Initial Evaporation Chamber P. (psig)	Total Injected Liquid Fuel Mass (g)	Sweep Speed of Oscilloscopes (sec/cm)	Fuel Injection Rate (g/sec)	Experiment Group Number
900	400	18.091	0.10	29.657	1
		15.484			
		12.917			
		10.468			
		7.861			
		6.305			
		18.091	5.00		2
800	450	18,091	0.10	32.596	1
		15.484			
		12.917			
		10.468			
		7.861			
		6.305			
		18.091	5.00		2
800	400	18.091	0.10	29.902	1
		15.484			
		12.917			
		10.468			
		7.861			
		6.305			
		18.091	5.00		2
800	400	18.091	0.10	32.305	1
		15.484			
		12.917			
		10.468			
		7.861			
		6.305			
		18.091	5.00		2

TABLE 6-1. Continued.

Initial Evaporation Chamber T. (°F)	Initial Evaporation Chamber P. (psig)	Total Injected Liquid Fuel Mass (g)	Sweep Speed of Oscilloscopes (sec/cm)	Fuel Injection Rate (g/sec)	Experiment Group Number
700	500	18.091	0.10	32.363	1
		15.484			
		12.917			
		10.468			
		7.861			
		6.305			
		18.091	5.00		2
700	450	18.091	0.10	31.963	1
		15.484			
		12.917			
		10.468			
		7.861			
		6.305			
		18.091	5.00		2
700	400	18.091	0.10	32.479	1
		15.484			
		12.917			
		10.468			
		7.861			
		6.305			
		18.091	5.00		2

TABLE 6-2

EXPERIMENTAL PARAMETER COMBINATIONS

Initial Evap. Chamber Temp. (°F)	Initial Evap. Chamber Pres. (psig)	Total Injected Liquid Fluid Mass (g)	Sweep Speed of Oscilloscope (sec/cm)	Fuel Injection rate (g/sec)	Fuel	Injector Plate Type
700	400	18.091	0.10	32.52	Ethyl Alcohol	8-hole
			5.00			
800			0.10			
			5.00			
900			0.10			
			5.00			
700		23.40	0.10	35.79	Water	16-hole
			5.00			
800			0.10			
			5.00			
900			0.10			
			5.00			
700		23.40	0.10	36.01		8-hole
			5.00			
800			0.10			
			5.00			
900			0.10			
			5.00			
700		23,40	0.10	36.15		1-hole
800						
900						

TABLE 6-3 LIFETIME OF ETHYL ALCOHOL SPRAYS. IDEAL GAS SOLUTIONS. 16-HOLE IMPINGING INJECTOR PLATE.

T_o (°F)	P_o (psig)	t_L (m sec)	κ	$\dot{m}_2$(g/sec)
700	400	241±7	0.27±.01	32.48
700	450	222±7	0.25±.01	31.96
700	500	217±7	0.23±.01	32.36
800	400	224±7	0.31±.01	32.31
800	400	242±7	0.30±.01	29.90
800	450	219±7	0.30±.01	32.60
900	400	203±7	0.30±.01	29.66

TABLE 6-4 LIFETIME OF ETHYL ALCOHOL SPRAY. NON IDEAL SOLUTIONS. 16-HOLE IMPINGING INJECTOR PLATE.

T_o(°F)	P_o(psig)	t_L (m sec)	κ	$\dot{m}_2$(g/sec)
700	400	180±3	0.23±.01	32.48
700	450	149±3	0.22±.01	31.96
700	500	144±2	0.22±.01	32.36
800	400	158±3	0.25±.01	32.31
800	400	169±4	0.25±.01	29.90
800	450	144±3	0.22±.01	32.60
900	400	165±4	0.30±.01	29.66

TABLE 6-5 LIFETIME OF ETHYL ALCOHOL SPRAYS. NON-IDEAL GAS SOLUTIONS. 8-HOLE SELF-IMPINGING INJECTOR PLATE

T_o (°F)	P_o (psig)	t_L (m sec)	κ	$\dot{m}_2$ (g/sec)
700	400	196±4	.26±.01	32.52
800		169±4	.27±.01	
900		178±4	.33±.01	29.89

TABLE 6-6 LIFETIME OF WATER SPRAYS. NON-IDEAL GAS SOLUTIONS. 16-HOLE SELF-IMPINGING INJECTOR PLATE

T_o (°F)	P_o (psig)	t_L (m sec)	κ	$\dot{m}_2$ (g/sec)
700	400	512±12	0.40±.01	35.79
800		480±12	0.44±.01	
900		422±10	0.45±.01	

TABLE 6-7 LIFETIME OF WATER SPRAYS. NON-IDEAL GAS SOLUTIONS. 8-HOLE SELF-IMPINGING INJECTOR PLATE

T_o (°F)	P_o (psig)	t_L (m sec)	κ	$\dot{m}_2$ (g/sec)
700	400	558±14	.43±.01	36.01
800		516±12	.48±.01	
900		462±12	.48±.01	